

The GeSn Alloy and its Optoelectronic Properties: A Critical Review of the Current Understanding.

Andrea Giunto and Anna Fontcuberta i Morral*
*Laboratory of Semiconductor Materials, Institute of Materials,
 École Polytechnique Fédérale de Lausanne, Lausanne, Switzerland*
 (Dated: September 20, 2023)

CONTENTS

I. Introduction	1
II. Historical Perspectives	1
III. Physical Properties of GeSn	4
A. GeSn: a Metastable Alloy	4
B. Crystal Lattice	4
C. Band Structure	5
IV. Challenges of the GeSn Alloy	6
A. Epitaxial Relaxation Defects	6
B. Sn Segregation and Thermal (In)stability	7
V. Epitaxial Growth of GeSn, Ge	11
A. Epitaxy of GeSn towards optoelectronic devices	11
B. State-of-Art of GeSn Sputtering Epitaxy	12
C. Ge Buffer Epitaxial Growth on Si Substrates	13
VI. Strain Relaxation Mechanisms and Defects in GeSn, Ge	15
A. Strain Relaxation during Epitaxial Growth of Ge on Si(001)	15
B. Annealing of Ge buffer	19
C. Strain Relaxation during Epitaxial Growth of GeSn on Ge buffer	21
D. Point Defects in Ge	22
E. Point Defects & Sn Clustering in GeSn	23
VII. Optoelectronic Properties of Ge & GeSn	24
A. Absorption Coefficient of GeSn	24
B. Trap states in Ge & GeSn	24
C. Unintentional Doping Concentration	28
D. Carrier Lifetime	32
VIII. Conclusions	36
Acknowledgments	36
References	36

I. INTRODUCTION

GeSn is nowadays recognized as a promising candidate to enable monolithic on-chip Si photonics operating in the near-infrared (NIR) and short-wave infrared (SWIR) wavelengths [1]. The addition of Sn to the Ge lattice induces a red-shift in the material bandgap (BG), extending the absorption cut-off wavelength towards the infrared. In addition, above 7-9 *at. %* Sn [2–4], the GeSn alloy acquires a direct BG, enabling its use as active material in SWIR light-emitting devices. Ge-rich GeSn alloys have been demonstrated in a plethora of optoelectronic devices including photodetectors [5–8], lasers [4, 9–11] and light emitting diodes (LEDs) [12–14]. Furthermore, the high theoretical mobility of GeSn [15, 16] motivated research for GeSn high-mobility field-effect transistors (FETs) [17–19], while the possibility of monolithic integration on Si platforms has also pushed the investigation of GeSn for on-chip thermoelectric applications [20, 21]. However, despite more than 15 years of intensive research in the field, there exists no commercial device to date based on GeSn. In fact, there are numerous challenges hindering the rise of this material for the next-generation (opto)electronics.

In the following sections, we give a concise review of the historical achievements in GeSn research and the withstanding challenges. This will be followed by a detailed description of the GeSn physical properties relevant for its use in optoelectronic devices.

II. HISTORICAL PERSPECTIVES

In 1982, C.H.L. Goodman first proposed crystalline GeSn (cGeSn) as a group-IV direct-BG material, hypothesizing alloy properties governed by Vegard’s law between Ge and the diamond cubic phase of Sn (i.e., α Sn) [22]. In addition, a high mobility was predicted due to the absence of polar scattering, typical in III-V and II-VI compounds. The Ge-Sn solid solution was thus suggested as alternative to III-V and II-VI materials for high-mobility FETs and infrared photodetectors in the SWIR (1.5 μm –3 μm), medium-wave infrared (MWIR) (3 μm –8 μm), and long-wave infrared (LWIR) wavelengths (8 μm –15 μm). Challenges in experimental realization of this material were expected due to the low solubility limit of 1 *at. %* of Sn in Ge (and vice-versa) [23, 24], and the lack of a lattice-matched substrate to stabilize metastable GeSn phases. Nevertheless, metastable, micro-crystalline GeSn

* anna.fontcuberta-morral@epfl.ch

with more than 20 *at.*% Sn was demonstrated one year later, thanks to the use of out-of-equilibrium synthesis [25]. $\text{Ge}_{0.78}\text{Sn}_{0.22}$ was crystallized from amorphous $\text{Ge}_{0.70}\text{Sn}_{0.30}$ by means of a UV pulsed laser. Initial theoretical studies of the GeSn alloy band structure using tight-binding models predicted an indirect-to-direct BG transition around 20 *at.*% Sn [26], similar to what expected from Vegard's law, now known to be overestimated [2]. The first epitaxial metastable GeSn film appeared in 1987, with growth up to 8 *at.*% Sn on a Ge(001) substrate by sputtering [27]. The growth temperature was maintained at 150°C to prevent Sn segregation due to the reduced solubility in Ge.

Slow, but notable progress in out-of-equilibrium synthesis processes was obtained in the 20 years following the demonstration of epitaxial GeSn on Ge(001). In 1989, Pukite *et al.* [32] employed the molecular beam epitaxy (MBE) method to push the Sn content to 30 *at.*% in polycrystalline GeSn films on Si(100) at 170°C. Despite the successful sputtering growth of GeSn epitaxial films, MBE became the growth method of choice in the 1990s, hence seeing considerable improvements in the following years. After a few more studies reporting polycrystalline growth [33, 34], monocrystalline MBE-grown GeSn was obtained in 1992 on Ge(001), but only up to thicknesses of 2 nm due to Sn segregation and the low growth temperatures employed [35]. In fact, low growth temperatures ($T < 200^\circ\text{C}$) reduce the adatom mobility, causing kinetic roughening and strain-induced roughening [36], limiting the epitaxial thickness to tens of nm for Sn fractions higher than 10 *at.*% [37–39]. Issues with Sn segregation and low-temperature growth were overcome in 1995 with the introduction of ion-assisted (Ar^+) MBE [40]. Mimicking the analogous effect in sputtering, light Ar bombardment was understood to induce collisional mixing of Sn adatoms with the film, increasing Sn incorporation and limiting its segregation [29]. With this method, He *et al.* [29] obtained 20-nm-thick monocrystalline GeSn films on Ge-buffered Si(001) substrates with Sn contents up to 34 *at.*%. In 1997, the same research group experimentally observed direct-BG behavior in GeSn for the first time [41] and realized the first pseudomorphic GeSn film on Ge(001) [42] in 2000, using standard thermal MBE. The BG crossing from indirect to direct character was found to occur around 11 *at.*%, a Sn alloy fraction considerably lower in comparison with the cross-over composition theoretically calculated at the time. This discrepancy was understood in the 2000s with first-principle computations [43] and subsequent experimental observation [44]. In fact, the behavior of the GeSn band energies follows a positive deviation from Vegard's law, described with the use of a bowing parameter (b):

$$E_{\text{GeSn}} = (1 - x)E_{\text{Ge}} + xE_{\alpha\text{Sn}} - b(1 - x)x \quad (1)$$

where E is the BG energy of the respective materials [45]. Numerous measurements and computations of b have been reported in the literature since then, with values generally spanning between 2.0 eV and 2.5 eV (see Tab. I,

discussed in Sec. III). The positive value of b implies that the BG crossover occurs at lower x compared to what predicted by Vegard's law, explaining the early disagreement between theoretical and experimental data. This discovery significantly boosted the prospects of the GeSn alloy, as it signified that the material BG can be strongly red-shifted with only a few *at.*% of Sn, simplifying the material synthesis process and benefiting optoelectronic SWIR applications.

To overcome the limitations of MBE associated with low-temperature growth and kinetic roughening [36], in the 2000s the attention was shifted towards different growth methods. Magnetron sputtering (MS) was successfully employed to grow few-hundred-nm-thick GeSn films on Ge(001) up to 14 *at.*% Sn [46, 47], while chemical vapor deposition (CVD) growth was demonstrated in 2001 by Taraci *et al.* thanks to the introduction of stable Sn precursors [48–50]; films up to 200 nm with 20 *at.*% Sn were obtained on Si(100) by ultra-high vacuum (UHV) CVD [44]. At the same time, the first SiGeSn films were demonstrated [51] with the potential of delivering a higher thermal stability and a decoupling of lattice parameter and BG energy [52].

The promising advances in epitaxy led to a growing interest in GeSn in the research community, evident in Fig. 1 from the increase in number of published works on GeSn from 2009 onwards. Researchers gained a deeper understanding of GeSn synthesis processes and properties, such as Ge surface reconstruction in presence of Sn [53], composition-dependent epitaxial strain relaxation [54], and BG alloy dependence on composition and strain [55]. With the introduction of doping methods of GeSn [56], the first optoelectronic device was demonstrated in 2009 by Mathews *et al.*, with the fabrication of a CVD-grown n - i - $\text{Ge}_{0.98}\text{Sn}_{0.02}/p$ -Si photodiode (PD), sensitive up to 1750 nm [31]. This detector possessed quantum efficiencies lower than 0.1% but, only 2 years later, an improved design in MBE-grown p - i - $\text{Ge}_{0.97}\text{Sn}_{0.03}/n$ -Si demonstrated a responsivity in the SWIR comparable to commercial Ge devices [57]. In 2011, GeSn p-type metal-oxide-semiconductor field-effect transistors (MOSFETs) were demonstrated with higher hole mobility than conventional Ge MOSFETs [58, 59]. Furthermore, following demonstration of GeSn photoluminescence (PL) [30], the first GeSn-based LED was fabricated, showing room-temperature electroluminescence and a clear red-shift in emission with respect to Ge LEDs [60, 61]. In the same year, Vincent *et al.* achieved GeSn epitaxial growth by atmospheric-pressure chemical vapor deposition (AP-CVD) with commercially available precursors, demonstrating the viability of vacuum-free alloy growth, thus significantly simplifying the synthesis process [62]. Growth of epitaxial GeSn on Si(100) with industry-compatible reduced-pressure chemical vapor deposition (RP-CVD) was shown in 2013 by Wirths *et al.* [63].

One of the most remarkable steps in the development of GeSn-based technology was the demonstration of the first

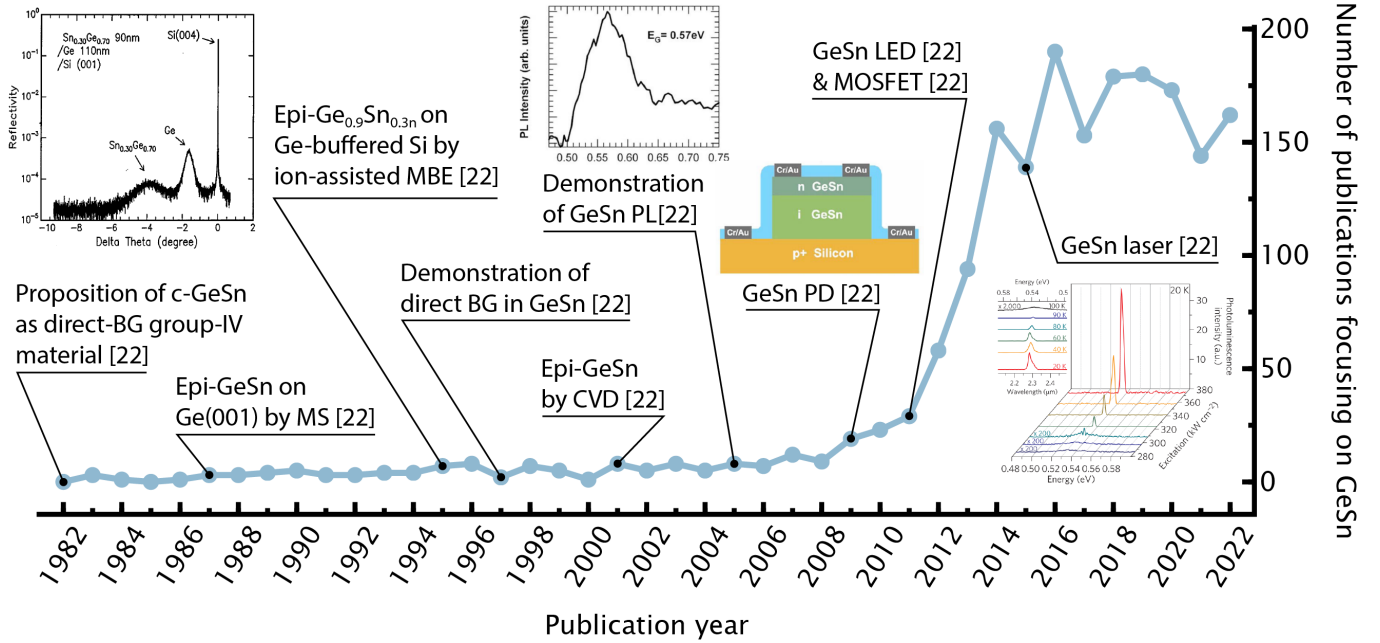


FIG. 1. Plot of number of publications per year focusing on GeSn, showing some of the milestones achieved in the field. Publication data was selected using the software *Dimensions.ai* [28], searching for entries from relevant fields of research with the following keywords in the title or abstract: “GeSn”, “SnGe”, “Ge_{1-x}Sn_x”, “Sn_xGe_{1-x}”, “Ge_{1-x}Sn_x”, “Sn_xGe_{1-x}”. Figures in the insets are reprinted with permission from the corresponding authors: respectively, from left to right, He *et al.* [29], © 1995 Elsevier; Soref *et al.* [30], © 2006 Springer Nature; Mathews *et al.* [31], © 2009 AIP Publishing; Wirths *et al.* [4], © 2015 Springer Nature.

optically-pumped GeSn laser operating at $T < 90$ K with 12 at.% Sn at wavelengths of $\sim 2.3 \mu\text{m}$ [4]. Being the last long-sought building block required for SWIR monolithic group-IV on-chip Si photonics [64], this work set off a race towards the first electrically pumped GeSn laser operating at room temperature, yet to be realized. Breakthroughs were achieved in 2020 with the first electrically-injected laser operating up to 100 K [65], and in 2022 with room-temperature lasing obtained in optically-pumped Ge_{0.86}Sn_{0.14} devices [66]. These works currently set the state-of-the-art operating temperatures for the respective injection modes. Factors limiting laser performance are the low carrier lifetimes in GeSn due to material defects, and the limited GeSn BG directness, i.e., the difference in energy between the indirect L- and direct Γ -valleys [4], which respectively increase the lasing threshold and decrease the maximum operating temperature [67]. Common strategies to increase the BG directness, and thus the lasing temperature, are to induce tensile strain in the GeSn gain material or increase the Sn fraction in the alloy [66, 68, 69], though the former is preferable to avoid the increase in defect concentration associated with large Sn contents [66]. Material defects inducing high lasing thresholds come from the bulk [70], surface [11] and interface [68] of the active material. Surface traps can be prevented via proper passivation of the material, though no absolute passivation scheme has been established for GeSn, resulting in each group using different methods [7, 71–73]. Interface defects come from arrays of

misfit dislocations from GeSn epitaxy and are physically unavoidable on mismatched substrates. In microdisk laser architectures, misfit dislocations can be etched away to improve the lasing threshold [68]. Alternatively, type-I GeSn/SiGeSn and GeSn/Ge multi quantum well (MQW) structures have been employed to confine carriers away from the epitaxial interface [70, 74, 75]. On the other hand, there is no clear strategy to decrease the material bulk defect concentration, mainly because GeSn bulk defects and electrical properties are poorly understood, as elaborated later in Sec. VII.

Present challenges prevent room-temperature operation of electrically-injected GeSn lasers, hindering their commercialization. In fact, though promising improvements have been achieved in the years, the very same factors limit the performance of GeSn as active material in photodetectors. GeSn PDs have been realized with CVD [5, 76], MBE [8, 77, 78], and magnetron sputtering (MS) [79]. State-of-the-art GeSn *p-i-n* SWIR PDs were obtained with Ge/GeSn MQW architecture, showing cut-off frequency of 10 GHz at $2 \mu\text{m}$ with low dark currents of 44 mA/cm^2 at a bias of -1 V , similarly to commercial Ge photodiodes [80], though with a limited responsivity of 15 mA/W [76]. Trying to extend the wavelength sensitivity range with increasing Sn contents results in the degradation of GeSn quality due to increased defect concentration [1]. Atalla *et al.* [5] achieved sensitivity up to $2.6 \mu\text{m}$ with a Ge_{0.885}Sn_{0.115} *p-i-n* PD. At a reverse bias of 0.5 V , they obtained a peak respon-

sivity of 0.3 A/W at 2 μm , with a noticeable drop in above 2.25 μm that reached ~ 60 mA/W at 2.6 μm . They achieved high cut-off frequency of 7.5 GHz at -5 V, which reduced to ~ 1 GHz at -1 V. However, as expected from the higher Sn content, the average dark current in these PDs was 6.5 A/cm², demonstrated by the authors to come from bulk material defects. Currently, the dark currents due to Shockley-Read-Hall (SRH) generation mechanisms in GeSn alloys are too high to be competitive with III-V technology [81]. Despite the potential of GeSn suggested by theoretical studies to reach the MWIR (i.e., 3 μm -8 μm) wavelengths [55, 82], the inherent epitaxial compressive strain on Ge and Si substrates increases the BG energy, significantly complicating the experimental realization of MWIR devices. As a consequence, there are only a handful of studies focusing on operation in this wavelength range [5]. Strain engineering is thus an essential point to consider to extend the wavelength operation range into the MWIR [1]. Waveguides [83, 84] and photonic crystals [85] have been proposed to enhance absorption and thus improve responsivity. To the same goal, GeSn avalanche photodiodes (APDs) have been fabricated [8, 77, 78], while GeSn single-photon avalanche photodiodes (SPADs) are yet to be demonstrated.

While GeSn laser devices fabricated to date employ exclusively CVD-grown materials, LEDs have been realized with both CVD and MBE methods [86]. Emission at 3.3 μm has been achieved with Ge_{0.85}Sn_{0.15}/Ge heterostructures [12], and a simple gas detector was demonstrated [87]. Though comparable with commercial MWIR LEDs [1], the GeSn LED quantum efficiency remains suboptimal due to trap recombination mechanisms caused by material defects [87, 88]. Alternative architectures employed SiGeSn/GeSn MQW carrier confinement to improve the quantum efficiency [88, 89], though it was effective only compared to indirect BG GeSn [1], and waveguides [90]. From the point of view of GeSn electronic devices, recently, GeSn FETs for complementary metal-oxide-semiconductor (CMOS) beyond-Si electronics were fabricated with improved performance with respect to the pure Ge counterpart [91]. Lastly, the field of research on GeSn nanostructures including nanowires, quantum wells and quantum dots has been equally progressing in the last decade. These works have been thoroughly reviewed by Doherty *et al.* [92].

III. PHYSICAL PROPERTIES OF GESN

In the following section, we introduce the basic physical properties of GeSn. We review the GeSn phase diagram and the metastability of the alloy, and then introduce recent discoveries on the arrangement of Sn solute atoms in the material. Finally, we describe the band structure of GeSn, and its dependence on the alloy composition and strain state of the material.

A. GeSn: a Metastable Alloy

GeSn is an alloy obtained from a solid solution of two group-IV elements, namely Ge and Sn. The Ge-Sn phase diagram is shown in Fig. 2(a). Ge is an indirect-BG semiconductor with diamond face-centered cubic (FCC) crystal structure (space group (SG): Fd $\bar{3}$ m), shown in the inset of Fig. 2(b), with lattice constant of 5.658 Å [22]. Sn instead can be found in two phases, the high-temperature metallic β Sn phase, and the low-temperature semi-metallic α Sn phase, with a thermodynamic phase transition of 13.2°C. In the case of GeSn alloys, α Sn is the phase of reference, since it also has a diamond FCC crystal structure, with lattice constant of 6.489 Å [22]. Ge and Sn can thus be mixed in a solid solution to obtain a non-polar semiconductor (or semi-metal, depending on the composition), with the same diamond FCC crystal structure of the two elemental materials. However, as a consequence of the large lattice mismatch between Ge and α Sn of 14.7 %, the solubility of one element in the other is low. Evident from the Ge-rich zoomed region of the phase diagram in Fig. 2(b), the solubility of Sn in Ge is limited to a bare 1.1 *at.*% at 400°C, and drops well below 1 *at.*% at room temperature. Ge-Sn are mostly immiscible, with an eutectic temperature of 231°C, and single-phase GeSn is therefore a metastable material across most of its compositions. Hence, phase-separation during growth or post-growth thermal processing is of concern. If not kinetically hindered by out-of-equilibrium processing, Sn will tend to segregate out of the Ge crystal, forming a metallic β Sn phase that is detrimental for optoelectronic devices. In this review, we discuss the Ge-rich phase of the GeSn alloy, as it is technologically more relevant for the targeted optoelectronic applications in the SWIR, MWIR, and LWIR wavelength ranges.

B. Crystal Lattice

The diamond FCC lattice parameter of GeSn follows Vegard's law [95–98], i.e., it varies linearly with composition between the lattice constants of Ge and α Sn. In agreement with *ab-initio* calculations [99], extended x-ray absorption fine structure (EXAFS) studies found that the Sn-induced strain in the GeSn alloy is accommodated by both bond stretching and bond bending, with a slightly larger contribution from the latter [100, 101].

For years, GeSn has been considered to be a homogeneous random solid solution following both computational predictions of the alloy properties [55, 95] and experimental studies [102]. A fully random solution implies the absence of any short- or long-range atomic order of the solute species. However, recent works showed that the GeSn alloy may possess a short-range order (SRO) [103, 104]. Combining statistical sampling and *ab initio* calculations, Cao *et al.* [103] suggested the presence of a SRO at Sn atoms, with the first coordination

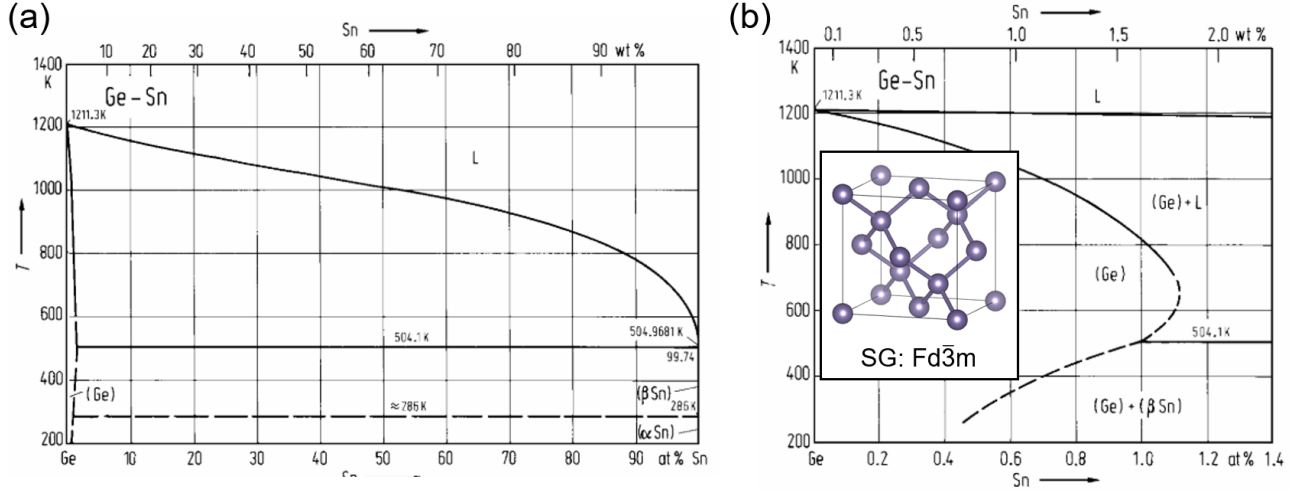


FIG. 2. (a) Phase diagram of the Ge-Sn alloy, and (b) zoom on the Ge-rich compositions. In the inset of (b) is the diamond FCC crystal unit cell, produced with the software *VESTA* [93]. Figures (a,b) reproduced with permission from Predel [94], © 1996 Springer Nature.

shell nearly devoid of other Sn atoms. With this assumption, they provided better predictions of the GeSn BG energy at high Sn contents, comparing it with experimental results previously fit with the random alloy assumption. The SRO was later demonstrated experimentally by EXAFS characterization of strain-free $\text{Ge}_{0.906}\text{Sn}_{0.094}$ nanowire shells grown around a compliant Ge core by CVD [104]. The observed SRO may be rationalized as an effect of the large size of Sn atoms, whose self-repulsion may allow local strain accommodation with reduced bond distortions. This idea is reflected by a significant Sn-Sn repulsion calculated by density-functional theory (DFT) in the first coordination cell of Sn [105]. The repulsion energy quickly drops moving away from the first coordination shell, becoming negligible at the fourth coordination cell [105].

A previous experimental study by atom probe tomography (APT) reported the absence of SRO in CVD-grown $\text{Ge}_{0.82}\text{Sn}_{0.18}$ [102]. The lack of observation of SRO has been suggested to be owed to the temperatures employed during growth of the material [106]. In Ref. [106], Windl *et al.* employed Monte Carlo methods to simulate the effect of growth temperature on the alloy by relaxing an 8000-atom cell with average composition corresponding to $\text{Ge}_{0.86}\text{Sn}_{0.14}$; they observed a significant reduction in SRO at the growth temperatures of 300–400°C, typically used in CVD epitaxy of GeSn. Furthermore, Lentz *et al.* [104] suggested the employed growth rate may also play a role in the final alloy SRO, as their GeSn layer was grown at 275°C at a slow rate of 1 nm/min in contrast with the rate of 1.5–2.8 nm/min employed in the GeSn film stack studied in Ref. [102]. Additional experimental studies on GeSn films are required to confirm the presence of SRO and to assess its dependence on growth conditions.

Lastly, APT studies suggested that compressive strain in GeSn may favor the presence of Sn-Sn bonds [107], in contrast with the SRO observed in strain-free GeSn [104]. If confirmed, this would suggest the importance of strain engineering to prevent phase separation when trying to achieve large Sn contents in the GeSn alloy.

C. Band Structure

The GeSn band structure evolution with composition can be qualitatively understood by observing the band structure of the constituent elements – Ge and αSn – shown in Fig. 3(a). Ge is an indirect-BG semiconductor with BG energy of 0.66 eV at the L-valley, and direct Γ -valley energy of 0.80 eV [108]. αSn , on the other hand, is a semi-metal with direct BG energy of -0.41 eV, and BG energy at the L-valley of 0.09 eV [108]. The Ge-Sn energy difference at Γ - and L-valleys are respectively of 1.21 eV and 0.55 eV. Assuming the bandgap energies vary linearly with compositions, one can therefore expect that by adding Sn to Ge the Γ -point energy will red-shift faster than the L-point, inducing a cross-over from indirect to direct BG behavior in the material. Experimentally, this is indeed the case, though we have seen in Sec. II that the cross-over occurs at lower Sn fractions compared to the linear prediction, with the bandgap energies following a bowing behavior described by eq. 1. The bowing behavior of the GeSn alloy is the result of coupling of states through a non-diamond-like potential [45]. This asymmetric potential originates from the difference in electronegativity of the constituent elements, and the lattice distortions (i.e., bond stretching and bending [109]) due to their different atomic sizes [45]. This explains why early works using highly symmetric potential-averaged

virtual crystal approximations, such as that from Jenkins *et al.* [26], failed to capture the large bowing behavior of the material. On a side note, DFT studies by Yin *et al.* [45] found that the total bowing behavior originates equally from Ge-Sn charge and structural differences, while Chibane *et al.* [110] determined a dominant contribution from the latter. Discrepancies in the result may have arisen from the different GeSn compositions and supercell sizes considered in the studies (see Tab. I).

In Tab. I, we report the measured and computed values of bowing parameters of the GeSn Γ - and L-energy gaps (b_Γ , b_L). From these results, it is clear that there is no close agreement on these values in the literature. In general, $2\text{ eV} < b_\Gamma < 3\text{ eV}$, while $b_L \sim 1\text{ eV}$. The large variability of the reported experimental values of b_Γ comes from the complexity of the material system: Besides possible experimental systematic errors coming from the different employed techniques, the atomistic structure of the alloy may vary depending on the employed growth technique and parameters, resulting in different physical properties. For example, Sn-clustering has been observed in GeSn [107, 112], and it has been predicted to lower the material bandgap [110], consequently inducing an apparent larger bowing parameter. Additionally, the strain state of the material affects BG energies shifts, as shown in Fig. 3(b). In particular, compressive strain has the opposite effect of Sn alloying on the conduction band (CB) valleys [55, 113], increasing the BG energy, and thus decreasing the apparent bowing behavior. Strain also splits the heavy-hole (HH)-light-hole (LH) degeneracy, with compressive strain lifting the HH, and tensile strain producing the opposite effect [114, 115]. Failure of appropriately taking into account the strain state of the material will result in experimental errors. Concerning theoretical computations of the alloy bowing parameter, DFT model on strain-free material considered the GeSn alloy to be fully random, while recent works demonstrated the presence of a SRO in GeSn [103, 104]. The absence of Sn atoms in the first coordination shells of Sn yields a larger BG energy [103, 110], and thus b is overestimated when fitted over the entire alloy spectrum; this is the case for Refs. [95, 116], which report $b_\Gamma > 3\text{ eV}$. Lastly, Gallagher *et al.* [3] found their data was better fitted with composition-dependent bowing parameter, also proposed with DFT-based calculations by Chibane *et al.* [110]. On the other hand, Yin *et al.* [45] computed by DFT a negligible dependence on composition of the bowing parameter. Furthermore, D’Costa *et al.* [117] argued that with the composition-dependent b_Γ from Gallagher *et al.* pseudomorphic GeSn would not show a direct-bandgap behavior for any composition. Fernando *et al.* [118] predict the indirect-to-direct crossover behavior of pseudomorphic GeSn on Ge(001) to be at 26 *at.*%, though extrapolated from samples with $x_{\text{Sn}} < 0.11$, and calculated without considering any SRO. The latter is expected to further push the crossover composition to larger Sn contents [103]. More theoretical work is necessary to determine the exact behavior of the bowing parameter. On

the other hand, experimentally determined values may vary due to the intrinsic differences in the alloy atomistic arrangements influenced by the employed growth technique and growth parameters.

Until recently, GeSn was expected to show a hard crossover from an indirect to direct BG behavior. Several groups tried to measure and/or compute the crossover alloy composition. Inevitably, the large scatter in the reported values of bowing parameter (see Tab. I) produced an equally large scatter in the reported alloy crossover compositions, spanning between 6 *at.*% and 10 *at.*% Sn [123]. In fact, recent works demonstrated that GeSn has a soft transition from an indirect to a direct BG behavior due to band mixing [1, 124, 125]. In GeSn, the CB edge states were found to consist in a linear combination of the Γ (Γ_{7c}) and L states (L_{6c}). This behavior originates from the large differences in covalent radius and electronegativity of the alloy constituent elements and was demonstrated by measuring the GeSn bandgap hydrostatic pressure coefficient (dE_g/dp) of GeSn [124]: In Ge, the pressure coefficient of the direct BG ($\Gamma_{7c} - \Gamma_{8v}$) is 3 times that of the indirect BG ($L_{6c} - \Gamma_{8v}$). By measuring dE_g/dp , it is thus simple to discern the BG behavior of the material. In GeSn, experimental values of dE_g/dp progressively increase from dE_L/dp to dE_Γ/dp for increasing Sn content ($x_{\text{Sn}} < 0.15$ [1]), indicating that the band mixing evolves progressively with x_{Sn} [124]. DFT computations confirmed the progressive increase of dE_g/dp in GeSn, corroborating the experiments [124, 125]. Furthermore, O’Hallaran *et al.* [125] found evidence of band mixing also in the previously reported DFT calculations, e.g., from Polak *et al.* [95], emphasizing the importance of atomistic computations in capturing the electronic behavior of the GeSn alloy. The band mixing behavior may explicate to some extent the variability in the reported experimental crossover alloy compositions.

In general, we can conclude that the lattice ordering and band structure of the GeSn alloy are fairly well understood qualitatively, but still lack accurate quantitative interpretation. Nevertheless, the knowledge accumulated until now allowed significant progress in the performance of GeSn-devices, as seen in Sec. II.

IV. CHALLENGES OF THE GESN ALLOY

The main challenges associated with GeSn processing are briefly discussed in the following sections. More thorough elucidations are given in Secs. VI and VII.

A. Epitaxial Relaxation Defects

To maximize the material performance, GeSn should be integrated in devices in a monocrystalline structure, since group-IV grain boundaries are known to be sources of trap states [126–129] and act as scattering centers dur-

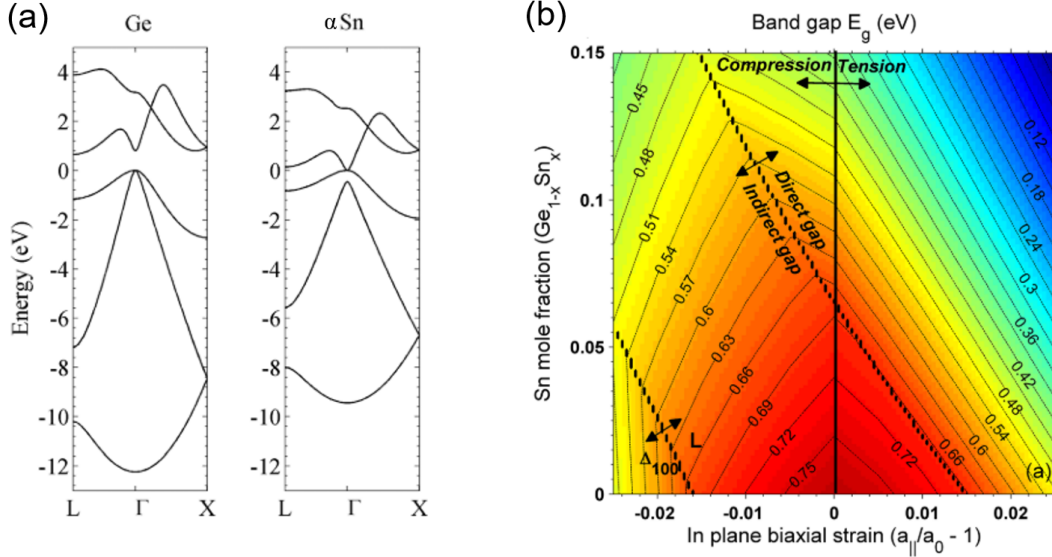


FIG. 3. (a) Band structures of Ge and α Sn. (b) Calculations of BG energy dependence on strain, using $b_T = 2.1$ eV. Figure (a) adapted with permission from Moontragoon *et al.* [111], © 2012 AIP Publishing. Figure (b) reprinted with permission from Gupta *et al.* [55], © 2013 AIP Publishing.

ing charge transport [130]. Monocrystalline GeSn can be obtained by epitaxial growth on substrates with a suitable crystal structure and similar lattice parameter. Undoubtedly, the ideal substrate from the technological point of view is Si, which has a diamond cubic FCC structure, with a lattice constant of 5.431 \AA that corresponds to a lattice mismatch of 4.18% with pure Ge. GeSn, possessing a lattice parameter larger than Ge, will thus grow in a compressive strain on Si substrates. However, with such large lattice mismatch, as the epitaxial film grows coherently on the substrate, it accumulates enough elastic energy to overcome the nucleation energy of dislocations, and the strain is thus (partially) relaxed via the formation of misfit dislocations (MDs) and threading dislocations (TDs), as shown in Fig. 4(a). The critical thickness of strain relaxation (t_{cr}) on Si is of only a few nm [131], and thus relaxation defects in GeSn are unavoidable on this substrate material for any thickness technologically relevant for optoelectronic applications. To partially accommodate the compressive strain, GeSn is grown on Ge-buffered Si substrates (also called Ge virtual substrate (vGe)), or directly on Ge substrates. This yields considerably larger t_{cr} , which however drops as the lattice mismatch increases with the Sn fraction in the alloy. The dependence of t_{cr} on GeSn composition is plotted in Fig. 4(b) using People and Bean's model, which is based on a thermodynamic energy-balance approach [131]. This model has been verified to correctly predict the critical thickness of GeSn grown on Ge [46, 132].

Dislocations limit the thermal stability of GeSn [133, 134] and are a source of electronic deep trap states [135–137], detrimental for the performance of GeSn-based op-

toelectronic devices. For example, in GeSn PDs, trap states increase the dark currents via SRH and trap-assisted tunneling (TAT) carrier generation mechanisms in the junction depletion regions [138]. Hence, epitaxial relaxation defects require appropriate management for the optimization of optoelectronic device performance. Extensive research on dislocation engineering showed that the threading dislocation density (TDD) in Ge and GeSn films can be reduced via nano- and micro-patterning of the substrate [139, 140], thick (graded) buffers [141], thermal processing [142, 143], or any combination of these strategies [140]. A more thorough discussion will thus follow in Secs. VI and VII. Because of the technological relevance of Ge buffers, their growth, relaxation phenomena, and electrical properties are presented as well throughout this review.

B. Sn Segregation and Thermal (In)stability

In the following section, we revise the understanding of the driving forces at play during Sn segregation in metastable GeSn, discussing the material thermal stability. We review the current understanding of Sn diffusion phenomena, the mediating role of defects in GeSn, and the efforts to elucidate the interplay between the alloy composition, strain relaxation and Sn out-diffusion.

As we have seen in Sec. III, GeSn is metastable for all compositions with $x_{Sn} > 1 \text{ at.}\%$. According to the Ge-Sn phase diagram in Fig. 2, at room temperature thermodynamics predict a phase separation of GeSn into a Ge-rich phase with less 1 at.% Sn, and a β Sn phase. However, this process is kinetically hindered by the low atomic diffusiv-

TABLE I. Summary of bowing parameters determined by experiments and computations. In the header, $x_{Sn,max}$ refers to the maximal Sn fraction considered in the study. Acronyms: CER, VASE, PR, OT, DSR.

	Ref.	b_T (eV)	b_L (eV)	Method	$x_{Sn,max}$	Comments
Experiments	Zelazna, 2015 [119]	1.8	-	CER	0.11	MBE, pseudomorphic on Ge. Compressive strain compensated in fits.
	Gallagher, 2014 [3]	2.66– 5.4 x_{Sn}	1.11– 0.78 x_{Sn}	PL	0.11	UHV-CVD, on Ge/Si. Compressive strain compensated in fits
	Jiang, 2014 [120]	2.46	1.03	PL	0.06	CVD, on Si. Compressive strain compensated in fits
	Lin, 2012 [121]	2.43	-	PR	0.064	MBE, on lattice-matched $In_yGa_{1-y}As/GaAs$
	Pérez Ladrón, 2007 [122]	2.30	-	OT	0.14	MS, on Ge(100). Strain unspecified, thickness of few 100s nm
	D'Costa, 2006 [44]	2.3	-	VASE & PR	0.20	UHV-CVD, on Si(100). Slight compressive (DSR _c 90%).
	He, 1997 [41]	2.8	-	OT	0.15	MBE, on Ge/Si(100). Fully relaxed within experimental error.
Computations	Song, 2020 [108]	2.28	2.86	30-band k·p	0.3	Strain-free. Less precise than DFT.
	Polak, 2017 [95]	3.02	1.23	DFT	1	Strain-free. 54-atom supercell, fully random alloy
	Zelazna, 2015 [119]	1.97	0.26	DFT	0.08	Strain-free. 54-atom supercell, non-random
	Eckhardt, 2014 [116]	3.1	-	DFT	1	Strain-free. 216-atom supercell, fully random alloy
	Chibane, 2010 [110]	1.94	0.90	DFT	0.25	Strain-free. 16-atom supercell, Sn-clustered & non-clustered cells.
	Yin, 2008 [45]	2.55	0.89	DFT	0.75	Strain-free. 64-atom supercell, fully random alloy.

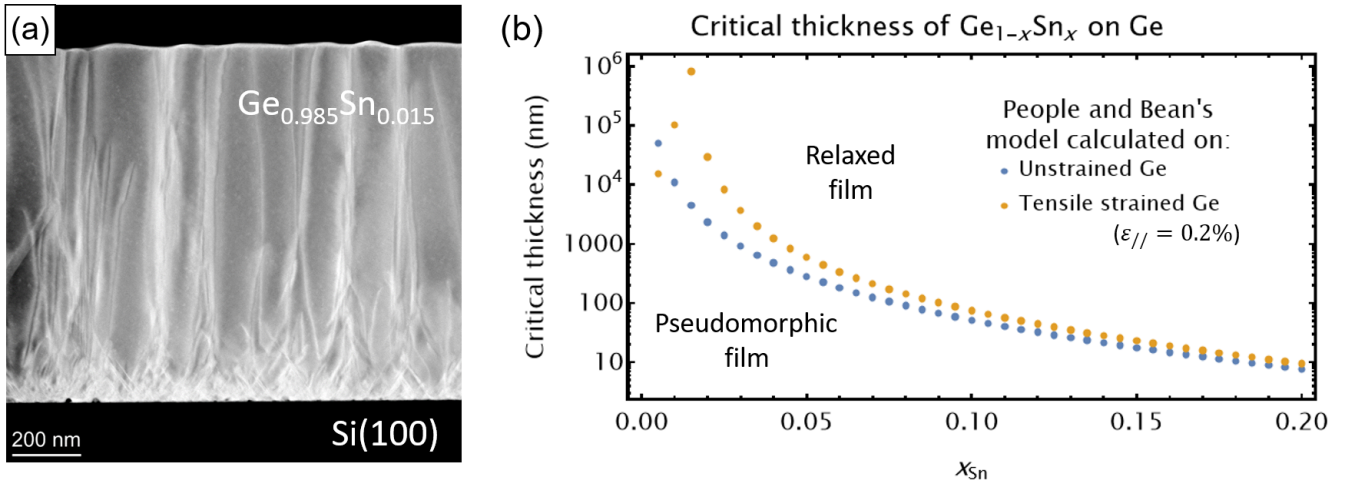


FIG. 4. (a) XTEM of $Ge_{0.985}Sn_{0.015}$ epitaxially grown on Si(100) by MS, rich in dislocations due to epitaxial strain relaxation. (b) People and Bean's thermodynamic model for GeSn critical thickness (t_{cr}) on Ge(100) substrates. On tensile-strained Ge, t_{cr} is increased.

ity at room temperature. On the other hand, upon thermal processing of the material, may it be for annealing, doping, or any CMOS post-growth process that requires heating, Sn atoms may acquire sufficient thermal energy to diffuse to the surface of the material [144, 145], and/or

cluster in the bulk into a β Sn phase [145]. Sn segregation may also occur during growth if the substrate temperatures are too elevated [146–148]. The resulting film will show several Sn droplets on surface, similar to the one reported in the scanning electron microscopy (SEM) im-

age of Fig. 5(a). The Sn out-diffusion from the Ge matrix increases the effective bandgap of the material, defeating the purpose of alloying with Sn. Additionally, the metallic behavior of the segregated β Sn phase will be detrimental in optoelectronic devices. Hence, in general, it is necessary to prevent the Sn segregation by maintaining a low thermal budget both during growth and post-growth processes. Exceptions where the Ge-Sn phase separation is sought obviously exist [149].

Experimental investigations have elucidated the driving forces for Sn segregation and the influence of material defects on the latter. Sn diffusion in Ge is mediated by vacancies [150–152], whose formation energy in group-IV semiconductors is known to depend on the strain state of the material [153–155]. In particular, the vacancy formation energy decreases under compressive strain. Therefore, in compressively strained GeSn films, the associated increase in vacancy concentration is expected to increase the Sn diffusion coefficient, facilitating Sn segregation. However, a study from von den Driesch *et al.* [144] in nearly dislocation-free GeSn films showed that this cannot be the only contributor to Sn out-diffusion. In fact, they observed that given an equal Sn composition and film compressive strain, Sn out-diffusion in $\text{Si}_{0.040}\text{Ge}_{0.895}\text{Sn}_{0.065}$ is accelerated compared to $\text{Ge}_{0.94}\text{Sn}_{0.06}$ due to the larger metastability of the ternary alloy, concluding that the principal driving force for Sn out-diffusion is given by the thermodynamic instability of the material. In support of this conclusion, they further observed two regimes of Sn diffusion depending on the annealing temperature. By gradually increasing temperature (T) from 500°C, they first found a low activation energy [156] regime, with enhanced diffusion due to the large metastability of the material. Around 650°C, as the Sn progressively diffused out of the Ge matrix, its diffusion activation energy increased and matched that of Sn in non-metastable, Sn-doped Ge [151]. The authors attributed this behavior to the loss of metastability-enhanced diffusion as the Sn concentration decreased to values within the solubility limit in Ge [144].

As a consequence of the strong influence of the alloy metastability on Sn segregation, the thermal stability of GeSn decreases with increasing Sn content, making it progressively more difficult to achieve large Sn fractions in GeSn. Zaumseil *et al.* [157] showed that the decrease is almost linear with Sn content, with phase-separation temperatures reported to be between 600°C and 350°C for Sn fractions respectively between 4.8 *at.%* and 11.7 *at.%*. This is in close agreement with other reports [158].

The presence of extended defects in GeSn has been found to strongly affect the Sn segregation behavior during thermal treatments. In pseudomorphic GeSn, Sn segregation occurs gradually via vacancy-mediated diffusion [144, 157], while in strain-relaxed GeSn the segregation process is considerably different due to the presence of misfit dislocations (MDs) and threading dislocations

(TDs) in the film. By investigating the atomic structure of segregated GeSn by APT, Mukherjee *et al.* [134] observed that during annealing of GeSn – with step-graded increase in Sn content from 8 *at.%* to 18 *at.%* – there is a tendency of diffusing Sn atoms to accumulate at the cores of both at MDs [157] and TDs [133, 134]. This is rationalized in terms of larger space available for Sn atoms at the dislocation cores, which allows to decrease the lattice local strains. Fig. 5(b) shows a Sn-decorated TD, as reconstructed from APT in the work of Nicolas *et al.* [133]. The upward increase in Sn concentration in the TD core along the epitaxial growth direction allowed to confirm that TDs act as preferential pathways for Sn diffusion to the film surface, a mechanism referred to as *pipe diffusion* [134]. The Sn diffusion coefficient is estimated to increase up to 4 orders of magnitude in presence of linear defects [133, 157]. Moreover, Mukherjee *et al.* [134] observed that, for a short annealing time, while Sn was accumulating at dislocation cores, the GeSn film was pristine far from the core, with no sign of Sn clustering. This observation allowed to conclude that dislocations do not merely facilitate Sn segregation, but they also act as initiators of phase separation as a consequence of the local strain fields they induce around their core. Hence, Sn segregation is enhanced in presence of relaxation defects, also confirmed by systematic studies: Stanchu *et al.* [159] showed that Sn segregation increased with higher density of dislocations, while Bonino *et al.* [160] demonstrated an improved thermal stability by etching relaxation defects in microstructured GeSn, achieving stability of $\text{Ge}_{0.831}\text{Sn}_{0.169}$ for temperatures as high as 400°C. This thermal stability range is considerably higher than what observed by Zaumseil *et al.* for relaxed films of similar alloy compositions [157]. Finally, the presence of a GeSn surface oxide – formed by annealing GeSn in rough vacuum – has also been found to affect the Sn segregation behavior, inhibiting Sn out-diffusion and improving the material thermal stability [161].

The Sn segregation behavior during annealing of GeSn has been modeled by Groiss *et al.* [146]. The authors showed that, once a consistent amount of Sn atoms reach the surface, Sn atoms can easily nucleate liquid droplets. These droplets move on surface through a self-maintained segregation process, schematized in Fig. 5(c); Sn liquid droplets tend to dissolve the metastable GeSn film at their front, depositing a layer of Ge at their back with Sn concentration around the solubility limit as a result of solute supersaturation. Due to a better wetting of Sn on the GeSn film compared to Ge, the droplet tends to advance in the opposite direction from the Ge deposited layer, often along the $\langle 110 \rangle$ and $\langle 100 \rangle$ crystal orientations. The wetting behavior explains the motion of droplets on the surface of the GeSn film, which leave a trail of precipitated Ge at the back. This results in characteristic trails associated with β Sn segregation droplets on the surface of phase-separated GeSn films, visible in Fig. 5(a). Besides surface phenomena, upon annealing of (partially) relaxed films, Sn clustering has been observed

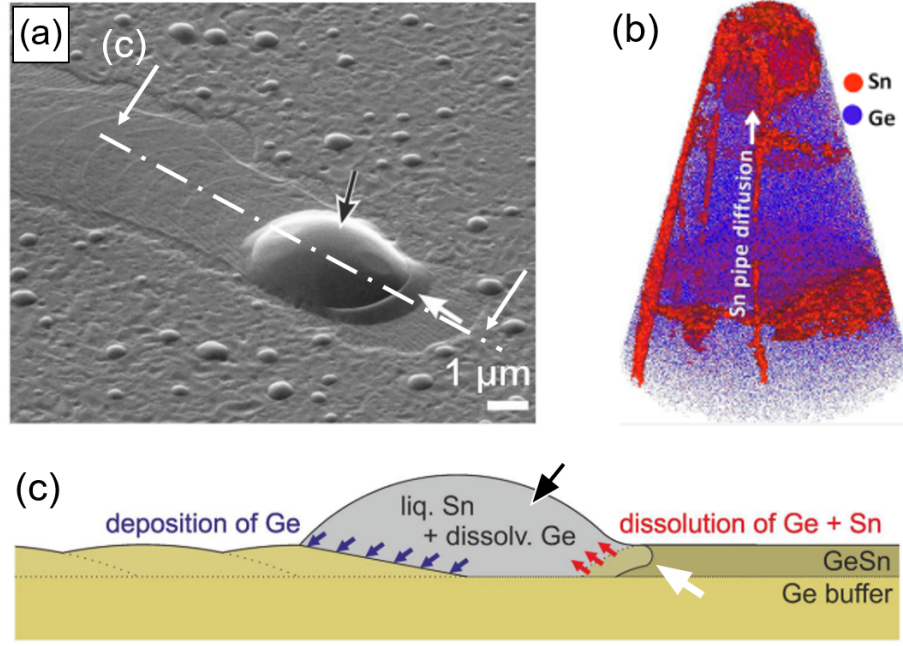


FIG. 5. (a) SEM image of a β Sn segregation droplet on the surface of a GeSn film. (b) Pipe diffusion of Sn along a dislocation core, as measured by APT. (c) Cross-section schematic view of a Sn droplet on surface. Figures (a,c) adapted from Ref. [146], under terms of the CC-BY license. Figure (b) reprinted with permission from Nicolas *et al.* [133], © 2020 American Chemical Society.

in the bulk [145] and at the film/substrate interface [157]. Bulk Sn clustering has been linked with large concentration of vacancies induced by the low-temperature growth of GeSn [157], while clustering at the interface occurs due to accumulation of Sn at the core of MDs [157].

In light of the above results, several studies tried to elucidate the interplay between alloy composition, strain relaxation and Sn segregation during annealing of GeSn. With in-situ annealing X-ray diffraction (XRD) studies, Zaumseil *et al.* [157] observed a gradual Sn out-diffusion with increasing temperature in RP-CVD-grown GeSn pseudomorphic films on fully relaxed vGe, with epitaxial strain progressively released through Sn diffusing out of the Ge matrix. On the other hand, partially relaxed films with Sn content from 5 *at.*% and 12 *at.*% showed further strain relaxation through elongation of MDs starting at approximately 300°C, followed by a “sudden” complete Sn segregation out of the Ge matrix when a higher critical temperature was reached [157]. This behavior was attributed to the activation of fast Sn pipe diffusion through TDs. In the study from Zaumseil *et al.* [157], the onset of vacancy-mediated Sn out-diffusion occurred at the same temperature in pseudomorphic and metamorphic $\text{Ge}_{0.95}\text{Sn}_{0.05}$ ($T \sim 500^\circ\text{C}$), but the segregation took place at a considerably higher rate in the former, indicating a strong driving force from the compressive strain of the film. Despite of these differences, it is interesting to notice that both samples reached the equilibrium Sn concentration of 1 *at.*% at approximately 650°C.

On the other hand, in metamorphic films with larger composition, the critical temperature for pipe diffusion was lower than the onset of vacancy-mediated diffusion, and therefore the latter was not observed prior to full Sn segregation. In agreement with Ref. [157], strain relaxation through solely Sn out-diffusion was also observed in Ref. [144] in pseudomorphic RP-CVD-grown GeSn with 6 *at.*% and 9 *at.*% Sn on fully relaxed on vGe, with no dislocation nucleation taking place. On the other hand, in MBE-grown $\text{Ge}_{0.92}\text{Sn}_{0.08}$, relaxation of pseudomorphic films was observed to occur first via dislocation formation up to temperatures of $\sim 550^\circ\text{C}$, and then also through Sn out-diffusion [145, 162]. Contrary to Ref. [157], no “sudden” segregation of Sn through pipe diffusion was observed, possibly due to the different experimental time scales in play (40-sec-rapid thermal annealing (RTA) in Ref. [162] and 5-min-RTA in Ref. [145], as opposed to 15–20 min for each 12.5°C step in *in situ* XRD in Ref. [157]). The different GeSn strain relaxation behavior may be due to the larger TDD in the thin Ge buffers employed – 210 nm in Ref. [145], 250 nm in Ref. [162] – which also partially relaxed upon annealing. In addition, to explain the discrepancies in the reported studies, the presence of vacancies generated by the low-temperature MBE growth may also have played a role in the relaxation-segregation behavior, favoring Sn diffusion, or conversely decreasing the metastable driving force for segregation due to local stabilization through the formation of Sn-vacancy complexes. Systematic studies with comparable time scales

are required to shed light on the role of point defects.

Until now we have discussed phase separation of the metastable GeSn alloy during post-deposition annealing (PDA) of the material. It is however important to make a distinction with the Sn segregation behavior during the growth process itself. While phase separation during PDA requires bulk Sn diffusion, during epitaxy Sn segregation can occur via adatom surface diffusion and nucleation of β Sn droplets. Surface adatom diffusion rates are considerably more elevated than Sn bulk diffusion, as the latter requires breaking of covalent bonds. As a result, the processing temperatures withstood by GeSn during growth are lower than the thermal stability after growth [134, 163]. Evidently, Sn segregation is also facilitated by larger Sn nominal fractions during growth as a result of the increased concentration of Sn adatoms and consequent larger β Sn nucleation probability [163]. On the contrary, increasing the growth rate of the film reduces the adatom diffusion length, hindering Sn segregation [164].

In conclusion, the described works illustrate the physics of Ge-Sn phase separation and its driving forces. The interplay between strain state of the material, defects, and alloy composition influences its thermal stability. During growth, the thermal stability of GeSn is decreased further.

V. EPITAXIAL GROWTH OF GESN, GE

In this section, we report the main advancements in epitaxy of GeSn, and the efforts towards higher incorporation of Sn in the alloy for MWIR and LWIR devices. Epitaxial growth by CVD and MBE methods has already been extensively reviewed [1, 52, 165–167]. We aim to complement these works by reviewing the studies of sputtering epitaxy of Ge and GeSn and their main findings.

A. Epitaxy of GeSn towards optoelectronic devices

GeSn must be grown epitaxially in monocrystalline form to obtain the desired optoelectronic properties in the material. For technologically relevant studies, GeSn growth is investigated on Si(100) substrates, with or without Ge buffer. To study pseudomorphic GeSn free of linear defects, GeSn is sometimes grown directly on Ge(001). Since the early studies on GeSn thin-film growth, researchers emphasized the need of out-of-equilibrium synthesis methods to prevent Sn segregation. Several epitaxial techniques have been thereby successfully reported with compositions up to 10 *at.%* Sn, mostly focusing on CVD and MBE growth as widely recognized standard epitaxial methods, reviewed in Refs. [1, 52, 165–167]. A handful of groups employed different techniques, including MS epitaxy [79, 168–171], solid-phase epitaxy (SPE) [172–175] and a few more exotic methods such

as liquid-phase epitaxy (LPE) [176, 177] and flash-lamp annealing (FLA) of Sn-implanted Ge [178]. The main focus of the more recent studies on GeSn epitaxy has been to improve the material crystal quality and push the Sn content to access the MWIR and LWIR wavelengths. Assuming a strain-free material, Sn fractions of ~ 16 *at.%* and ~ 26 *at.%* are respectively required to access these wavelength ranges [108]. However, GeSn crystal quality and thermal stability quickly degrade with increasing Sn fractions, posing major challenges to the synthesis and use of these materials in actual devices [1].

In Tab. II, the highest Sn compositions achieved in epitaxial, monocrystalline GeSn films are reported, together with a few representative films grown with more than 15 *at.%* Sn. A common strategy to maximize Sn incorporation avoiding segregation is the use of low substrate temperatures ($T < 150^\circ\text{C}$) in physical vapor deposition (PVD) growth processes [179–183]. High growth rates have been shown to provide the same benefits [184]. However, while low substrate temperatures prevent Sn segregation, the associated reduced adatom mobility is detrimental for the material crystal quality [185, 186] and limits the maximal epitaxial thicknesses due to kinetic roughening phenomena [36, 39]. The latter takes place at low temperatures due to the presence of a potential barrier at atomic terrace steps, termed *Erlich* barrier [187]. With low thermal energy available from the system, adatoms cannot overcome this potential barrier, and are forced to remain on their atomic plane. This leads to an unbalance of flux between atomic planes, and to increased nucleation of 2D islands on terraces, with consequent progressive 3D roughening and faceting of the film [36]. After a certain *critical thickness*, the film roughness prevents filling of trenches and the epitaxial growth breaks down, with the film growing first in highly defective [39] or polycrystalline fashion, and then purely amorphous [188]. In presence of Sn, the Ge adatom mobility and interlayer mass-transport (i.e., adatom up- or down-stepping at terraces) is increased [39], and therefore kinetic roughening is partially suppressed [39]. Nonetheless, with increasing Sn content, compressive strain increases in the film – on Ge and Si substrates – leading to a hybrid strain-roughening mode, where the reduced kinetics induce the surface oscillations necessary to allow strain relaxation through roughening [36]. Pure strain-induced roughening effects are normally observed at high temperature due to the large mass-transport involved [189]. Hybrid kinetic-strain roughening is exacerbated with larger Sn contents, as the compressive epitaxial strain increases in the film [39]. This poses a fundamental limit to the maximal epitaxial thickness at large Sn contents achievable at low growth temperatures. Evident from Tab. II, GeSn films with the highest compositions ever obtained are only a few-nm-thick. The epitaxial critical thickness is improved at higher growth temperatures, but these are limited in MBE by the increased tendency of segregation with higher Sn contents.

On the other hand, CVD growth can take place at

TABLE II. Summary of highest Sn fractions achieved in epitaxial, monocrystalline GeSn films. Acronyms: graded GeSn buffer (grGeSn), monolayer (ML).

Sn <i>at.</i> %	Growth method	Substrate	Thickness (nm)	Growth <i>T</i> (°C)	Ref.
35.4	UHV-CVD	Si(100)	49	220	Mircovich, 2021 [186]
34	Ar ⁺ MBE	Ge/Si(100)	20	150	He, 1996 [179]
30	UHV-CVD	Si(100)	40	245	Xu, 2019 [190]
28	MS	grGeSn/Ge(100)	20	100	Zheng, 2018 [180]
27	MBE	Ge(100)	120	100	Imbrenda, 2018 [181]
25	MBE	Si(100)	48	120	Oehme, 2014 [182]
22.3	RP-CVD	grGeSn/Ge/Si(100)	Few MLs ^a	200	Dou, 2018 [191]
18.3	MBE	Ge(100)	100	90	Hickey, 2017 [183]
18	LP-CVD	grGeSn/Ge/Si(100)	40	280	Assali, 2019 [192]
16	MBE	Ge/Si(100)	250	150	Rathore, 2021 [193]
15	UHV-CVD	Si(100)	245	285	Xu, 2019 [190]

^a The composition of this film is not uniform over its thickness. Only the top few MLs of the film showed the max Sn content of 22.3 *at.*% reported in the table.

higher deposition temperatures thanks to the different growth dynamics involving gaseous species. This has been the motivation since the early studies on CVD [48]. Common precursors are Ge and Sn hydrides/chlorides [52]. In CVD growth, Sn incorporation depends on the strain state of the film and increases for decreasing compressive strain, a phenomenon known as strain-relaxation enhancement of Sn incorporation [191, 192, 194]. This does not occur in MBE films [193]. Strain engineering is therefore key in maximizing Sn incorporation in CVD-grown GeSn [1]. Hence, graded GeSn buffers with progressively increasing Sn content have been proposed to gradually relax the film, preventing Sn segregation, to maximize the Sn content at the top of the GeSn stack [109, 141, 192, 195, 196]. On the other hand, other groups argued that growing directly on Si(100) allows for increased strain relaxation, and thus larger Sn incorporation in CVD [186] and lower strain-induced roughening, with consequent larger critical epitaxial thickness [182]. Recently, by growing directly on Si(100) and switching the Sn precursor from SnD₄ to SnH₄, Mircovich *et al.* [186] demonstrated a record 35.4 *at.*% Sn content in UHV-CVD 49-nm-thick GeSn.

Nevertheless, achieving the large compositions from Tab. II is not necessarily sufficient to access the MWIR (3 μm –8 μm) and LWIR wavelengths (8 μm –15 μm). In fact, the inherent compressive strain induced by epitaxial mismatch during growth on Ge or Si substrates causes a blue-shift in the GeSn film BG energy [55, 113, 197]. This implies that a compressive strained film requires higher Sn content to red-shift its BG to the desired energies. Strain engineering thus becomes essential in achieving full relaxation of the compressive strain to operate at

long wavelengths [186]. In addition, the crystal quality of GeSn is known to degrade with increasing Sn contents [57], complicating the realization of optoelectronic devices. For these reasons, while numerous GeSn-based optoelectronic devices have been demonstrated to operate in the SWIR wavelengths (1.4 μm –3.0 μm), only a handful of them could reach the MWIR [102, 198] despite the large Sn contents achieved in GeSn epitaxial films, as reported in Tab. II. The alloy compositions in the works reported in Tab. II are also in principle sufficient to access the LWIR; nevertheless, up to date, there exists a few studies of bandgap energy measurements [181, 190], but the fabrication of devices in the LWIR is lacking. Employing GeSn of such large Sn contents in actual devices remains an open challenge.

The element currently hindering the commercialization of GeSn-based devices is the material crystal quality. The main challenge remains the thorough understanding and management of linear and point defects in GeSn alloys. While the former can be avoided to some extent by engineering the growth processes, e.g., with (graded) buffer layers, the latter are poorly understood. In Sec. VI and VII, we review the research done towards the understanding of defect nucleation, and their influence on carrier trap states in the material.

B. State-of-Art of GeSn Sputtering Epitaxy

Despite its poor reputation for thin film epitaxy, magnetron sputtering (MS) may represent a plausible solution for industrial scale-up of GeSn. Compared to mainstream epitaxial methods such as MBE and CVD, MS tools are relatively simple, and they allow large growth

rates, film homogeneity over large substrates and the use of non-toxic Ge and Sn targets. An additional advantage related to MS growth of GeSn is that ion impingement enhances the incorporation of Sn adatoms via collisional mixing inhibiting segregation, as demonstrated in early works with ion-assisted MBE [29] and sputtering growth [27]. This allows to employ higher substrate temperatures compared to other PVD methods such as MBE, leading in principle to a lower concentration of point defects [199, 200]. Experimental verification is required to confirm this hypothesis. However, while CVD and MBE have been extensively studied for epitaxy of GeSn, MS was investigated only by a handful of groups [27, 46, 79, 168–171, 201, 202]. A summary of the works on sputtering epitaxy of GeSn is reported in Tab. III. Monocrystalline GeSn with Sn content up to 28 *at.*% has been demonstrated [180], among the highest Sn fractions observed in the literature with any growth technique. GeSn films are generally sputtered using Ar gas and substrate temperatures between 100°C and 300°C, which are higher than MBE, but lower than CVD. Macroscopic structural properties of the layers are well documented, with reported values of alloy composition, film roughness, and DSR. However, while structural characterization may give good indications of the promise of a material, it does not offer a full picture of its potential for use in optoelectronic devices. The latter is given exclusively by accurate optoelectronic characterization of the layer, currently lacking in the literature for sputtered epitaxial GeSn. Up to date, there has been only one report demonstrating direct-BG in Ge_{0.87}Sn_{0.13} grown on Si, Ge and GaAs substrates [201]. No study focused on the BG crossover composition. Room-temperature PL was shown in MS Ge_{0.97}Sn_{0.03} by Miao *et al.* [169], while Zheng *et al.* [203] are the sole to have demonstrated the use of MS GeSn in an optoelectronic device. They fabricated a *p-i-n* photodetector using Ge_{0.94}Sn_{0.06} as active material and showed performances comparable with devices realized with MBE or CVD at the time. Despite the promising results, no GeSn-based device made from MS has been reported ever since.

The poor reputation of MS epitaxy is likely owed to the association of the ion impingement occurring during deposition to the detrimental effects taking place during ion implantation processing, e.g. for material doping. In the latter, implanted species accelerated at energies of few keV are known to generate defects and even amorphization in the implanted layer [209]. However, energies of sputtered atoms impinging on surface during MS are considerably lower, of a few tens of eV [210, 211], and thus the interaction with the film is fundamentally different. With these kinetic energies, impinging atoms will only the surface layers of the film, inducing some atomic displacement [212]. It is true that ions from the working gas (i.e., Ar) neutralized and reflected at the target can possess higher energies up to a few hundred of eV [210, 211], but with appropriate cathode design the acceleration voltages at the target can be kept low enough

to limit the Ar energy to values similar to the sputtered atoms [210], limiting bombardment and implantation effects. Furthermore, being the growing film and substrate heated during growth, the thermal energy will allow for crystal reorganization and annihilation of the eventual defects caused by ion surface impingement. Aurret *et al.* [213, 214] showed that while Ar plasma exposure of Ge at room temperature generated some trap levels in Ge, no electrically active Ar-related defects could be observed in the material, and additionally all traps generated by the process were removed by annealing at 250°C. Hence, with growth temperatures well above 250°C and appropriate cathode design, MS should yield films free of ion-impingement-induced defects, though this conclusion should be experimentally verified for GeSn alloys.

From the works reported in Tab. III, the investigations of GeSn MS epitaxy have allowed to establish a few guidelines for optimization of the material crystal quality:

- **Substrate T:** As explained in the above paragraph, it should be kept as high as possible, avoiding Ge-Sn phase separation [168].
- **Sputtering gas:** H₂ is often added to the Ar sputtering gas, as reactive H species from the plasma are expected to passivate dangling bonds and prevent Sn segregation [208]. In MBE, the presence of H₂ during growth has been found to be beneficial in reducing adatom diffusion length [215, 216]. Via DFT-based calculations, Johll *et al.* [217] showed that hydrogenated epi-surface promotes Sn incorporation in the film, preventing Sn segregation. H₂ has also been found to induce strain relaxation in sputtered films [208].
- **Growth rate:** Large growth rates reduce adatom diffusion length, promoting Sn incorporation, hindering phase separation [168].

Systematic studies on the effect of gas pressure have not been reported, despite its role in determining the ion impingement energy through scattering mechanisms in the gas phase. Several other questions regarding GeSn MS epitaxy remain open. For example, contrasting observations have been reported regarding Sn distribution uniformity along the epitaxial thickness, with studies showing both uniform [204] and non-uniform [169] distributions. Both theoretical and experimental investigations in defect levels and electronic properties in sputtered GeSn are missing.

C. Ge Buffer Epitaxial Growth on Si Substrates

Epitaxial growth of Ge has been investigated for years, with well-established recipes for MBE and CVD methods [218]. As for the GeSn alloy, MS epitaxy of Ge has been investigated to a lesser extent.

TABLE III. Summary of monocrystalline GeSn films grown by the magnetron sputtering (MS) method, except for Ref. [27], where DC diode sputtering was employed. Acronyms: t_f , graded GeSn buffer (grGeSn), low-temperature GeSn buffer (LT-GeSn), GR, R_{rms} , SIMS, RF, HiPI.

Ref.	Comp. Sn at. %	Substrate	Growth T (°C)	t_f (nm)	Power (W) Ge Sn	Gas (mTorr)	p (nm/min)	GR R_{rms} (nm)	Claims
Lin, 2023 [202]	16.2	(grGeSn)/Ge(001)	259	60, 120	DC 51	DC 6.5	Ar	3.7 12	High DSR. Relaxation mechanisms w/o grGeSn buffer.
Tsukamoto, 2023 [204]	9	Ge(001)	215 – 250	70, 390	DC 70	DC 5	Ar + 5% H ₂	3 24	Uniform Sn profile, and limited diffusion in substr.
Huang, 2022 [171]	13	Ge/Si(001)	180 – 300	350	DC 140	RF 40	Ar	3 8.4	Highest x_{Sn} on Si(100) by sputtering.
Khelidj, 2021 [205]	~ 10	Ge/Si(001)	< 360	100	DC 150	DC 15	Ar	2.25 62.5	96-sec growth during cooling from 360°C. O, C contamination < $2 \cdot 10^{19} \text{ cm}^{-3}$.
Qian, 2020 [201]	~ 13	Ge(001)/Si(001)	-	330	RF 100	RF 20	Ar	3 5.5	Direct-BG demonstrated via OT and PL.
Dascalescu, 2020 [170]	~ 12.5	Ge/Si(001)	200 – 250	~ 120	HiPI	DC	Ar + 5% H ₂	3 1	First growth by HiPI sputtering. Polycryst. defects.
Tsukamoto, 2019 [206]	9	(LT-GeSn)/Si(001)	300	100	-	-	Ar + 5% H ₂	-	Low- T GeSn buffer allows to prevent Sn segregation. ~ 1.7
Yang, 2019 [207]	7	Ge(100)	160	400	RF 120	RF	Ar	3 12 – 30	TDD ~ 10^9 cm^{-2} .
Miao, 2018 [169]	< 3	Ge/Si(100)	160	400	RF 120	RF	Ar	3 12 – 30	SIMS shows non-uniform Sn distribution along thickness. Showed GeSn PL.
Zheng, 2018 [180]	20 28	grGeSn/Ge(100)	100 – 160	20	RF 70	RF 9–30	Ar	3 10 – 14.5	< 0.5 est x_{Sn} achieved by sputtering. Thermal stability of 350°C for Ge _{0.80} Sn _{0.20} .
Zheng, 2017 [208]	12	grGeSn/Ge(001)	140	140	-	-	Ar + H ₂ 0 – 40%	3 -	Sn uniform along z . H ₂ decreases Sn diff. length and helps strain relaxation.
Tsukamoto, 2015 [163]	8.5 11.5	Si(001)	250 – 300	100	DC	DC	Ar + 5% H ₂	- -	Sn segregation occurs more easily during growth.
Tsukamoto, 2015 [168]	≤ 11.5	Si(001)	200 – 300	100	DC	DC	Ar + 5% H ₂	- 25.2	< 1 High GR allows high gr. $T = i$ better cryst.
Zheng, 2014 [79]	≤ 6	Ge/Si(001)	150	450	RF 70	RF 5–15	Ar	3 ~ 10.2	- Thermal stability of 700°C for Ge _{0.975} Sn _{0.025} , 500°C for Ge _{0.94} Sn _{0.06} .
Pérez Ladr., 2003 [46]	≤ 14	Ge(001)	150 – 170	≤ 800	RF	-	Ar	- -	- People's model [131] describes well $t_{cr, GeSn}$ on Ge.
Shah, 1987 [27]	≤ 8	Ge(001) GaAs(001)	90 – 150	1000	DC	DC	Ar	25 12	First epi-GeSn. Absence of magnetron required substrate bias for low-energy ion bombardment.

Due to the large epitaxial mismatch of 4.2%, strain-induced roughening and islanding tend to occur during Ge heteroepitaxy on Si [36, 219]. Ge is therefore generally grown in a 2-step method, introduced by Colace *et al.* [220]. A first flat Ge layer is grown at low-temperature (LT) as the film relaxes the epitaxial strain. The LT serves to reduce the adatom mobility to hinder 3D growth. This layer is typically thinner than 100 nm, since $t_{cr,Ge}$ on Si is of the order of few nm [131, 221]. A second Ge layer is then grown to the desired final thickness at a high-temperature (HT) to maximize the crystal quality. Growth of the Ge buffer is followed by thermal annealing at T typically higher than 800°C to fully relax the film and reduce the TDD [218], as elucidated in the next section. Besides the reduced TDD, the annealing of the Ge buffer has an additional benefit for GeSn epitaxy. Thanks to the high temperatures used during annealing, after cooling, the Ge buffer will be left with $\sim 0.2\%$ tensile strain due to the differential thermal expansion coefficient (TEC) between the Ge film and the Si substrate [222]. The built tensile strain in Ge will provide a decrease in lattice mismatch for GeSn epitaxy, increasing the t_{cr} for strain relaxation and thus extending the thickness limits for GeSn pseudomorphic growth. It is important to avoid additional nucleation of relaxation defects during growth of GeSn to optimize the material performance in optoelectronic devices. The improvement is shown in t_{cr} with tensile strain is shown in Fig. 4(b), using People and Bean's model for GeSn grown on a vGe with 0.2% tensile strain, a typical value for annealed Ge on Si [222]. One should however note that relaxation of GeSn films on Ge-buffered Si may not follow closely the People and Bean's (P-B) model as a result of the presence of dislocations in the film threading from the buffer. The behavior may be better described by the Matthews and Blakeslee (M-B) model, which takes into account the presence of TDs in the film.

In the next paragraph, we briefly review the literature on Ge MS epitaxy summarized in Tab. IV. Surprisingly, no study reports the growth via a 2-step deposition, despite being well known to yield higher crystal quality. Monocrystalline Ge films on Si(100) have been achieved using both DC and RF power sources. With DC sputtering, root mean square roughness (R_{rms}) ~ 0.3 nm were obtained, optimal for the use of Ge as an epitaxial buffer layer. R_{rms} for sputtered Ge were noticeably better than for GeSn (see Tab. III) likely due to the higher Ge growth T that limits kinetic roughening. In a few studies, the resistivity of the Si substrate has been found to play a major role in achieving flat Ge layers [223, 224]. In particular, highly doped Si substrates, independently on their doping type, reduced Ge surface adatom mobility, preventing Si-Ge intermixing and strain-induced roughening at 350°C. This phenomenon is not yet well understood. A reduction in adatom mobility was also observed at high sputtering powers as a result of the increased growth rate [225], analogously to GeSn [168]. Zeng *et al.* [226] showed an

improvement in crystal quality with the application of a positive substrate bias to reduce ion bombardment by decelerating Ar^+ ions from the plasma. This work highlighted the importance of tuning the ion impingement energy, an aspect often overlooked. The annealing of sputtered Ge was demonstrated to reduce TDD [227–229] and annihilate stacking fault (SF)s [230]. A few studies reported also the electrical properties of the films, showing *p-type* unintentional doping concentration (n_{un}) of $10^{16} - 10^{17} \text{ cm}^{-3}$ [228, 231], and room-temperature hole mobility (μ_p) values of $1000 \text{ cm}^2/\text{Vs}$ [228], which are not too far from intrinsic bulk Ge μ_p of $\sim 1900 \text{ cm}^2/\text{Vs}$. These properties are in line with other epitaxial techniques, as discussed in Sec. VII.

VI. STRAIN RELAXATION MECHANISMS AND DEFECTS IN GESN, GE

For an extensive summary of the different types of dislocations in the group-IV FCC lattice, the reader is directed to the work from Arroyo Rojas Dasilva *et al.* [233]. It contains extensive explanations on the different types of extended defects in group-IV materials, and their visualization at transmission electron microscopy (TEM).

A. Strain Relaxation during Epitaxial Growth of Ge on Si(001)

In the following paragraphs, we give a brief review of the phenomena occurring during strain relaxation in epitaxial Ge growth on Si(001) substrates. Models of critical thickness of strain relaxation predict a t_{cr} of few nm for epitaxial growth of Ge on Si [131]. According to People and Bean's model [131], at $t_f = t_{cr}$ the elastic strain energy accumulated in the film due to misfit strain will match the energy necessary to nucleate new dislocations. 60° MDs nucleate on surface to plastically release the misfit strain and, driven by the misfit stress field, they glide down the $\{111\}$ planes via the formation of dislocation half-loops [234], represented schematically in Fig. 6(a). When a half-loop reaches the Ge/Si interface, it will form a misfit dislocation (MD) with Burger's vector (\mathbf{b}) along one of the $\langle 110 \rangle$ directions. The dislocation will thread to the surface via two segments of mostly screw character [234], the latter being known as threading dislocations (TDs). The Burger's circuit around a 60° MD dislocation core with $\mathbf{b} = a/2\langle 011 \rangle$ is shown in Fig. 6(b). Since \mathbf{b} has an in-plane edge component, the formation of a such MDs will contribute to the release of the epitaxial strain. On the other hand, due to their antiparallel \mathbf{b} , the TD pair does not release misfit strain [235]. However, TDs are electrically active, i.e., source of trap states, and are therefore undesired.

A representative XTEM image of a Ge epitaxial film on Si(001) along the $\langle 110 \rangle$ zone axis is shown in Fig. 6(c), with MDs and TDs indicated by arrows and lines, respec-

TABLE IV. Summary of monocrystalline Ge films grown by the magnetron sputtering (MS) method, except for Ref. [232], where RF diode sputtering was employed. Acronyms: GR pDC, CW, SF, n_{un} , GS-MBE.

Ref.	Growth T ($^{\circ}\text{C}$)	t_f (nm)	Power (W)	Gas (mTorr)	P	GR (nm/min)	R_{rms} (nm)	Claims
Zeng, 2021 [226]	600	450	RF 75–125	Ar + H ₂ 0–15%	1.2	-	0.58	Improved crystal quality and R_{rms} with positive substrate bias to reduce Ar ⁺ ion impingement energy. H ₂ enhanced relaxation.
Liu, 2018 [227]	400	100–200	RF	-	1.1	4	-	Reduction of 3 orders of magnitude in TDD upon CW laser annealing above $T_{m,Ge}$.
Otsuka, 2017 [230]	350	6	DC	Ar	2	17.4	0.39	RTA at 720 $^{\circ}\text{C}$ annihilates SFs in Ge film, though slightly degrading R_{rms} to 0.54 nm.
Tsukamoto, 2015 [225]	450	200	DC 100	Ar + 5%H ₂	3	20	0.23	TDD $\sim 2 \cdot 10^9 \text{ cm}^{-2}$. Higher sputtering power decreases adatom diffusion length, limiting islanding. Si-Ge interface intermixing observed at low power.
Yeh, 2014 [228]	< 360	1000	DC 100	Ar	2.5	126	-	Demonstrate TDD reduction with annealing at 800 $^{\circ}\text{C}$. μ_p improves to > 1000 cm ² /Vs; n_{un} decreases at LT, but increases at $T > \sim 150 \text{ K}$.
Tsukamoto, 2013 [224]	350	≤ 100	DC 10	Ar + 5%H ₂	3	2	0.3	B-doping of Si sub. has same effect as P in Ref. [223]. Doping type of sub. not important.
Steglich, 2013 [231]	380	120	DC 10	Ar	7.5	4.5	-	Oxide contamination on surface did not prevent epitaxy at 380 $^{\circ}$, but did at 320 $^{\circ}\text{C}$. Measured $n_{un}(300\text{K}) \sim 10^{17} \text{ cm}^{-3}$.
Hanafusa, 2012 [223]	350	≤ 60	DC	Ar + 5%H ₂	3	2.2	0.31	Si sub. P-doping reduces adatom diff. length, influencing Ge islanding and strain relxn. Si-Ge intermixing observed at low Si doping. Sub. doping has no effect in GS-MBE.
Pietralunga, 2009 [229]	170 370	100–200	pDC 550,800	Ar	13 17	4.5	~ 1	Unintentional p-type doping observed in Ge. RTA at 400 $^{\circ}\text{C}$ improved crystal quality.
Bajor, 1982 [232]	470	1500	RF	Ar	15	14.5	-	Strong Si-Ge interface intermixing, likely due to initial ion etching. $n_{un}(300\text{K}) \sim 10^{17} \text{ cm}^{-3}$, $\mu_p = 1280 \text{ cm}^2/\text{Vs}$

tively. Besides the aforementioned 60° MDs and TDs, at the Si-Ge interface we also find several 90° full edge dislocations with $\mathbf{b}=\pm a/2[1\bar{1}0]$ or $\mathbf{b}=\pm a/2[110]$, known as Lomer dislocations [234]. A 90° MD is imaged by XTEM in Fig. 6(d), with its Burger's circuit showing that \mathbf{b} lies in the (001) plane. Thanks to their full edge character, Lomer dislocations release twice the misfit strain of 60° MDs [236]. However, while 60° MDs are glissile as their slip plane [237] is the $\{111\}$ family, Lomer MDs are sessile as their slip plane is the (001) plane, which is not a close-packed slip plane of the FCC lattice. 90° MDs therefore cannot nucleate directly as half-loops on surface and glide to the Si/Ge interface [236]. At high processing temperatures, Lomer dislocations can move perpendicularly to their slip plane by *climb*, involving vacancy-assisted atomic diffusion, but this does not explain their presence at the Ge/Si interface at the growth T used for Ge epitaxy [234], since their *climbing* would require the presence of extremely large concentrations of vacancies. In fact, Lomer MDs have been found to be the result of the reaction

$$a/2[10\bar{1}] + a/2[011] = a/2[110] \quad (2)$$

which describes the recombination of two 60° MDs with parallel dislocation cores [234], shown in Fig. 6(f) after Ref. [234]. Perpendicular 60° MDs may also recombine into a Lomer MD, as schematized in Fig. 6(g) for specific combinations of \mathbf{b} [234].

The large occurrence of 90° MDs in epitaxial Ge on Si(001) has been explained by the fact that in high-misfit epitaxial systems the nucleation of a first 60° MD induces the nucleation of a second 60° MD in the near vicinity. In a 3-nm Ge film grown on Si(001) by CVD, Marzeggalli *et al.* [236] showed the formation of 60° MD pairs at the film interface in Fig. 6(e). They reported an occurrence of 88% of these pairs, with the remaining 12% being isolated 60° or 90° MDs, and they elucidated this phenomenon with dislocation dynamics simulations. They found that after a first MD has nucleated and glided to the interface, its strain field is felt at the film surface, and the surface nucleation of a *complementary* 60° MD becomes energetically favored. Its most likely position is off the gliding plane of the first 60° MD, explaining the large occurrence of the MD pair, with dislocation cores distanced by ~ 1 nm. On the other hand, nucleation of the complementary dislocation can statistically still occur in the mirror-like gliding plane of the *parent* MD, with consequent gliding and recombination into a Lomer MD. With high processing temperatures, e.g. during growth of the HT Ge layer in a 2-step process, or during annealing, the 60° MD pair can recombine via short-range climbing, explaining the predominance of Lomer dislocations observed at high processing temperatures [236]. The authors, however, point out that the experimental reports of statistics of Lomer MDs could be affected by the difficulty of discerning a 60° pair from a Lomer dislocation. In Fig. 6(e), they show that the Burger's vectors of a 60° MD pair and a Lomer MD are the same, and that the

two can be easily confused given the small distance between the dislocation cores in the 60° MD pair. Lastly, it should be mentioned that the elucidated mechanism of 60° -MD-induced nucleation is typical of only largely mismatched heteroepitaxial systems, such as the 4.2% of Ge on Si substrates. At low misfit ($< 1.5\%$ [240]), such as that of Si-rich SiGe grown on Si, the t_{cr} is too large for this phenomenon to occur; as the first 60° MD nucleates and glides to film/substrate interface, its strain field will not be felt at the surface. Hence, there will be no preferential nucleation of a complementary MD. In this system, Lomer dislocations are thus not observed after growth [234].

Stacking faults (SFs) has also been observed in epitaxial Ge on Si(001) in few-nm-thick films [215, 230], Ge islands [241], and growth on patterned substrates [242, 243]. The presence of SFs is due to the splitting of a 60° MD into two Shockley partial dislocations ($90^\circ + 30^\circ$) [233]. This process is driven by the reduction in energy associated with the MD self-energy, proportional to b^2 [35]. After dissociation of the 60° MD, the two partials split apart, connected by a SF, reaching an equilibrium distance determined by the interplay between the mutually exerted repulsive force from two partials, and the attractive force due to energetically unfavorable lengthening of the SF [35]. Of course, the misfit strain will also play a role in the stability of this dislocation complex. In particular, in compressively strained Ge films on Si(001), after a critical thickness of a few nm the two partials are expected to glide under the driving force of the misfit stress and recombine [244]. This explains the presence of SFs in thin Ge films on Si(001), and their absence in thick films. Alternative mechanisms of SF formation in few-monolayer-thick Ge films have been proposed [245]. After annealing, SFs have been found to disappear in thin films [215, 230] due to recombination of the partial dislocations into a MD.

As a result of the elucidated strain relaxation phenomena, the as-grown Ge epitaxial films on Si(001) will present numerous TDs and short segments of MDs at the Ge/Si interface, as shown in Fig. 6(c). In the ideal case, an array of regularly spaced Lomer dislocations with a pitch of ~ 9 nm with no TD is sufficient to fully relax the misfit strain of 4.2% [234, 246]. This configuration, however, cannot be achieved through spontaneous strain relaxation during epitaxy. At the onset of plastic relaxation, i.e., $t_f=t_{cr}$, 60° MDs will nucleate at stress concentrators, which consist in impurities or surface steps [235]. Their density will thus determine the initial TDD, typically of the order of 10^{11} – 10^{12} cm $^{-2}$ [234]. As the film grows, the TDs propagate in the new monolayers and, developing mostly in inclined directions with respect to the (001) growth plane, there is an increasingly high probability that they meet a neighboring TD as the film grows [235]. When two TDs with opposite components of \mathbf{b} come within each other's strain field, they can glide/climb under the effect of mutual elastic interactions. They can repel each other, or fuse/annihilate,

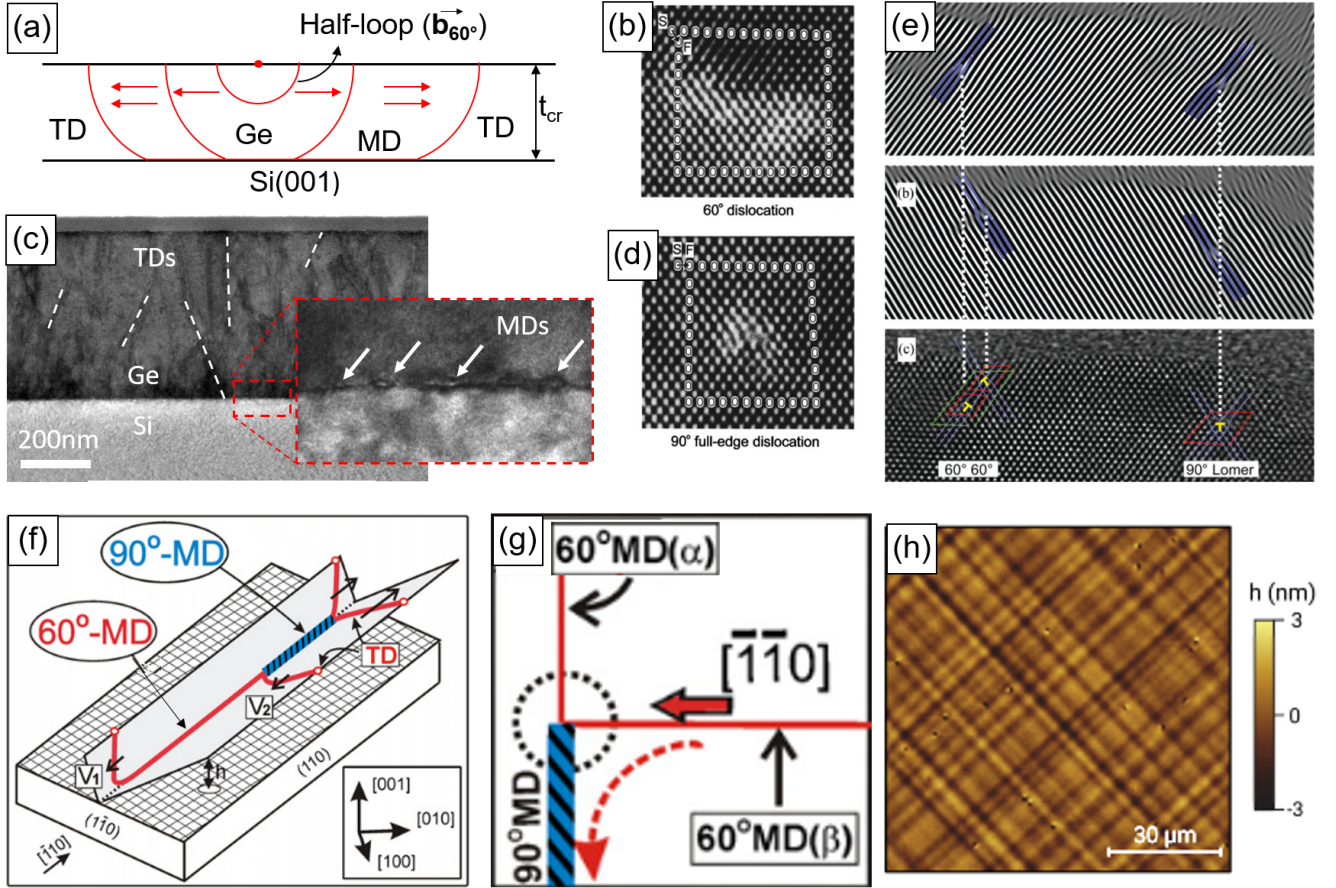


FIG. 6. (a) Schematics of 60° dislocation half-loops nucleating on surface at t_{cr} , and gliding to the Ge/Si interface to form a 60° MD + two screw TDs. (b, d) XTEM image parallel to the dislocation core (zone axis $\langle 110 \rangle$) of respectively a 60° and 90° MD showing their Burger's circuit and \mathbf{b} . (c) XTEM of an as-grown epitaxial Ge film on Si(001). (e) XTEM showing the subtle difference between a 90° MD and a pair of 60° MDs having the same \mathbf{b} . (f, g) Schematics of two 60° MDs with (f) parallel and (g) perpendicular dislocation cores recombining in one 90° MD. Figures (b, d) are adapted from Ref. [238] with permission from the authors, © 1997 AIP Publishing. (e) is reprinted with permission from Marzegalli *et al.* [236], © 2013 American Physical Society. (f, g) are adapted with permission from Bolkhovityanov *et al.* [234], © 2012 IOP Publishing. (h) is reprinted with permission from Rovaris *et al.* [239], © 2019 American Physical Society.

decreasing the average TDD in the film [247]. As a consequence, experimentally it is observed that the thicker the Ge film is grown, the lower its final TDD is [142]. For very large thicknesses of few μm , this geometric effect saturates due to the low TDD and consequent decrease in probability of interaction [248]. To reduce the final TDD without thermal processing, SiGe buffer layers may be introduced to act as dislocation filters, causing bending of existing TDs into MDs at the Ge/SiGe interface [248], and favoring nucleation of Lomer MDs over 60° MDs to relax more efficiently the misfit strain with lower MDs densities [234].

During growth of a Ge film, dislocations will tend to diffuse (i.e., glide or climb) under the effect of the resolved shear strain in their slip plane, in an Arrhenius-like thermally activated process [249]. In epitaxial Ge on Si, strain acting on dislocations is induced by the lattice mismatch, and by the interaction with other dislo-

cations, which may be of attractive or repulsive character. TDs glide by thermally activated motion of kinks along the threading segment [249]. TD pairs tend to move apart under the effect of misfit strain, elongating the associated MD core at the Ge/Si interface. They can remain blocked by the repulsive field of a perpendicular MD [250, 251], or by a parallel TD with opposite \mathbf{b} that causes cross-slip [234, 252]. Dislocations may thus remain pinned by the interactions with other dislocations, or also by point defects [142]. Depending on the growth temperature, kinetic barriers of dislocation diffusion may not be overcome, and the Ge film may be left with residual global – i.e., lattice mismatch – and local strains – i.e., dislocation-dislocation interactions – acting on dislocations. Annealing the film at high temperatures, typically $\geq 800^\circ\text{C}$, activates dislocation diffusion driven by the felt shear stresses. The resulting recombination of dislocations allows to improve the structural and elec-

trical properties of the material, and is thus essential in the absence of different strain engineering strategies. Effective strain relaxation in the film, may it be thanks to the high growth temperature or annealing, is recognized by cross-hatch surface roughness patterns, shown in Fig. 6(h). These patterns are associated with surface Ge adatom diffusion driven the strain induced by buried networks of elongated MDs at the Ge/Si interface [239]. In the following section, the dynamics of dislocations during annealing of Ge will be elucidated.

B. Annealing of Ge buffer

As elucidated in the previous section, as-grown epitaxial Ge films on Si(001) will contain several segments of MDs with their associated TDs, and possibly residual misfit strain. TDs additionally feel mutual stress fields from neighboring TDs, which can extend within a radius of 50 nm from their dislocation core [235], but their motion is hindered by the insufficient thermal energy to overcome kinetic diffusion barriers. Upon annealing, TDs glide and climb under the effect of global – i.e. misfit – and local – i.e. neighboring TDs – stress fields, pulling their associated MD segment behind. TD pairs will be pushed apart by the misfit stress, and the associated MDs will be elongated, resulting in the relaxation of misfit strain. As TDs feel the stress field from neighboring TDs, they may repel or attract each other, depending on their relative signs of \mathbf{b} . TDs can fuse into one TD, or fully annihilate if they have antiparallel \mathbf{b} . The film TDD will therefore decrease as a result of TD recombination, which can take place in 4 different modalities [235], illustrated in Fig. 7(a-d):

- (a) Dislocation loop self-annihilation, which can only occur upon reversal of film strain.
- (b) TDs on the same slip plane recombine by glide.
- (c) TDs on parallel slip planes recombine by glide+cross-slipping, or by climb.
- (d) TDs on non-parallel slip planes recombine by glide, climb, or a combination of the two.

Due to the inclined angle of TDs, their interaction probability increases with the film thickness. Wang *et al.* [143] constructed a simple thermodynamic model considering the energetics involved in reaction (b) to calculate the extent of TDD reduction in function of the Ge layer thickness. Their argument is that in absence of external stress, which is the case after the misfit stress is fully relaxed, the interaction energy has to be larger than the Peierls barrier –i.e. the energy barrier for dislocation glide– for TDs to move under the effect of mutual stress fields, independently on their attractive or repulsive interaction. Therefore, in their model, they calculate the *quasi-equilibrium* distance between two interacting

TDs dislocations by equating their interaction energy, dependent on the distance between 2 threading segments, to the TDs Peierls barrier. Their model, presented in Fig. 7(e), was found to describe well the experimental TDD measured in annealed Ge films on Si(001), with the average TDD scaling with the inverse square of the film thickness. They termed the so-calculated average TDD the *quasi-equilibrium* TDD, and not *equilibrium* TDD, as TDs are not an equilibrium defects that minimize the free energy of the system, and the history of the film processing can influence their final density. For example, micro-patterning of films is beneficial for achieving an improved TDD, as TDs can glide and annihilate at the edges of microstructures: In 10- μm mesas of Ge, Luan *et al.* [140] have demonstrated an order of magnitude improvement in TDD with respect to equally-thick Ge films. Additionally, also cyclic annealed Ge films are found to achieve lower TDD values than the quasi-equilibrium TDD [143], as discussed in the following paragraph.

In Tab. V, we report the results of a few experimental studies of annealing of Ge epitaxial films on Si(001). Ge is always annealed post-growth at $T \geq 800^\circ\text{C}$ for a few minutes. Terzieva *et al.* have shown that a higher annealing temperature of 850°C allows to achieve the quasi-equilibrium TDD with shorter annealing times [253]. On the other hand, temperature-swing annealing has been found to be a more effective process with respect to single-temperature annealing [140, 254], with the final TDD being potentially lower than the quasiequilibrium TDD. This is understood as an enhancement of TD diffusion – and probability of interaction – due to cycled compressive-tensile strains developing during cooling and warming owed to the differential TEC of the Ge film and Si substrate [255] [234]. However, as clearly visible from Tab. V, the high and low temperature limits in temperature-swing annealing are chosen arbitrarily, despite respectively having a major influence on the Si-Ge interdiffusion and dislocation glide velocity. Knowing that the activation energy for TD glide increases linearly with the Si fraction in SiGe [256], the Si-Ge intermixing occurring at excessively high annealing T may hinder the efficacy of the annealing process in reducing the TDD [143]. A systematic study on the effect of the high and low-temperature limits in cyclic annealing should yield the optimal temperatures to employ in the process.

Performing annealing steps during growth has also been found to be more effective in reducing the final TDD density with respect to post-growth annealing [254, 261]. This is because the annihilated TDs do not thread in the following grown layers, decreasing the amount of TD that has to recombine in the post-growth annealing step. This process has been observed to be more effective in Ge films with thickness $> 1\mu\text{m}$ [260], likely due to the saturation of geometric effect at the low TDD of thick films. Lastly, Nayfeh *et al.* [262] suggested that the presence of H_2 during annealing enhances Ge adatom mobility, enabling a decrease in surface roughness from 25 nm to ~ 3 nm. Their as-grown 200-nm-thick

TABLE V. Summary of a few works reporting Ge films annealing processes. Films are annealed after growth unless differently specified. Disclaimer: this table does **not report** an exhaustive list of all works on Ge annealed films.

Ref.	Growth method	Thick. (μm)	TDD (cm^{-2}) As-grown	TDD (cm^{-2}) After anneal.	Annealing process	Comments
Wei, 2020 [257]	MBE	0.5	$\sim 10^9$	$\sim 8 \cdot 10^7$	800°C	Same TDD obtained at 900°C, but with more Si-Ge intermixing.
Yamamoto, 2018 [254]	RP-CVD	1	-	$1.1 \cdot 10^7$	5 cycles: 750°C, 850°C 850°C cycles during growth	Annealing during growth yields lower TDD.
		5	-	$2.0 \cdot 10^6$		
		5	-	$1.3 \cdot 10^6$		
Yeh, 2014 [228]	MS	1	$2.6\text{--}40^6$	$\sim 40^4$	800°C (30 min)	Likely error in TDD measurements.
Tan, 2012 [258]	RP-CVD	0.98	-	$6 \cdot 10^6$	8 cycles: 825°C (10 min), 680°C (10 min)	
Shah, 2011 [259]	RP-CVD	0.76	$2.8 \cdot 10^8$	$4.6 \cdot 10^7$	830°C (10 min) in-situ	
		1.2	$1.7 \cdot 10^8$	$1.0 \cdot 10^7$		
Yamamoto, 2011 [260]	RP-CVD	1	$1.6 \cdot 10^9$	$6 \cdot 10^7$	800°C cycles during growth	Cyclic annealing only effective in films with $t > 1\mu\text{m}$
				$6 \cdot 10^7$	800°C post-growth	
		4.7	$4 \cdot 10^8$	$7 \cdot 10^5$	800°C cycles during growth	
				$8 \cdot 10^6$	800°C post-growth	
				$2.0 \cdot 10^7$	800°C (1 min)	
Terzieva, 2008 [253]	CVD			$1.5 \cdot 10^7$	800°C (3 min)	Higher annealing temperatures allow to reach quasi-equilibrium TDD faster.
		1.6	$1 \cdot 10^8$	$1.2 \cdot 10^7$	800°C (30 min)	
				$1.2 \cdot 10^7$	850°C (3 min)	
				$1.2 \cdot 10^7$	850°C (20 min)	
				$1.2 \cdot 10^7$	850°C (20 min)	
Choi, 2008 [261]	CVD	2.5	-	$5 \cdot 10^6$	Every 500 of film growth: 800°C (30 min)	Annealing during growth is more effective than same process after growth.
Hartmann, 2004 [246]	RP-CVD	0.73	$9 \cdot 10^8$	$< 2 \cdot 10^8$	10 cycles: 750°C (10 min), 875°C (10 min)	
		1.66	-	-		
Luan, 1999 [140]	CVD	1	$9.5 \cdot 10^8$	$2.3 \cdot 10^7$	10 cycles: 900°C (10 min), 780°C (10 min)	In 10- μm mesas, obtained TDD is $2.3 \cdot 10^6 \text{ cm}^{-2}$.

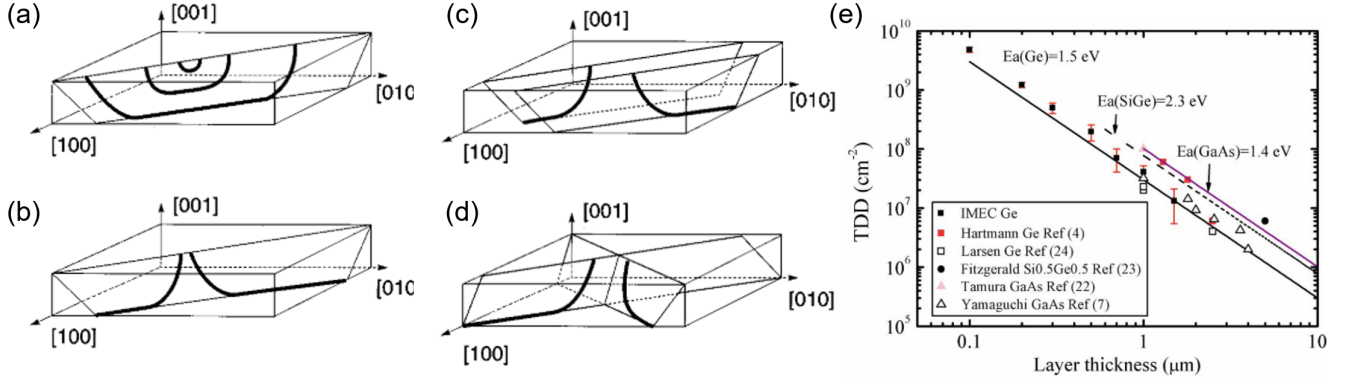


FIG. 7. Modes of TDs recombination: (a) Self-annihilation; (b) On same slip plane by glide; (c) On parallel slip planes by glide+cross-slip or climb; (d) Non-parallel slip planes by glide and/or climb. (e) Prediction of *quasi-equilibrium* TDD according to the model from Ref. [143]. Figures (a-d) reprinted with permission from Speck *et al.* [235], © 1996 AIP Publishing. Figure (e) reproduced with permission from Wang *et al.* [143], © 2009 AIP Publishing.

Ge films, however, had suboptimal R_{rms} levels. Annealing in H_2 has been observed to induce monolayer terracing in Ge(001) wafers [263], to reduce the roughness from 3.5 nm to 0.7 nm in Ge layers epitaxially overgrown on patterned Si substrates [264], and even to promote out-diffusion of oxygen impurities [265]. On the other hand, with ~ 1 nm R_{rms} in as-grown 150-nm-thick Ge, annealing in H_2 worsened the R_{rms} at $T > 650^\circ\text{C}$ [266]. Hartmann *et al.* [267] also observed the worsening of R_{rms} with increasing annealing time at 750°C in smooth 270-nm-thick Ge films on Si(001). In the same study, the authors showed that these annealing conditions had no effect on the roughness of 2.45- μm -thick films, which however considerably roughened with prolonged cyclic annealing between 750°C and 890°C . The data suggests that indeed H_2 enhances surface adatom mobility. This may be detrimental however when the film is under strain, e.g. with residual compressive strain in thin Ge epitaxial films, or in strain developed during cyclic annealing due to differential TEC, as strain-induced roughening mechanisms may lead to worsening of R_{rms} . Systematic studies of annealing with/without H_2 in (un)strained films would help clarifying the role of H_2 , often used during Ge annealing [228, 254, 258, 261].

After annealing and full strain relaxation of Ge on Si(001), arrays of regularly spaced MDs can be observed at the Ge/Si interface [228, 238, 257, 261], mainly of 90° character [234, 238, 257]. This is a consequence of the strain-driven diffusion of TDs, which causes the elongation of MDs segments for efficient misfit strain relaxation. The arrangement in regular spacing of MDs is instead owed to gliding of 60° and vacancy-mediated climbing of 90° MDs due to self-interactions [268]. A regular spacing between 9 nm and 10 nm is expected to fully release the Ge-Si misfit strain of 4.2% [234, 238, 246, 257]. The MD density will therefore increase as a result of annealing, which should be taken into consideration in case MDs are found to be electrically active. Currently, the electri-

cal activity of MDs is not understood.

C. Strain Relaxation during Epitaxial Growth of GeSn on Ge buffer

The strain relaxation behavior of GeSn on Ge is similar to that of Ge on Si due to the materials having the same crystal structures. There are however some differences due to the lower lattice mismatch of GeSn on Ge, and the metastability of GeSn at Sn contents larger than 1 *at.*%. As seen in Sec. IV, Sn out-diffusion in pseudomorphic GeSn films on Ge can in fact be a mechanism for strain relaxation [144, 157]. On the other hand, bulk Sn clustering has been ruled out to contribute to strain relaxation by APT studies [269]. Sn clustering is only driven by temperature increase due to the material metastability [269], and is enhanced in presence of linear defects [134, 270].

Wang *et al.* [132] demonstrated that GeSn relaxes on Ge(001) substrates following People and Bean's model for critical relaxation [131], in agreement with the critical thickness of strain relaxation (t_{cr}) reported in other studies where GeSn was grown by CVD [192], MBE [271], and MS [46]. Slightly lower values of t_{cr} were found in GeSn grown on Ge buffers [272], possibly due to the presence of TDs threading from the buffer during growth that reduce the nucleation energy of MDs [234], or due to different growth parameters (i.e., growth rate and T) [132]. On the other hand, Cai *et al.* [273] reported the MBE growth of GeSn on Ge(001) up to 9.7 *at.*% Sn significantly exceeding the t_{cr} predicted by the P-B model. The authors claimed this originated due to the low growth temperature of 150°C , though in strong contrast with the systematic study of Wang *et al.*, where GeSn films were deposited at the same growth rate and T . The results from Ref. [273] may in fact be affected by Sn-Ge intermixing, clearly visible by the asymmetry of the Bragg-Brentano

XRD curves of GeSn films with thickness larger than the t_{cr} predicted by the P-B model. Intermixing may arise from strain relaxation, and is known to occur in the Si-Ge system [168, 223, 274, 275]. Hence, the mechanism of strain relaxation in Ref. [273] may have been Sn-Ge intermixing rather than nucleation of MDs, explaining the observed t_{cr} exceeding the values predicted by the P-B model.

Upon relaxation of GeSn on Ge at $t_f = t_{cr}$, 60° half-loops will nucleate on surface [159, 192], gliding to the interface to form a network of MDs. The latter have been observed predominantly to be of 60° character [191, 202], in accordance with predictive models for low-misfit group-IV systems [234]. In contrast with the Ge-on-Si(001) system, after relaxation, SFs along the $\{111\}$ planes are often observed at the GeSn/Ge interface, extending in short segments across the interface [109, 191, 202, 276, 277]. Their origin is associated with two phenomena: (a) splitting of 60° MDs into the more energetically favorable Shockley partials, bound by a SF [191, 276], and (2) SF-bound Frank partial dislocations associated with vacancy complexes [191, 233]. The latter may be characteristic of the GeSn material system, where Sn-vacancy complexes are expected to form [165]. In addition, Dou *et al.* [191] observed the formation of full-edge Lomer dislocations from the reactions between Shockley and Frank partials. Relaxation by strain-induced roughening has also been observed [192].

In low-temperature growth ($T \sim 150^\circ\text{C}$), relaxation of GeSn on Ge occurs with slightly different mechanisms due to the limited thermal energy available in the system. In particular, in both MBE [132, 193, 278] and MS [208], it has been observed that only the upper part of GeSn films relaxes via the formation of dislocations, while the portion of the film close to the substrate remains fully strained. A model for this phenomenon was proposed by Wan *et al.* [278]. In their model, during growth of GeSn in kinetic roughening regime, surface roughness arises with the typical shape of mounds. Since surface roughness features can give rise to stress concentrators, facilitating dislocation nucleation, at $t = t_{cr}$, MD nucleation will be facilitated at the cusps formed between the mounds. Dislocations will propagate upwards as the film grows, while the downward propagation is believed to be hindered by the low temperatures [278], explaining the fully strained bottom region of the film.

Furthermore, the relaxation behavior of GeSn is affected by the layers beneath. For example, nucleation of MDs will be facilitated if the Ge buffer has a large TDD [234, 279]. In this situation, GeSn films are not expected to follow the P-B model for critical strain relaxation. On the other hand, on graded GeSn buffers, dislocations tend to be confined in the first layers, with limited propagation of TDs to the surface [191, 192, 280]. This is understood as the result of dislocation bending at the buffers interfaces, with resulting enhanced probability of interaction with dislocations with opposite components of \mathbf{b} [234] and due to Hagen-Strunk multiplication mech-

anisms that induce the nucleation of complementary 60° MD, with resulting formation of Lomer MDs [191, 192]. Lastly, large amounts of SFs have been found at the interface of GeSn with more than 20 *at.*% Sn grown directly on Si(001) [96, 186]. This is unexpected for such large compressive misfits [244], and may indicate different relaxation behaviors that remain to be understood to date.

Upon annealing GeSn films, strain relaxation may be activated in pseudomorphic or partially relaxed films. Experimental data suggests that MDs elongate during strain relaxation, but that no new MDs are formed [159]. In pseudomorphic films, strain relaxation takes place rather by Sn out-diffusion [144], although this behavior may be strongly composition-dependent [157, 273]. MDs may also nucleate from TDs present in the underlying Ge buffer [144, 165].

D. Point Defects in Ge

In pure intrinsic Ge, theory predicts a formation energy for monovacancy (V) defects of about 2.9 eV, which yields a practically null vacancy concentration at room temperature [281] [282]. Self-interstitials have even larger formation energies [282]. At room temperature, these defects are therefore absent in intrinsic Ge [283]. They can arise however from irradiation damage [284, 285], out-of-equilibrium growth processes [199, 200, 286–289], strain [153–155], and presence of impurities [290, 291]. Experimental studies of neutron-irradiated lightly n-doped Ge ($n_{sb} \sim 1.5 \cdot 10^{15} \text{ cm}^{-3}$) by positron annihilation spectroscopy (PAS) showed that Ge monovacancies are unstable above 65 K [292], as they tend to agglomerate into neutral divacancies [293]. Divacancies are stable at room temperature, and tend to agglomerate in larger-sized vacancy clusters after annealing at 200°C [291, 294], while negatively-charge divacancies are stable up to 400°C [284]. However, these defects disappear after annealing at 500°C [284, 295], indicating that after annealing of a Ge buffer for TDD reduction all intrinsic defects are expected to annihilate. Ge self-interstitials caused by irradiation also annihilate at $T > 150 \text{ K}$ [285]. Point defects remaining in the Ge buffer after annealing are therefore due to impurities present in the film, which may typically be H, N, O, C from the base vacuum pressure. In germanium, H sits in interstitial positions [296, 297], while N, O, C form stable vacancy complexes [298–304]. Their electrical activity will be reviewed in Sec. VII. Dopant elements, with the exception of B, also tend to form vacancy complexes that are more stable compared to Ge monovacancies [305]. On the other hand, the presence of Ar in the lattice is not expected to yield any electrically-active Ar-specific defect [306]. Surface defects due to Ar implantation are annealed at $T > 250^\circ\text{C}$ [213].

E. Point Defects & Sn Clustering in GeSn

When adding Sn to the Ge matrix, *ab-initio* calculations predict that Sn occupies preferentially substitutional positions in the lattice [307, 308], in agreement with experimental reports [309]. The fraction of Sn atoms occupying substitutional sites can be evaluated with Rutherford backscattering spectrometry (RBS) in channeling geometry, comparing the χ_{min} –i.e., ratio of aligned to random peak height– values of Ge and Sn [271]. With this technique, a full substitutional incorporation of Sn was found up to 14 *at.*% Sn in CVD [49, 310], MBE [311][312], and gas-source molecular beam epitaxy (GS-MBE) [97, 158]. Su *et al.* [311] measured a decrease in χ_{min} in MBE GeSn with increasing Sn content or decreasing growth temperature, indicating an worsening of crystal quality. Bhargava *et al.* [271] reported substitutional Sn fractions of at least 90% in MBE GeSn with 2.3–14.5 *at.*% Sn, with a decrease in substitutional fraction with increasing Sn content. Nonetheless, small deviations from full substitutional Sn occupations measured by RBS may in fact arise from measurement artifacts. To accommodate the local strain induced by Sn atoms in the Ge matrix, Ge-Sn bonds are distorted [100, 101], thus yielding reduced channeling in correspondence with Sn atoms even in a GeSn crystal with full Sn substitutional incorporation [97].

There is however an increase in point defect concentration associated with the presence of Sn in the Ge matrix, as Sn atoms act as vacancy sinks. Experimental studies of Sn-implanted Ge, backed by *ab initio* computations, demonstrated that Sn-V defects are more stable than isolated vacancies in Ge [105, 151, 298, 308]. Furthermore, due to opposite elastic fields, Sn-V pairs attract neighboring substitutional Sn atoms, favoring phase separation [313]. Intuitively, this can be understood as a vacancy accommodating local lattice strain induced by large Sn atoms in the Ge matrix [314]. The stability of Sn-V defects thus increases when $\text{Sn}_n\text{-V}_m$ complexes are formed [315]. Sn-V pairs arrange in split-configuration –i.e., Sn atom sitting at the bond-centered site– and are stable up to at least 400°C [308]. This suggests that it is not possible to annihilate them by heating GeSn if its Sn *at.*% is too large, as phase separation would likely occur first. As we will see in Sec. VII, Sn-V vacancy complexes are electrically active. It is therefore of primary importance to limit the amount of vacancies induced during growth, e.g., by low-temperature growth [286], excessive growth rate [287] and compressive strain [153–155], as they cannot be eliminated in post-growth processing. On the other hand, as the processing temperature is increased, the concentration of Sn-V pairs predicted by thermodynamics also increases [313]. This would suggest a trade-off between high-temperature CVD growth methods and low-temperature MBE is necessary for optimal optoelectronic properties of GeSn. The intermediate temperatures employed in MS GeSn epitaxy may turn out to be favorable in this sense. In this context,

an assessment of the electrical properties of MS GeSn is required.

Vacancies are difficult to observe in a material and, for this reason, there exists only a limited amount of studies of vacancy-related defects in epitaxially grown GeSn, which do not allow to draw final conclusions on optimal growth conditions of the material. PAS is the ideal technique to observe vacancy-related defects due to its versatility in measurement conditions and acceptable sensitivity range of $10^{15}\text{--}10^{19}\text{ cm}^{-3}$, depending on the charge state of the vacancy [316]. Assali *et al.* [317] studied thoroughly the presence of vacancies in 500–700-nm-thick relaxed GeSn with Sn contents of 6.5–13 *at.*% grown by low-pressure chemical vapor deposition (LP-CVD) at 330–300°C on νGe . With room-temperature PAS measurements, they observed the absence of monovacancies, and a predominance for divacancy complexes, with few higher-order vacancy clusters. On the other hand, in the Ge buffer they measured a predominance of vacancy clusters, attributed to the diffusion of (di)vacancies and clustering during high-temperature annealing of the material prior to GeSn growth. Interestingly, they also showed a decrease in vacancy clusters and concomitant increase in divacancies with increasing Sn fractions in the film, attributed to capturing of divacancies by the higher concentration of Sn atoms in the lattice. Slotte *et al.* [318] found somewhat contrasting results in PAS characterization of 400–500 nm GeSn with 6–12.6 *at.*% Sn (DSR \sim 70%). In a preliminary study, they observed a predominance of vacancy clusters over mono- or di-vacancies. The difference may arise from the growth conditions of the material, unspecified in Ref. [318]. Lastly, the PAS results from Kamiyama [319] in 200-nm-thick pseudomorph Ge(Sn) grown at 170°C by MBE on Ge substrates also hint at a higher vacancy concentration in $\text{Ge}_{0.983}\text{Sn}_{0.017}$ with respect to pure homoepitaxial Ge. On the other hand, they observed a lower positron lifetime –hence, vacancy concentration– with 0.1 *at.*% Sn, corroborated by electrical measurements, but they did not provide explanations of this result.

Another defect commonly observed in GeSn are few-atom-sized Sn clusters, considered to be the onset of phase separation in metastable GeSn. Atomistic calculations predict a repulsion between Sn substitutional defects in Ge [105, 313], which may explain the SRO recently experimentally observed by Lentz *et al.* [104]. Sn clusters are therefore expected to be stable only in the β -Sn phase. Sn clustering is favored by the presence of vacancies in the film, as Sn-V pairs attract neighboring substitutional Sn atoms [313], and is also favored by compressive strain [107]. Calculations from Chronopoulos *et al.* [315] predict $\text{Sn}_n\text{-V}_m$ complexes to be more stable with respect to simple Sn-V pairs. Experimentally, Sn clusters have been indirectly detected by APT in AP-CVD GeSn grown at 320°C with nominal Sn content of 5 *at.*% [112], where the authors deduced the presence of Sn_2V , Sn_3V , and Sn_4V_2 complexes. They also observed a higher concentration of these defects in a re-

laxed film, likely associated to solute segregation at dislocations [133, 134]. With successive investigations, the same research group concluded that Sn clustering is not involved in strain relaxation mechanisms, but it is rather driven by the material metastability [269]. Consistent with the tendency of Sn to segregate on surface, Liu *et al.* [107] found a higher concentration of Sn clusters towards the surface of their CVD $\text{Ge}_{0.86}\text{Sn}_{0.14}$ films. On the other hand, Rathore *et al.* [193] found no evidence of Sn clustering by APT in their MBE-grown $\text{Ge}_{0.84}\text{Sn}_{0.16}$ films up to thicknesses of 250 nm, suggesting that appropriate growth parameters allow to prevent Sn clustering.

The presence of Sn in the GeSn film has also been found to stabilize impurities. Sn-V pairs tend to attract impurities such as C [298], O [320], forming complexes that are more stable compared to impurity-V pairs. H/H₂ species have also been reported to interact with Sn-V complexes [321] while, to the best of our knowledge, no study has been reported on the behavior of N impurities in GeSn. Substitutional Sn atoms have been found to attract C [322] and repel O impurities [320]. Finally, due to the strong binding energy of Sn with vacancies, Sn-doping of Ge has been proposed as a method to prevent the formation dopant-V pairs that limit dopant activation in Ge [303, 323]. However, both As-V [323] and P-V pairs [303, 324–326] seem to be more stable than Sn-V pairs.

VII. OPTOELECTRONIC PROPERTIES OF GE & GESN

In this section, we review the work done to understand the optoelectronic properties of Ge and GeSn. We anticipate that the variety of the reported optoelectronic properties of GeSn thin films evidence a strong influence of the growth technique, parameters, and purity conditions. In order to control precisely the performance of a GeSn device, it is thus important to assess the experimental film properties, as they cannot be assumed from the literature.

A. Absorption Coefficient of GeSn

The optical properties of GeSn have been extensively investigated with both theory and experiments. Following the bandgap predictions reported in Sec. III, the absorption edge of GeSn shifts towards the infrared for increasing Sn content, as shown in Fig. 8(a) with experimental data plotted from Refs. [181, 190, 327]. MWIR wavelengths ($\sim 3\text{--}8\mu\text{m}$) can be accessed starting from 15/16 *at. %* Sn, while by extrapolation of the curves in Fig. 8(a) we can expect the absorption edge to reach the LWIR for $x_{\text{Sn}} > 0.3$. Fig. 8(b) shows experimental and theoretical values of GeSn absorption coefficient at $1.55\mu\text{m}$, wavelengths of interest e.g. for telecommunication and light detection and ranging (LiDAR) applications. The red, dashed line is a fit of theoretical absorption coefficient of unstrained GeSn from Ref. [328],[329] and serves as a guide to the eye. In spite of the considerable scattering in the data, the absorption coefficient grows visibly as the Sn fraction in the alloy increases. In addition, in Fig. 8(b), we report with a blue, dashed line, the absorption coefficient of $\text{In}_{0.53}\text{Ga}_{0.47}\text{As}$, the absorber material employed in commercial III-V technologies. Multiple experimental data suggests that a few *at. %* Sn in relaxed GeSn are sufficient to surpass the absorption coefficient of $\text{In}_{0.53}\text{Ga}_{0.47}\text{As}$, demonstrating the potential of GeSn for detector applications. On the other hand, in GeSn films the epitaxial compressive strain induces a blue-shift in bandgap energy, and is thus expected to limit the absorption coefficient. This effect however remains hidden by the large scattering in both experimental and computed data in Fig. 8(b). We conclude that a systematic analysis of the material absorption coefficient as a function of strain and material synthesis method is required to resolve the inconsistencies arising from the different experimental and computational methods employed.

B. Trap states in Ge & GeSn

Trap energy levels in the bandgap of an intrinsic semiconductor determine its electrical properties. Shallow trap levels act as acceptors/donors, releasing free carriers in the material – i.e., unintentional doping concentration – while deep trap levels induce SRH and TAT generation/recombination mechanisms, detrimental for device performance. The SRH recombination rate can be expressed as

$$R_{srh}(T) = \frac{pn - n_i^2}{\tau_{r,p} \left(n + N_C \cdot \exp\left(\frac{E_t - E_C}{kT}\right) \right) + \tau_{r,n} \left(p + N_V \cdot \exp\left(-\frac{E_t - E_V}{kT}\right) \right)} \quad (3)$$

where n_i the intrinsic material concentration, p (n) is the

hole (electron) concentration, $\tau_{r,p}$ ($\tau_{r,n}$) the hole (elec-

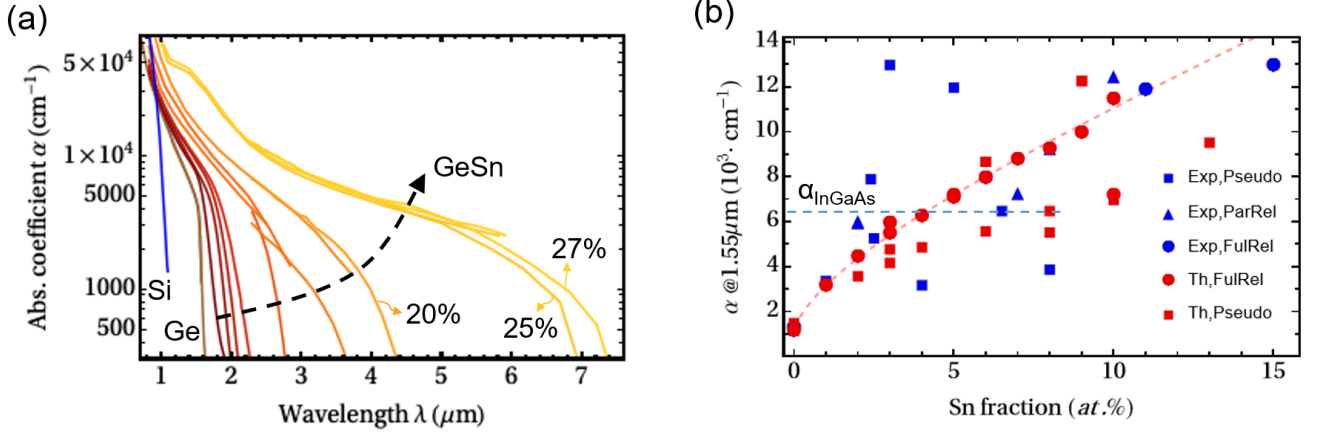


FIG. 8. (a) Shift of absorption edge in GeSn with increasing Sn *at.*%. Data plotted from Refs. [181, 190, 327]. (b) Absorption coefficient of GeSn at 1.55 μm plotted from both theoretical and experimental studies [41, 77, 330–340]. The blue, dashed line indicates the absorption coefficient of $\text{In}_{0.53}\text{Ga}_{0.47}\text{As}$ from Ref. [341], while the red, dashed line is a fit for the computed absorption coefficient of $\text{Ge}_{1-x}\text{Sn}_x$ from Ref. [328].

tron) lifetime, E_V (E_C) is the valence-band (conduction-band) energy, E_f is the Fermi energy, E_t is the trap energy level, k is the Boltzmann constant and T is the lattice temperature [130]. From eq. 3, one can deduce that SRH carrier generation has a strong dependence on temperature and on the trap energy level. Traps closer to the middle of the BG will facilitate SRH generation of carriers, as they will ensure the lowest possible rate-determining energetic barrier. TAT mechanisms have an analogous dependence on trap levels [342]. It is thus fundamental to review trap states that may arise from impurities and defects in intrinsic Ge and GeSn. There exist multiple studies reporting electronic levels in both materials, typically measured by deep-level transient spectroscopy (DLTS).

In Ge, electronic levels originating from defects and impurities have been partially reviewed in Refs. [130, 165, 343, 344]. Trap states observed in intrinsic Ge and GeSn are reported in Tab. VI. Intrinsic point defects in Ge are charged and in principle affect the material electrical properties. However, as discussed in Sec. VI, these defects annihilate at temperatures lower than those employed for Ge annealing [284, 285, 295]. Consequently, intrinsic Ge point defects are not expected to persist in the annealed Ge buffer layers. Threading dislocations generating from epitaxial strain relaxation are however electrically active. Due to the complexity of the system involved, to date electronic trap states in Ge have not been unambiguously assigned to the different linear defect types. In fact, while mid-gap trap states in Ge are beyond doubt associated with the presence of

TDs [135, 137, 343, 345, 346], a reduction in TDD does not always correspond to a proportional reduction in trap concentrations [347–349], clearly indicating the presence of other sources of deep traps [345]. Deep trap states can be generated by point defects, dislocations, and any combination thereof, substantially complicating the assignment of the measured trap levels to specific defects. A number of different mid-gap levels have been experimentally measured by DLTS, and reported in Tab. VI. It has been proposed in Ref. [346] that mid-gap traps arise from the interaction of dislocation cores with point-defect clouds [137, 346, 350], while clean TDs are expected to generate shallower levels, which may contribute to unintentional doping of the material. This remains however to be verified, since the referred works do not verify if dislocations are clean, or interacting with point defects [351, 352]. Studies in which the TDD is reduced by thermal annealing, such as those in Refs. [347, 348], may thus be influenced by the diffusion and clustering of point defects, which may explain the sub-proportional reduction in trap states with TDDs. The elongation of MDs upon annealing may additionally play a role in changing the electrical properties of annealed Ge. However, to the best of our knowledge, the investigation of the electrical activity of MDs in epitaxial Ge on Si has never been reported. Lastly, electronic states in the bandgap arise also from the interaction between dislocations [353] and from dangling bonds at grain boundaries [129, 346]. It is clear that further systematic studies backed by computational works are required to discern trap states induced by TDs, 60° MDs, 90° MDs, SFs and partial dislocations.

TABLE VI: Trap levels generated by defects in Ge and GeSn measured by DLTS, unless differently specified. This table was inspired from that of Ref. [165] and significantly expanded to include data for impurities and extended defects in Ge and GeSn. Used abbreviations: PD: point defect, D: dislocation, ED: extended defect (i.e. SF + partial Ds), GB: grain boundary, DB: dangling bonds BL: band-like states, int.: interface, rlx.: (partially) relaxed, str.: fully strained, vGe, Cz: Czochralski, e: electron, p: proton, n:neutron, γ : gamma-ray, SPC.

Defects		Activation energy (eV)		Sample condition
		Electron	Hole	
Point defects in Ge	Ge _i	0.11 ^f		e-irradiated Ge
	V ⁻ /0		0.02 ^{af}	Anneal+quench Cz-Ge
	V ⁻ -/-		0.26 ^{af}	Anneal+quench Cz-Ge
	V ₂	0.29 ^{ab,c} 0.31 ^{ac}		e ^{-ab} , n ^{-ab} , p ^{-c} irradiated, sputter- ^{ac} , e-beam-deposited ^{ad} Ge:Sb
	V ₂ ⁻ -/-		0.19 ^{ae}	p-irradiated Cz-Ge
	V ₃ ⁻ /0		0.08 ^{ae}	e-, p-irradiated Cz-Ge
	Small V cluster	0.1 ^{ab}		n-irradiated Ge:Sb
Linear defects in Ge	Decorated TDs		0.29 ^{k,l} , 0.25 ^l	vGe
	Clean? D		0.02 ^w , 0.10 ^w	D-rich pGe crystal
	Clean? D	0.09 ^w		D-rich nGe crystal
	D-related	0.3? ^m	0.16 ^m , 0.18 ^m	Relaxed Ge:B on Si
	D-V-related	0.28 ^o	0.18 ^o	Relaxed Ge on grSiGe/Si
	60°/90° partials	0.27 ⁿ	0.07 ⁿ , 0.19 ⁿ , 0.27 ⁿ	Plastically deformed Ge:Ga
DBs in Ge	DBs		Below VB ^{ak}	DFT calculations
	DBs at GB		0.05–0.10 ^{ai}	SPC poly-Ge*
	GB-related		0.32 ^k	poly-Ge
O in Ge	O _{Ge}	0.017, 0.04, 0.2		Unspecified, reported in Ref. [344]
	O ₄	0.017 ^d		Annealed O-rich Cz-Ge*
	VO ⁻ -/-	0.21 ^{a,aj} , 0.27 ^{c,aa}		γ ^{a,aj} -, p ^{c,aa} -, e ^{c,a} -irradiated Ge
	VO ⁻ /0		0.27 ^{a,aj}	γ ^{-a,aj} -, e ^{-a} irradiated O-rich Ge
	VO ₂ ⁻ -/-	0.195 ^b		e-irradiated O-rich Ge
	VO ₂ ⁻ /0	0.365 ^b		e-irradiated O-rich Ge
	O-related	0.14 ^c , 0.19 ^c		p-, e-irradiated O-rich n-Ge
	O-, H-related?		0.15 ^e	p-irradiated Ge:Sb
	I _{Ge} -O _{2i}	0.06 ^{f,aa} , 0.08 ^f		e ^{-f} , p ^{-aa} irradiated O-rich Ge:Sb ^f , Ge:P ^{aa}
C in Ge	C _{Ge}		Neutral ^q	
	V ₂ C ⁱ		Unknown	
H in Ge	H _i		Shallow acceptor/neutral ^r	p-irradiated Ge:Sb
	V ₂ H		0.07 ^q	γ-irradiated Ge
	HSi _{Ge} , HC _{Ge}		Shallow ^{p,q}	
	HO _i	Shallow ^{p,q}		
N in Ge	N _{Ge}	Shallow ^g		DFT calculations
	N _{2i}		Neutral ^g	DFT calculations
	V _n N _m ^j		Unknown	DFT calculations
Known defects in GeSn	Clean 60° ED		BL ≤ 0.15 ^s	Rlx. Ge _{0.922} Sn _{0.078} on Ge
	TD-related		BL 0.29 ^x	Str. Ge _{0.93} Sn _{0.07} on vGe
	VS ⁻ -/-		0.19 ^t , 0.14 ^{aa}	e ^t -, p ^{aa} -irradiated GeSn
	V ₂ Sn ^{ah}		Unknown	e-irradiated Ge:Sn [¶]
Unidentified defects in GeSn	Unassigned	0.12–0.14 ^{aa}	0.14 ^v , 0.075 ^v	Rlx. Ge _{0.9994} Sn _{0.0006} on nSi*
			0.08 ^{ag}	p-irr. rlx. GeSn(<i>x</i> _{Sn} < 0.1) on Si
				Rlx. Ge _{0.95} Sn _{0.05} on vGe [§]
	D-related?		≤ 0.05 ^u	Rlx. Ge _{0.94} Sn _{0.06} on pGe ⁺
			0.085–0.090 ^y	Rlx. GeSn(<i>x</i> _{Sn} ≤ 0.04) on vGe ⁺
	Sn-related PDs?	0.23 ^u , 0.27 ^u	0.14 ^y , 0.16 ^y	Str. GeSn(<i>x</i> _{Sn} ≤ 0.032) on nGe
	GeSn/Ge int.		0.20–0.25 ^z	Rlx. Ge _{0.962} Sn _{0.058} :B on nGe [‡]

*Measured by Hall effect, ⁺Measured by capacitance-voltage (CV), [§]Extracted from conductivity, [†]Measured by photoconductivity (PC), [‡]Simulated from I-V curves, [¶]Observed with Fourier-transform infrared (FTIR) spectroscopy.

References: ^a [301], ^b [354], ^c [355], ^d [356], ^e [357], ^f [285], ^g [358], ^h [359], ⁱ [298], ^j [300], ^k [346], ^l [360], ^m [349], ⁿ [361], ^o [350], ^p [362], ^q [363], ^r [364], ^s [276], ^t [324], ^u [365], ^v [366], ^w [351], ^x [367], ^y [136], ^z [368], ^{aa} [369], ^{ab} [370], ^{ac} [213], ^{ad} [371], ^{ae} [294], ^{af} [372], ^{ag} [373], ^{ah} [374], ^{ai} [129], ^{aj} [375], ^{ak} [282], ^{al} [344].

Additional sources of trap states in the bandgap are impurities introduced in the films during growth. Common impurities from background pressure in the growth chamber are O, C, N, H. In the following, we summarize the known trap states they can induce in pure Ge growth:

- **Oxygen impurity:** O occupies interstitial positions, but is electrically inactive [356]. On the other hand, upon annealing of O-rich Ge, O_4 clusters can form and lead to n-type doping of the material [356]. O also acts as vacancy sink, and O-V complexes have been found to induce both acceptor and donor deep levels in Ge [301, 355].
- **Carbon impurity:** C occupies neutral substitutional positions [362] and, due to its small size, the C_{Ge} defect has a structure similar to a Ge monovacancy [359]. It only weakly binds to vacancies, but it is stabilized by double vacancies [298]. It also tends to bind to and neutralize dopant-vacancy complexes, inactivating the dopant [376]. Despite its large contamination levels during epitaxy [377], trap levels induced by C complexes are seldom studied [283], and, to the best of our knowledge, there exists no information on their trap states. However, knowing that C is universally present in the base pressure, often due to the use of graphite heaters, it may be assumed that its contributions to the trap concentration in Ge are not dominant, since they have not been observed in experimental DLTS studies. There is data of C traps in Si, but the behavior of traps in Si and Ge is fundamentally different [283].
- **Hydrogen impurity:** Supported by experimental findings [364], first-principle calculations predict interstitial H^- impurities to behave as acceptors with shallow traps resonant or very close to the valence band (VB) [282, 296, 297]. In Ge, atomic H has been observed to induce shallow acceptor levels by forming complexes with isoelectric Si and C, and donor levels with O [362]. V_2H complexes instead induce shallow acceptor levels in pure Ge [363]. Contrary to Si, H does not passivate completely dangling bonds in Ge, with at best only 60% of the surface dangling bonds passivated upon annealing in H_2 [378]. On the other hand, it has been experimentally verified that H atomic species introduced from a H_2 plasma can passivate dislocations reducing their electrical activity in Ge [379]. The same effect was not observed in He plasma or simple annealing in H_2 atmosphere, demonstrating the passivation effect is induced by atomic diffusing H species generated by the plasma process. Dislocations act as sinks for vacancies and excess H [363], and therefore in vGe we can expect H impurities to be attracted by dislocations and passivate defects at dislocation cores. The effect of atomic hydrogen in sputtered Ge should thus be accurately evalu-

ated to see if it is negative or positive in terms of electrical properties.

- **Argon impurity:** The effect of Ar plasma or implantation was studied in Ge, and no Ar-specific trap levels were found [306, 380, 381]. All trap levels were induced by non-Ar-specific ion bombardment. This indicates that, as expected, Ar does not electrically interact with the material.
- **Nitrogen impurity:** Being from group-V in the periodic table of elements, N is expected to be a n-type dopant for Ge. However, N is a poor dopant [382] because it tends to form electrically inactive N interstitial pairs [358]. When in substitutional positions, N gives a shallow level close to the CB [358], although it has been suggested that it also gives rise to deep traps due to lattice distortions [382].

In low-Sn-content GeSn alloys, we can obviously find trap levels typical of pure Ge [383]. For example, intrinsic Ge point defects that are expected to annihilate during high-temperature annealing of the Ge buffer can instead be observed in GeSn, especially considering the low GeSn growth temperature compared to pure Ge. This may be the case of Ge divacancies, which have been reported to show mid-gap trap levels [213, 294, 370], and are expected to be stable up to 400°C [284], well above typical GeSn growth temperatures in PVD methods. As a consequence, vacancies forming in the film during growth will strongly affect the film electrical properties. The growth temperatures should therefore be maintained as high as possible to limit the formation of vacancies.

In addition to the Ge-related traps, in GeSn alloys there will be trap states induced by the presence of Sn in the material, which we summarize in the following. There exists several studies of defect levels arising in GeSn, but rarely the observed traps are unambiguously assigned to specific defects. Tab. VI reports the measured trap levels induced by the presence of Sn in the GeSn alloy. These are generally independent on the alloy composition [276, 365, 369]. Concerning point defects in GeSn, Markevich *et al.* [324] measured by DLTS hole trap levels 0.19 eV in electron-irradiated GeSn and assigned them to Sn-V complexes. Similar traps were measured in proton-irradiated GeSn [369]. As seen in Sec. VII, monovacancy complexes were not observed in as-grown GeSn epitaxial layers, as PAS characterisation showed that divacancies and larger complexes are present in significantly larger concentrations [317, 318]. Hence, we can deduce Sn-V complexes are annihilated at the temperatures employed for epitaxial growth. Sn-divacancies complexes have been observed in irradiated Sn-doped Ge [374, 384], but, to the best of our knowledge, their electrical levels have never been reported. In analogy with the SnV_2 defect in Si [385], we can expect SnV_2 complexes to introduce a deep level in Ge.

Dislocations present in GeSn will also affect its electrical properties. Besides the electronic levels known

to be induced in pure Ge, there have been reports of electronic trap states induced by dislocations in GeSn. Gupta *et al.* [276] studied by DLTS the trap levels in a $\text{Ge}_{0.922}\text{Sn}_{0.078}$ film grown by CVD on a n+Ge substrate. They observed band-like shallow acceptor defects with energies $\leq 0.15\text{ eV}$, and attributed them to clean extended defects (EDs) observed in proximity of the GeSn/Ge interface. These defects, consisting in SFs bound by Shockley partials, showed trap states similar to Shockley partials in pure Ge [361]. Despite the low activation energy of these EDs, the authors ruled out their role as acceptor dopants due to their small capture cross-sections, implying these defects act as donor-like repulsive centers. They further demonstrated that the EDs determined the SRH minority electron generation rate in GeSn, by analyzing the Arrhenius behavior of a pGeSn/nGe diode, where the GeSn was *p*-doped unintentionally. The presence of defects at the GeSn/Ge interface determining the dark currents of pGeSn/nGe diodes had already been supposed through simulations and fittings of the dark currents in an earlier work by the same authors, though the simulated trap levels yielded defects of 0.20–0.25 eV above the VB [368]. Kondratenko *et al.* [136] fitted PC curves to find activation energies of 85–90 meV above the VB, which they attributed to the large dislocation density in their CVD-grown relaxed GeSn ($x_{\text{Sn}} \leq 0.04$) films on vGe. On the other hand, in GeSn films with better structural properties – as measured by XRD – and larger Sn contents ($x_{\text{Sn}} > 0.04$) they found that dominant traps were placed at 0.14–0.16 meV above the VB. They suggested these traps were not related to dislocations, and tentatively associated them to SnV complexes [324, 369]. The latter trap level was also observed by Ryu *et al.* [366] with Hall measurements of CVD-grown relaxed $\text{Ge}_{0.9994}\text{Sn}_{0.0006}$ on nSi substrates. Furthermore, the authors reported the appearance of a *p*-type degenerate conductive layer at the GeSn/Si interface, attributing to the arrays of 90° MDs generated due to epitaxial strain relaxation. This result is in agreement with the decrease in lasing threshold observed when removing MDs in the active region of GeSn microdisks lasers [68].

In conclusion, the few studies reporting trap states of GeSn are mostly speculative, lacking unambiguous assignment of trap states to specific defects. The investigation of trap states in GeSn is still at its infant state, and more systematic studies are required to evaluate the influence of the epitaxial technique of choice, and of the employed growth parameters, which will ultimately determine the film electrical properties.

Lastly, it is important to mention possible defects arising from the atomic impingement of species from the plasma in plasma-based growth techniques, such as MS and plasma-enhanced chemical vapor deposition (PECVD). DLTS investigations of bulk Ge:Sb exposed to Ar plasma during sputtering have evidenced the absence of hole traps [214]. On the other hand, several electron traps were observed down to the first 400 nm

of the nGe crystal, mostly associated to Sb and Ge interstitial induced by Ar impingement. They reported only one intrinsic trap level — at 0.31 eV below the CB — tentatively attributed to Ge divacancies. All observed sputtering-induced defects were annihilated above 250°C [213, 214], suggesting the growth temperature should be above this value to prevent plasma-induced defects.

C. Unintentional Doping Concentration

Epitaxial GeSn alloys, including pure Ge, always show carrier concentration levels higher than the intrinsic values at room temperature, despite being nominally intrinsic. This charge carrier concentration is therefore termed *unintentional*, and originates from the presence of defects and impurities in the material. High levels of unintentional doping can be detrimental for the operation of diode devices. For example, they can increase the junction capacitance and decrease the frequency bandwidth of PDs [76], or induce breakdown in the GeSn absorber of eventual GeSn-on-Si SPADs [386]. Representative studies reporting unintentional doping levels in Ge and GeSn thin films are listed in Tab. VII. Carrier concentrations refer to majority holes at 300 K ($p_{300\text{K}}$) unless differently specified with the symbol “*n* =” inserted before the concentration values. In most cases, GeSn thin films show unintentional doping of type *p*, while pure Ge is reported possessing both *n*- and *p*-type unintentional doping.

In pure Ge films, unintentional doping concentrations in the 10^{16} cm^{-3} range can be achieved [198, 228, 257, 337, 369, 387]. To the best of our knowledge, a concentration in the 10^{15} cm^{-3} range was measured only by Roucka *et al.* [337], who reported $p_{300\text{K}} = 7 \cdot 10^{15}\text{ cm}^{-3}$ in Ge grown by GS-MBE. Unintentional doping in pure Ge is often attributed to the presence of multi-level vacancy complexes [165] or divacancies [317]. Considering the trap levels reported in the literature, summarized in Tab. VI, divacancies and vacancy clusters may effectively yield both *n*- and *p*-type doping. However, DLTS analysis of neutron- and proton-irradiated Ge [284, 295] showed that intrinsic vacancy defects in Ge annihilate completely at temperatures above 500°C. Hence, intrinsic Ge vacancies – or vacancy complexes – are not expected to be present in annealed Ge films and are unlikely to be the source of unintentional doping in the material. We thus discuss other possible sources of shallow traps that may lead to unintentional doping.

Clean dislocations have also been proposed as source of residual doping in Ge [346]. This may be in accordance with observations made in Ref. [228], by Yeh *et al.*, who measured the dependence of unintentional doping concentration on Ge film thickness, reported in Fig. 9(a). They observed a decrease in *p* with Ge film thickness, explained as a reduction in defect concentration. We believe there are two possible explanations for this behavior: (1) On the one hand, if we consider solely the film de-

fects, the TDD is well known to decrease with film thickness as a consequence of enhanced TD interaction due to the geometric effect [142]. On the other hand, there is no reason why the point defect concentration should change with film thickness if the growth conditions are kept constant. Hence, the results from Fig 9(a) would point at TDs contributing to unintentional p -type doping at room temperature. Tab. VI shows various trap levels measured in Ge and associated to the presence of TDs. (2) The decrease in apparent concentration with thickness can also be explained due to a fixed concentration of traps at the interface, e.g. MDs or impurities adsorbed on the substrate prior to film growth, whose contribution to the total amount of carriers in the film decreases with thickness, leading to an apparent decrease in film carrier concentration.

Annealing of Ge films has been reported to be beneficial for the material electrical properties. In particular, a reduction of unintentional doping and an improvement in mobility have been observed as a consequence of a decrease in defect concentration during annealing [228, 257]. Nevertheless, Hall measurements from 300 K to cryogenic temperatures revealed that the unintentional doping concentration does not decrease over the whole temperature range after annealing. Two examples are shown in Fig. 9(b-c). After annealing in vacuum a MBE Ge film, Wei *et al.* [257] measured a reduced carrier concentration across the entire temperature measurement range, shown in (b). However, a thermal treatment of 600°C allowed to obtain a lower unintentional doping levels compared to 800°C, except for room-temperature measurements, where p was equal. This suggests that shallow trap levels formed at higher processing temperatures, despite an overall reduction in defect concentration. On the same line, Yeh *et al.* [228], in (c), compared Hall measurements of MS Ge with and without thermal treatment (30 minutes at 700°C in $N_2+3.8\%H_2$). They observed a higher unintentional doping level after Ge annealing at 700°C between 300 K and ~ 150 K. On the other hand, at lower temperatures, the carrier concentration was strongly reduced with annealing. Hence, in this study, deeper trap levels, which contribute to unintentional doping at 300 K, formed during annealing, while shallower levels were annihilated during thermal processing, causing a decrease in unintentional doping at lower temperatures. The formation of deep trap levels after annealing cannot be associated to intrinsic point defects, nor TDs, since their concentration decreases with thermal processing. On the other hand, MDs elongate during annealing, and may be a source of deep traps. This could explain also the results in Fig. 7(b), where a higher density of MDs is expected following annealing at 800°C. In alternative, the increase in unintentional doping observed with annealing could also be associated to impurities. Indeed, the influence of impurities is mostly overlooked when trying to individuate the origin of the material unintentional doping. However, intrinsic defects in Ge, being V, V_2 , or larger clusters, may form

complexes with impurities that are stable at higher temperatures [324, 325] or may form during the annealing process through diffusion and recombination. In particular, Tab. VI shows that O- and H-related defects can be source of doping (n -type: $I_{Ge}-O_{2i}$, O_{Ge} , O_4 , HO_i . p -type: H_i , V_2H , HSi_{Ge} , HC_{Ge}). Trap levels associated with C and N complexes are unknown, but cannot be discarded a priori as source of doping. In addition, precise data on the thermal stability of these complexes is often lacking, complicating unambiguous individuation of the source of shallow traps. The different impurity levels, growth techniques and thermal processes of the grown Ge films can therefore explain the apparent inconsistencies found in the literature.

On a side note, it is interesting to observe the analogous temperature-dependence of p in as-grown MS and MBE Ge films in Figs. 7(b-c); as the films are cooled down from 300 K, the carrier concentration first decreases and, round 150 K p starts increasing again. It then saturates around 100 K, remaining unchanged as the film is further cooled down to $T < 20$ K. Yeh *et al.* explain the saturation behavior at low temperatures with the presence of an impurity band formed due to defects at energies approximately 20 meV above the VB, schematized in Fig. 7(c). This impurity band disappears upon annealing as a consequence of the reduction in defect concentration. From Tab. VI, plausible defects with trap energy of 20 meV are dislocations [351]. This is in line with the strong decrease in TDD occurring upon annealing. Monovacancies ($V^{-/0}$) also show the same trap level, but they are not expected to be stable above 65 K [292], and are thus to be excluded as possible source of this behavior[392].

In contrast to Ge, whose unintentional doping type is equally reported to be n - or p -type, GeSn alloys are predominantly reported to be p -type, as shown in Tab. VII. Typical room-temperature carrier concentrations are in the order of $10^{16}-10^{17} \text{ cm}^{-3}$. Concentrations in the order of 10^{15} cm^{-3} have never been reported to the best of our knowledge. The fact that GeSn is consistently reported to be p -type, with generally increasing p for higher Sn contents [198, 340, 369, 387, 390, 391], could suggest that there exists a Sn-related dominant acceptor trap that overshadows any other defect. This is often associated to Sn-vacancy complexes [198, 276, 387]. In agreement with this hypothesis, Kamiyama *et al.* [319] have observed a proportionality between vacancy concentration measured by PAS and hole doping in Ge and GeSn. However, the exact nature of this defect remains unknown: Sn-V pairs are expected to induce hole trap levels between 140 meV and 190 meV, as shown in Tab. VI, but PAS characterization of epitaxial GeSn revealed a predominance of divacancies and vacancy clusters [317, 318]. Sn_2-V [374] and higher order Sn_nV_m complexes [315] are thus more likely candidates, though their trap energies remain unknown to date. Alternatively, acceptor defects in GeSn may also arise from dislocations [136, 365], or their interaction with Sn, since most studies are performed on

TABLE VII. Unintentional doping concentrations in $\text{Ge}_{1-x}\text{Sn}_x$ thin films reported in the literature. Concentrations refer to holes (p), unless differently specified (n). Acronyms: amrp.: amorphous, CV and e-CV measurements, DLTS, SOI, VdP, GOI, PDA, R .

Ref.	Comp. Sn $at.\%$	Substrate	Growth method	Gr. T ($^{\circ}\text{C}$)	Thick. (nm)	$p_{300\text{ K}}$ (cm^{-3})	Meas. method	Comments
Mizoguchi, 2021 [388]	1.2–4.0	SiO_2	MBE amrp. + PDA + SPC	*	150	$> 5\text{E}17$	Hall VdP	*: 500–700 $^{\circ}\text{C}$ PDA for 2 h. Then SPC in N_2 at 400–650 $^{\circ}\text{C}$ for 40 h gave poly-GeSn.
Atalla, 2021 [198]	0–17	$\text{Ge}/\text{Si}(001)$	LP-CVD	-	120–160	Pure Ge: $7\text{E}16$ $x_{\text{Sn}} \geq 10.5\%$: $1\text{--}5\text{E}17$	CV	Increase in dark current in GeSn PD with larger Sn $at.\%$.
Hogsed, 2020 [369]	0–9.4	$\text{Si}(001)$	CVD	-	300–800	Pure Ge: $n = 5\text{E}16$ $x_{\text{Sn}} = 2\%$: $2\text{E}16$ $x_{\text{Sn}} = 9.4\%$: $2\text{E}17$	CV DLTS	Measured in pm devices. p increases with $at.\%$ Sn.
Tao, 2020 [340]	0–14	$\text{Ge}(001)$	MBE	200	30	Pure Ge: $n = 5.8\text{E}17$ $x_{\text{Sn}} = 4\%$: $n = 3.9\text{E}17$ $x_{\text{Sn}} = 8\%$: $n = 5.2\text{E}17$ $x_{\text{Sn}} = 14\%$: $n = 5.4\text{E}17$	Hall	Films reported partially relaxed, but MBE 30-nm-thick GeSn with $x_{\text{Sn}} \leq 8\text{ at.}\%$ is expected to be pseudomorphic on Ge [132]. Carriers are n-type also in GeSn.
Wei, 2020 [257]	0	$\text{Si}(001)$	MBE	200	500	As-grown Ge: $9\text{E}16$ PDA $\geq 500^{\circ}\text{C}$: $\sim 2\text{E}16$	Hall	$p_{<300\text{ K}}$ is higher with PDA of 800 $^{\circ}\text{C}$ compared to 600 $^{\circ}\text{C}$.
Julsgaard, 2020 [389]	12.5	$\text{Ge}/\text{Si}(001)$	CVD	-	350	$9\text{E}17$	e-CV	
Scajev, 2020 [373]	5	$\text{Ge}/\text{SiGe}/\text{Si}(001)$	MBE	150	200	$1.1\text{E}17$ $p_{200\text{ K}} = 6\text{E}16$	R	TDD $\sim 3 \cdot 10^6\text{ cm}^{-2}$. Hole activation energy of $80 \pm 10\text{ meV}$.
Gupta, 2018 [276]	7.8	$\text{Ge}(001)$	CVD	320	315	$2\text{E}16$	CV	GeSn is partially relaxed.
Schulte-Braucks, 2017 [390]	0–12.5	$\text{Ge}/\text{Si}(001)$	CVD	350	2500 768 835 414	Pure Ge: $4\text{E}17$ $x_{\text{Sn}} = 8.5\%$: $5\text{E}17$ $x_{\text{Sn}} = 10\%$: $1.5\text{E}18$ $x_{\text{Sn}} = 12.5\%$: $4\text{E}18$	Hall	Cooling down, $p_{200\text{ K}}$ lower by 1 order of magnitude in GeSn, and by 2.5 in Ge.
Asano, 2015 [216]	5	$\text{Ge}(001)$	MBE	150	55–70	$8\text{E}17$ no H_2 $1\text{E}17$ with H_2	CV	Growth in partial pressure of H_2 . Pseudomorphic films.
Kamiyama, 2014 [319]	0–1.7	GOI(001)	MBE	170	200	Pure Ge: $1.7\text{E}17$ $x_{\text{Sn}} = 0.1\%$: $2.4\text{E}16$ $x_{\text{Sn}} = 1.7\%$: $5.5\text{E}17$	Hall	Carrier type unspecified. PAS used to measured vacancy concentration in films, which matched p (n).
Oehme, 2014 [387]	0–4.2	$\text{Ge}/\text{Si}(001)$	MBE	160	300	Pure Ge: $\sim 1\text{E}16$ $x_{\text{Sn}} = 2\%$: $\sim 1\text{E}16$ $x_{\text{Sn}} = 4.2\%$: $\sim 1\text{E}17$	CV	Carrier type unspecified. Indirect measurements of conc. in $p\text{Ge-}i\text{GeSn-}n\text{Ge}$ PD.

Yeh, 2014 [228]	0	Si(001)	MS	< 360	1000	As-grown Ge: 5E16 PDA 700°C: 1.3E16	Hall	p_{200K} is higher in film annealed at 700°C.
Nakatsuka, 2013 [321]	0-2	SOI(001)	MBE	200	-	Pure Ge: ~ 1E18 $x_{Sn} = 0.01, 2\%$: ~ 1E18 $x_{Sn} = 0.1\%$: ~ 1E17	Hall	Anneal in H ₂ decreases p by one order of magnitude.
Ryu, 2012 [366]	0.06	Si(001)	UHV CVD	390 + RTA 680°C	800	1.4E16	Hall VdP	Degenerate p -type conductive layer at GeSn/Si interface due to MDs.
Roucka, 2011 [337]	0	Si(001)	GS-MBE	390	350 900	Pure Ge $n = 7E15-5E16$	Hall	
Nakatsuka, 2010 [391]	0-5.8	SOI(001)	MBE	200	160-170	> 7E17 as-grown 3E17 after PDA	Hall VdP	Anneal in N ₂ at 500°C for 60 min decreases p . Slight increase in p with Sn <i>at.</i> %.
Soref, 2006 [30]	2	-	CVD	-	-	5.6E16	Hall	PDA improved mobility and decreased p .

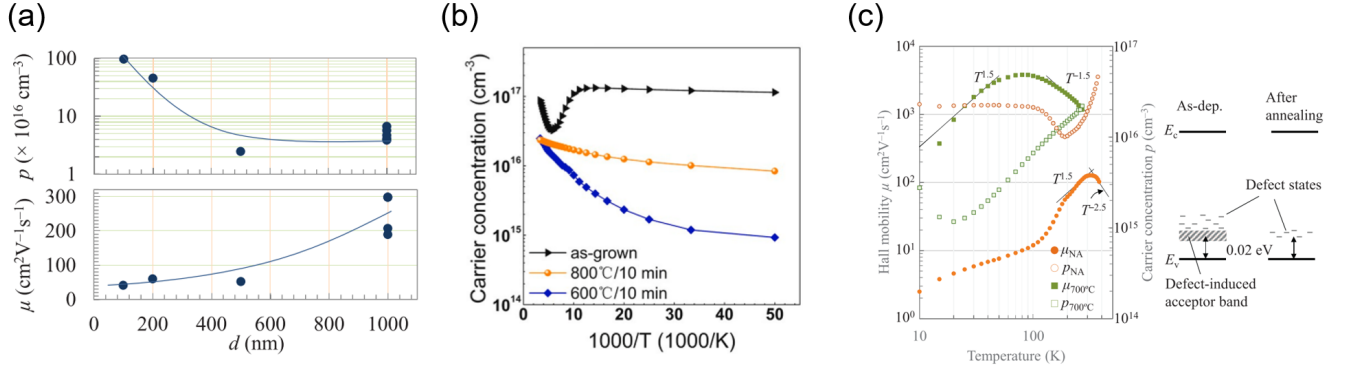


FIG. 9. Hall measurements of Ge films from (a,c) Ref. [228] and (b) [257]. More details of these studies are reported in Tab. VII. In both cases Ge is unintentionally doped *p*-type. Figures (a,c) reproduced from Ref. [228] under terms of the CC-BY license. Figure (b) with permission from Wei *et al.* [257], © 2020 Elsevier.

relaxed GeSn films. A systematic comparison of pseudomorphic and relaxed GeSn would shed light on the role of dislocations, though Asano *et al.* [216] reported high concentrations of *p*-type dopants in pseudomorphic GeSn, suggesting dislocations are not the source of *p*-type doping.

Ultimately, the growth conditions and impurity levels will govern the electronic trap states in the material and thus its unintentional doping concentration. The consistency in *p*-type doping in GeSn, as opposed to the inconsistency in majority carrier type observed in Ge, may also arise from the lower deposition temperature employed for the alloy. Higher growth temperatures have been reported to be beneficial to reduce the concentration of point defects in the film [199, 200], and thus in principle the unintentional doping. Nevertheless, a systematic study of the effect of temperature on *p* has not been performed to the best of our knowledge. The presence of H₂ gas in the growth atmosphere has been reported to be beneficial in reducing *p* by almost one order of magnitude, possibly due to point defect passivation from H species [216]. Post-deposition annealing (PDA) at 500–700°C was also seen to be beneficial in reducing *p* [30, 391], especially when performed in H₂ ambient [321]. This possibility is however limited with GeSn alloys possessing significant Sn fractions, as we reviewed in Sec. IV.

D. Carrier Lifetime

The free carrier lifetime is a key figure of merit of semiconductor materials employed in optoelectronic devices. It determines the device performance, affecting its noise and efficiency [70, 109, 373, 386, 393]. The term *lifetime* can refer to both carrier generation and recombination phenomena, and the relative importance depends on the type of optoelectronic device. For example, in optical detectors, the *generation* lifetime determines the rate at

which free carriers are generated in the reverse-biased depletion region in dark conditions. These *dark* carriers induce currents that affect the noise performance of the device [386, 393]. In this case, eq. 3 can be used to calculate the device dark currents, assuming generation is governed by SRH processes. Eq. 3, expressed in function of the recombination lifetimes (i.e., τ_r), can be simplified in function of the generation lifetime (τ_g) with $G \sim n_i/\tau_g$ [347], considering that $n_i^2 \gg pn$. The recombination and generation lifetimes are thus not equal, but are related via material's parameters [394], and it thus suffices to measure one of the two to know both.

The carrier lifetime is highly sensitive to electronic trap states in a semiconductor, and can thus be employed to assess its crystal quality. The recombination lifetime τ_r can be measured by injecting carriers in a material and monitoring their decay time with time-resolved measurements. In this setup, τ_r depends non-linearly on the excess carrier density (Δn), and can be decomposed in three contributions [394]:

$$1/\tau_r = 1/\tau_{SRH} + 1/\tau_{rad} + 1/\tau_{Auger} = A + B(\Delta n) + C(\Delta n)^2 \quad (4)$$

where A, B, C are material constants, and $\tau_{SRH}, \tau_{rad}, \tau_{Auger}$, are the SRH, radiative and Auger lifetimes, respectively. The latter becomes important only at high injection regimes, generally not employed when assessing carrier lifetime in thin films. In a highly-defective material, $\tau_{SRH} \ll \tau_{rad}$, and thus $\tau_r \sim \tau_{SRH}$. In this situation, τ_r and τ_g are related via [395]

$$\tau_g \simeq 2\tau_r \sqrt{\sigma_n/\sigma_p} \cosh[(E_T - E_g/2)/kT] \quad (5)$$

where σ_n (σ_p) is the electron (hole) capture cross-section of a trap with energy E_T [394].

Tab. VII summarizes carrier lifetimes reported for Ge and GeSn films in the literature. In Ge crystals, bulk recombination lifetimes ($\tau_{r,B}$) have been measured to be between 100 μ s and 5000 μ s [396, 397]. These values are

however far from the reported carrier lifetimes in Ge films grown on Si substrates, which are of only a few ns [398–400]. This is attributed to the large density of dislocations generated by epitaxial relaxation phenomena, and to the presence of a surface and an interface in the vicinity of injected carriers [401]. In thin films, carriers can in fact diffuse and recombine at surface traps with a non-negligible contribution to the overall carrier recombination time. The measured effective carrier lifetime can thus be decomposed in two separate contributions [396]:

$$\tau_r = \left[\frac{1}{\tau_{r,B}} + \frac{1}{\tau_{r,S} + \tau_D} \right]^{-1} \quad (6)$$

where $\tau_{r,S} = d_{eff}/v_{r,S}$ is the surface recombination lifetime, and $\tau_D = d_{eff}/(\pi^2 D)$ is the carrier diffusion time. $v_{r,S}$ is the surface recombination velocity, D the carrier diffusion coefficient, and d_{eff} the effective probed depth of the material. τ_D takes into account the loss of carriers due to diffusion out of the probed region, and can be mostly neglected with the low $\tau_{r,B}$ measured in epitaxial Ge and GeSn thin films. $\tau_{r,B}$ is a proper figure of merit of material quality, while $\tau_{r,S}$ is indicative of the presence of trap states at the film surface or at the film/substrate interface. $\tau_{r,S}$ is also sensitive to surface roughness [402]. In configurations where $\tau_{r,S}$ is comparable to $\tau_{r,B}$, the resulting measurements of τ_r are strongly affected by the film thickness, as carriers can diffuse and recombine at the interfaces. Thicker films will be less sensitive to $\tau_{r,S}$, yielding longer recombination lifetimes. This situation is typical of few- μm -thick Ge films grown and annealed on Si substrates, as dislocations remain confined near the interface after a PDA process [142]. To properly account for the effect of this defective interface on τ_r , eq. 6 can be fitted over τ_r measured at different film thicknesses – i.e., d_{eff} – [399]. This yields an effective $\tau_{r,S}$ that describes the recombination rate at the defective epitaxial interface or film surface [403]. Doing so, Ge bulk lifetimes ($\tau_{r,B}$) from few ns [398] up to 11 ns [399] were reported, with recombination velocities ($v_{r,S}$) of tens of m/s at the Si/Ge interface. An exceptional $\tau_{r,B} = 91$ ns was measured by Kako *et al.* [403], possibly due to a low TDD in the film owed to its large thickness $> 3 \mu\text{m}$.

For GeSn thin films, recombination lifetimes are even lower than in Ge. Measurements of τ_r in GeSn have been reported in a handful of studies, summarized in Tab. VII. Direct measurements of carrier lifetime in pseudomorphic GeSn on vGe yielded $\tau_{r,300K}$ from a few hundreds of ps [4, 373, 389, 405, 407] to 1–2 ns [404–406]. Considerably larger $\tau_{r,300K}$ of tens of ns was measured by μW -PCD in a study by Hudait *et al.* [402] on GeSn grown pseudomorphic (or lattice matched) [410] on III-V-buffered GaAs substrates, possibly due to the absence of dislocations in the film. While in studies concerning pure Ge the surface and bulk recombination rates are often distinguished through fitting of eq. 6 measured in films with different thickness, this is not the case for GeSn, as typically only the effective τ_r is reported. This value is thus dependent on the film thickness in few-hundred-

nm-thick GeSn films, as confirmed in Refs [109, 402]. In addition, Rogowicz *et al.* [404] showed that measured PL lifetimes of a few hundred of ps are consistent with surface-recombination phenomena, rather than the film bulk properties. With TRDR measurements of various GeSn films with different compositions, they consistently observed two different decay lifetimes, attributed to surface and SRH bulk recombination processes. TRPLS measurements of the same samples yielded PL lifetimes matching almost perfectly the fast TRDR decay owed to surface processes. Their work highlighted the importance to decompose the bulk and surface lifetimes to accurately evaluate material performance.

From the measurements of carrier lifetime in Ge and GeSn thin films we can draw a few conclusions. A clear correlation between the TDD and τ_r has been observed in multiple works [109, 347, 399, 402, 405]. Vitiello *et al.* [405] measured τ_r in $\text{Ge}_{0.92}\text{Sn}_{0.08}$ films with constant composition and different TDD. They observed a linearly proportional decrease in τ_r , and could estimate a recombination velocity at TD lines of $(1.77 \pm 0.03) \cdot 10^5$ cm/s, which is 2- to 10-fold higher than $v_{r,S}$ at Si/Ge interfaces. A clear proportionality between TDD and τ_r in this study was enabled by controlling the TDD in the films through their thickness and resulting DSR. On the other hand, Gonzalez *et al.* [347] found that a decrease in TDD obtained through high-temperature PDA processing of the film led to a subproportional increase in lifetime, indicating that at high-temperature processing other defect reactions influence the trap concentration, and thus the carrier lifetime. This is in line with the investigations of unintentional doping concentrations in annealed films discussed in the previous section.

The GeSn alloy composition has also been found to influence carrier recombination lifetimes. A few studies reported that τ_r decreases with increasing Sn content in the alloy [404, 405, 407]. In particular, a large difference in carrier lifetime was observed between pure Ge and GeSn alloy films. A 10-fold decrease in τ_r was measured between a Ge buffer layer and a pseudomorphic GeSn film grown on the buffer itself [407]. Since the TDD should be the same in the two materials, one can speculate the resulting lower τ_r in GeSn is owed to the increased concentration of vacancies that induce mid-gap traps, enhancing SRH recombination processes. As elucidated in the previous sections, vacancies are expected in considerably lower concentrations in pure Ge as a consequence of the higher growth temperature and PDA processes of Ge films. Lowering the growth temperature has been demonstrated to decrease the lifetime in GeSn [402]. Furthermore, the concentration of vacancies is known to increase with increasing Sn content [317, 319], explaining the observed trends in τ_r with alloy composition.

To conclude, the measured recombination lifetimes in GeSn films are always attributed to SRH or surface recombination phenomena. In GeSn, τ_r measures a few ns in the best cases, which is considerably smaller than its computed radiative recombination lifetimes [411]. From

TABLE VII. Carrier lifetimes reported in the literature. Introduced acronyms: surface recombination velocity ($v_{r,s}$), bulk and surface recombination lifetimes ($\tau_{r,B}$, $\tau_{r,s}$), PECVD, LITG, EL, μ W-PCD, TRDR, TRPLS IR broadband pump-probe differential transmission measurements ($\Delta T/T(t)$), IC-PCD.

Ref.	Comp. Sn <i>at.</i> %	Substrate	Growth method	Gr. T (°C)	Thick. (nm)	τ_r (ns)	τ meas. method	Comments
Hudait, 2022 [402]	0-6	III-V buf./ GaAs	MBE	175- -250	50-600	@300 K: 90-470	μ W-PCD	GeSn lattice matched or pseudomorphic. $\tau_r = \tau_{SRH}$, increased with higher gr. T or lower R_{rms} . $\tau_{r,s}$ not properly considered.
Rogowicz, 2021 [404]	6-12	Ge/Si(001)	RP-CVD	-	36-60	$\tau_{r,B}$ @300 K: 1.5 with 6 <i>at.</i> % Sn, 1.2 with 11 <i>at.</i> % Sn. $\tau_{r,s}$ @300 K: 0.7-0.5	TRPLS TRDR	Pseudomorphic GeSn. Slightly longer lifetimes with less Sn. Report T-dependence of $\tau_{r,B}$ and $\tau_{r,s}$.
Julsgaard, 2020 [389]	12.5	Ge/Si(001)	CVD	-	350	0.22 @20 K Same @300 K	TRPLS	Claim $\tau_r = \tau_{SRH}$. Modest variation with measurement T.
Scajev, 2020 [373]	5	Ge/SiGe/ /Si(001)	MBE	150	200	0.05-0.15 @ 50-350 K	LITG	Pseudomorphic GeSn, with TDD $\sim 3\text{E6 cm}^{-2}$ inherited from buffers. At 300 K, $\tau_h > \tau_e$. Measured diffusion length of 450 nm.
Vitiello, 2020 [405]	2-10	Ge/Si(001)	RP-CVD	200- -300	150 45 35 70 40 40	@10 K: 2 <i>at.</i> % Sn: 0.70 3 <i>at.</i> % Sn: 0.75 4 <i>at.</i> % Sn: 0.90 6 <i>at.</i> % Sn: 2.5 8 <i>at.</i> % Sn: 0.65 10 <i>at.</i> % Sn: 0.4	Hanle effect	GeSn pseudomorphic on 600-nm-thick Ge buffer. Claim $\tau_r = \tau_{SRH}$. Not a clear trend on alloy composition, justified with different growth conditions. Observed a proportional decrease in τ_r with TDD.
De Cesari, 2019 [406]	5	Ge/Si(001)	RP-CVD	280	70	1.1 @300 K 0.9 @210 K	TRPLS	GeSn pseudomorphic on 650-nm-thick Ge buffer. Traps at 13 meV and 17 meV above Fermi level.
Geiger, 2016 [407]	0-12.5	Ge/Si(001)	RP-CVD	350- -390	2700 800 560	@300 K: Pure Ge buffer: 2.6 8.5%-0.47(0.43@20K) 12.5%:0.26(0.17@25K)	IR $\Delta T/T(t)$	Ge buffer underwent PDA. τ_r slightly decreases at ~ 20 K compared to 300 K. Pure Ge shows 10-fold longer τ_r compared to GeSn.
Wirths, 2015 [4]	8-13	Ge/Si(001)	RP-CVD	350- -390	200-560	0.35 @300 K 2.1 @15 K	Indirect	τ_r extracted from PL measurements. Fit SRH temperature behavior of τ_r and obtain $E_t - E_F = 19$ meV.
Gallagher, 2015 [109]	0-11	Ge(001)	UHV CVD	285- -320	400-700	@300 K Rlxd. 400nm: 30 Rlxd. 700nm: 95 Psdmrp.: 100-300	Indirect	τ_r extracted from EL measurements in <i>pin</i> diodes. Strong reduction of τ_r in presence of interface relaxation defects.

Kako, 2015 [403]	0	Si(001)	CVD	-	230–3150	Pure Ge @300 K: $\tau_{r,B} \sim 91$ ns $v_{r,S} \sim 130$ m/s	TRPLS	Surface recombination dominated by defective Ge/Si interface. Demonstrate fitting PL decay time with bulk and surface components.
Srinivasan, 2015 [408]	0	SOI	-	-	350	Pure Ge @300 K: 1.6 $v_{r,S} < 200$ m/s	TRPLS	τ_r measured in Ge waveguides. $v_{r,S}$ at Ge/Si interface.
Saito, 2014 [398]	0	Si(001)	CVD	PDA	500	Pure Ge @300 K: 2 $\tau_{r,B} = 3.5$ ns $v_{r,S} < 55$ m/s	TRPLS	They consider τ_r is equal to twice the PL decay time. Growth T and PDA conditions unspecified.
Geiger, 2014 [400]	0	Si(001) GOI	PECVD	500+ PDA	1700 2600	Pure Ge @300 K: 2.0 ($v_{r,S} \sim 850$ m/s) 5.3 ($v_{r,S} \sim 490$ m/s)	IR $\Delta T/T(t)$	6-cycle PDA between 800°C and 600°C. Report $\tau_r = \tau_{r,S}$, assuming recombination occurs only at defective interface with substrate.
Conley, 2014 [409]	10	Ge/Si(001)	RP-CVD	< 450	95	120–1000 @ 77K	Indirect	τ_r extracted from optical responsivity at 1.55 μ m. They however used an unrealistic abs. coeff. of 19200 cm^{-1} for $\text{Ge}_{0.093}\text{Sn}_{0.07}$. Mesa diameter determines τ_r , indicating an unaccounted contribution of $\tau_{r,S}$.
Sheng, 2013 [399]	0	Si(001)	MBE	-	3500	Pure Ge @300 K: 7 TDD $\sim 3.3\text{E}7 \text{ cm}^{-2}$; $\tau_{r,B} = 8.2$ ns TDD $\sim 1.6\text{E}7 \text{ cm}^{-2}$; $\tau_{r,B} = 11$ ns	μ W-PCD	Strong decrease in τ_r near Ge/Si interface. $\tau_{r,B}$ reflects TDD.
Gonzalez, 2011 [347]	0	Si(001)	CVD	450	330	Bulk Ge @300 K: TDD $\sim 1.6\text{E}10 \text{ cm}^{-2}$; $\tau_g = 0.5$ ns TDD $\sim 4.2\text{E}8 \text{ cm}^{-2}$; $\tau_g = 6.8$ ns	Indirect	PDA (850°C, 3 min, in N_2) decreased TDD 40-fold, but τ_g increased only 14-fold. τ_g was extracted from dark currents in Ge pFET, and found to be governed by SRH and TAT generation.
Gaubas, 2006 [396]	0	None	Cz, FZ	-	-	Bulk Ge @300 K: $1 - 5 \cdot 10^5$	μ W-PCD	Study on Ge Czochralski (Cz) or float-zone (FZ) bulk Ge crystals.
Derhacopian, 1994 [397]	0	None	-	-	-	Bulk Ge @300 K: $\tau_{r,B} = 5 \cdot 10^6$ ns $v_{r,S} = 13$ m/s	IC-PCD	Study on bulk Ge crystal, with nominal doping $< 10^{10} \text{ cm}^{-3}$.

Ref. [411], τ_r in GeSn is computed to decrease with Sn content, but still remains above 100 ns up to 18 *at.*% Sn; this computed lifetime is two order of magnitudes higher than any experimental carrier lifetime measured in GeSn on (Ge-buffered) Si substrates. Hence, the reviewed experimental results elucidate the difficulty in achieving efficient room-temperature emission and lasing. More systematic studies are required to understand the material defects in depth, and find effective passivation techniques for linear and point defects in order to increase the non-radiative lifetimes in GeSn. For example, H species have been observed to passivate point defects in GeSn [321].

VIII. CONCLUSIONS

The current bottleneck of the use of GeSn in commercial optoelectronic devices is the lack of a thorough understanding of its defects and trap states, and how they can be controlled during the growth of epitaxial films. The literature evidenced a general lack of agreement regarding the source of trap states leading to high unintentional doping concentrations, generally attributed to vacancy complexes. However, threading dislocations have also been associated to unintentional doping. A sys-

tematic study of unintentional doping concentrations in pseudomorphic GeSn – i.e., free of dislocations – grown on Ge(001) may allow to rule out the latter. Furthermore, impurities have been found to generate deep trap states, decreasing the carrier lifetime in the material, thus worsening its optoelectronic properties. Electrical characterization of annealed Ge films has evidenced a complex interaction between impurities and intrinsic material defects, which may lead to an increase in unintentional doping upon annealing. These interactions are extremely important to control the film electrical properties, but are currently not understood. We conclude stressing the importance of thorough investigations of the electrical properties of GeSn films to achieve a more in-depth understanding and a higher degree of control that would enable its deployment to commercial devices.

ACKNOWLEDGMENTS

This work was supported by Innosuisse, SNSF NCCR QSIT, Max Planck Institut für Festkörperforschung, and Max Planck Graduate Center for Quantum Materials.

Author contributions: A.G. conceived the structure of the review and wrote the manuscript, with inputs from A.F.M.

-
- [1] O. Moutanabbir, S. Assali, X. Gong, E. O'Reilly, C. A. Broderick, B. Marzban, J. Witzens, W. Du, S.-Q. Yu, A. Chelnokov, D. Buca, and D. Nam, Monolithic infrared silicon photonics: The rise of (Si)GeSn semiconductors, *Applied Physics Letters* **118**, 110502 (2021), arXiv:2101.03245.
 - [2] S. A. Ghetmiri, W. Du, J. Margetis, A. Mosleh, L. Cousar, B. R. Conley, L. Domulevicz, A. Nazzal, G. Sun, R. A. Soref, J. Tolle, B. Li, H. A. Naseem, and S. Q. Yu, Direct-bandgap GeSn grown on silicon with 2230 nm photoluminescence, *Applied Physics Letters* **105**, 6 (2014).
 - [3] J. D. Gallagher, C. L. Senaratne, J. Kouvetakis, and J. Menéndez, Compositional dependence of the bowing parameter for the direct and indirect band gaps in Ge_{1-y}Sn_y alloys, *Applied Physics Letters* **105**, 142102 (2014).
 - [4] S. Wirths, R. Geiger, N. von den Driesch, G. Musler, T. Stoica, S. Mantl, Z. Ikonik, M. Luysberg, S. Chiussi, J. M. Hartmann, H. Sigg, J. Faist, D. Buca, and D. Grützmacher, Lasing in direct-bandgap GeSn alloy grown on Si, *Nature Photonics* **9**, 88 (2015), arXiv:1603.03454.
 - [5] M. R. M. Atalla, S. Assali, S. Koelling, A. Attiaoui, and O. Moutanabbir, High-Bandwidth Extended-SWIR GeSn Photodetectors on Silicon Achieving Ultrafast Broadband Spectroscopic Response, *ACS Photonics* **9**, 1425 (2022), arXiv:2111.02892.
 - [6] E. Talamas Simola, V. Kiyek, A. Ballabio, V. Schlykow, J. Frigerio, C. Zucchetti, A. De Iacovo, L. Colace, Y. Yamamoto, G. Capellini, D. Grützmacher, D. Buca, and G. Isella, CMOS-Compatible Bias-Tunable Dual-Band Detector Based on GeSn/Ge/Si Coupled Photodiodes, *ACS Photonics* **8**, 2166 (2021).
 - [7] H. Tran, T. Pham, J. Margetis, Y. Zhou, W. Dou, P. C. Grant, J. M. Grant, S. Al-Kabi, G. Sun, R. A. Soref, J. Tolle, Y.-H. Zhang, W. Du, B. Li, M. Mortazavi, and S.-Q. Yu, Si-Based GeSn Photodetectors toward Mid-Infrared Imaging Applications, *ACS Photonics* **6**, 2807 (2019).
 - [8] D. Zhang, X. Hu, D. Liu, X. Lin, W. Wang, Z. Ding, Z. Wang, B. Cheng, and C. Xue, GeSn on Si avalanche photodiodes for short wave infrared detection, in *Optical Sensing and Imaging Technologies and Applications*, December 2018, edited by D. Liu, H. Gong, M. Guina, and J. Lu (SPIE, 2018) p. 54.
 - [9] Y. Kim, S. Assali, D. Burt, Y. Jung, H.-J. Joo, M. Chen, Z. Ikonik, O. Moutanabbir, and D. Nam, Improved GeSn microdisk lasers directly sitting on Si, in *Silicon Photonics XVII*, March, edited by G. T. Reed and A. P. Knights (SPIE, 2022) p. 21.
 - [10] S. Ojo, Y. Zhou, S. Acharya, N. Saunders, S. Amoah, Y.-T. Jheng, H. Tran, W. Du, G.-E. Chang, B. Li, and S.-Q. Yu, Silicon-based electrically injected GeSn lasers, in *Physics and Simulation of Optoelectronic Devices XXX*, March, edited by M. Osinski, Y. Arakawa, and B. Witzigmann (SPIE, 2022) p. 15.
 - [11] B. Marzban, L. Seidel, T. Liu, K. Wu, V. Kiyek, M. H. Zoellner, Z. Ikonik, J. Schulze, D. Grützmacher, G. Capellini, M. Oehme, J. Witzens, and D. Buca, Strain Engineered Electrically Pumped SiGeSn Microring Lasers on Si, *ACS Photonics* **10**, 217 (2023).

- [12] C. Cardoux, L. Casiez, N. Pauc, V. Calvo, N. Coudurier, P. Rodriguez, J. Richy, P. Barritault, O. Lartigue, C. Constancias, M. Frauenrath, J.-M. Hartmann, A. Chelnokov, O. Gravrand, and V. Reboud, Room temperature spectral characterization of direct band gap Ge_{0.85}Sn_{0.15} LEDs and photodiodes, in *Silicon Photonics XVII*, March, edited by G. T. Reed and A. P. Knights (SPIE, 2022) p. 12.
- [13] B.-J. Huang, C.-Y. Chang, Y.-D. Hsieh, R. A. Soref, G. Sun, H.-H. Cheng, and G.-E. Chang, Electrically Injected GeSn Vertical-Cavity Surface Emitters on Silicon-on-Insulator Platforms, *ACS Photonics* **6**, 1931 (2019).
- [14] C. Chang, T.-w. Chang, H. Li, H. H. Cheng, R. Soref, G. Sun, and J. R. Hendrickson, Room-temperature 2- μ m GeSn P-I-N homojunction light-emitting diode for inplane coupling to group-IV waveguides, *Applied Physics Letters* **111**, 141105 (2017).
- [15] J. D. Sau and M. L. Cohen, Possibility of increased mobility in Ge-Sn alloy system, *Physical Review B* **75**, 045208 (2007).
- [16] S. Mukhopadhyay, B. Mukhopadhyay, G. Sen, and P. K. Basu, Maximum theoretical electron mobility in n-type Ge_{1-x}Sn_x due to minimum doping requirement set by intrinsic carrier density, *Journal of Computational Electronics* **20**, 274 (2021).
- [17] M. Liu, K. Mertens, N. von den Driesch, V. Schlykow, T. Grap, F. Lentz, S. Trelenkamp, J.-m. Hartmann, J. Knoch, D. Buca, and Q.-t. Zhao, Vertical heterojunction Ge_{0.92}Sn_{0.08}/Ge gate-all-around nanowire pMOS-FETs with NiGeSn contact, *Solid-State Electronics* **168**, 107716 (2020).
- [18] Y.-S. Huang, Y.-j. Tsou, C.-H. Huang, C.-H. Huang, H.-s. Lan, C. W. Liu, Y.-C. Huang, H. Chung, C.-P. Chang, S. S. Chu, and S. Kuppura, High-Mobility CVD-Grown Ge/Strained Ge 0.9 Sn 0.1 /Ge Quantum-Well pMOS-FETs on Si by Optimizing Ge Cap Thickness, *IEEE Transactions on Electron Devices* **64**, 2498 (2017).
- [19] W. Wang, D. Lei, Y.-C. Huang, K. H. Lee, W.-K. Loke, Y. Dong, S. Xu, C. S. Tan, H. Wang, S.-F. Yoon, X. Gong, and Y.-C. Yeo, High-performance GeSn photodetector and fin field-effect transistor (FinFET) on an advanced GeSn-on-insulator platform, *Optics Express* **26**, 10305 (2018).
- [20] A. Portavoce, H. Khelidj, N. Ouedna, S. Amhil, M. Bertoglio, D. Manginck, L. Essaleh, and K. Houm-mada, Thermoelectric power factor of Ge_{1-x}Sn_x thin films, *Materialia* **14**, 100873 (2020).
- [21] D. Spirito, N. von den Driesch, C. L. Manganelli, M. H. Zoellner, A. A. Corley-Wiciak, Z. Ikonik, T. Stoica, D. Grütz-macher, D. Buca, and G. Capellini, Thermoelectric Efficiency of Epitaxial GeSn Alloys for Integrated Si-Based Applications: Assessing the Lattice Thermal Conductivity by Raman Thermometry, *ACS Applied Energy Materials* **4**, 7385 (2021).
- [22] C. Goodman, Direct-gap group IV semiconductors based on tin, *IEEE Proceedings I Solid State and Electron Devices* **129**, 189 (1982).
- [23] F. A. Trumbore, Solid Solubilities and Electrical Properties of Tin in Germanium Single Crystals, *Journal of The Electrochemical Society* **103**, 597 (1956).
- [24] R. W. Olesinski and G. J. Abbaschian, The Ge-Sn (Germanium-Tin) system, *Bulletin of Alloy Phase Diagrams* **5**, 265 (1984).
- [25] S. Oguz, W. Paul, T. F. Deutsch, B. Tsaur, and D. V. Murphy, Synthesis of metastable, semiconducting Ge-Sn alloys by pulsed UV laser crystallization, *Applied Physics Letters* **43**, 848 (1983).
- [26] D. W. Jenkins and J. D. Dow, Electronic properties of metastable GeSn alloys, *Physical Review B* **36**, 7994 (1987).
- [27] S. Shah, J. Greene, L. Abels, Q. Yao, and P. Raccach, Growth of single-crystal metastable Ge_{1-x}Sn_x alloys on Ge(100) and GaAs(100) substrates, *Journal of Crystal Growth* **83**, 3 (1987).
- [28] D. W. Hook, S. J. Porter, and C. Herzog, Dimensions: Building Context for Search and Evaluation, *Frontiers in Research Metrics and Analytics* **3**, 23 (2018).
- [29] G. He and H. A. Atwater, Synthesis of epitaxial Sn_xGe_{1-x} alloy films by ion-assisted molecular beam epitaxy, *Nuclear Instruments and Methods in Physics Research Section B: Beam Interactions with Materials and Atoms* **106**, 126 (1995).
- [30] R. Soref, J. Kouvetakis, and J. Menendez, Advances in SiGeSn/Ge Technology, *MRS Proceedings* **958**, 0958 (2006).
- [31] J. Mathews, R. Roucka, J. Xie, S. Q. Yu, J. Meñdez, and J. Kouvetakis, Extended performance GeSn/Si(100) p-i-n photodetectors for full spectral range telecommunication applications, *Applied Physics Letters* **95**, 1 (2009).
- [32] P. R. Pukite, A. Harwit, and S. S. Iyer, Molecular beam epitaxy of metastable, diamond structure Sn x Ge 1-x alloys, *Applied Physics Letters* **54**, 2142 (1989).
- [33] H. Gossmann, Determination of critical layer thicknesses in IV-IV-alloy systems using reflection high energy electron diffraction intensity oscillations: Ge(100)/Ge x Sn 1-x, *Journal of Applied Physics* **68**, 2791 (1990).
- [34] A. Harwit, P. R. Pukite, J. Angilello, and S. S. Iyer, Properties of diamond structure SnGe films grown by molecular beam epitaxy, *Thin Solid Films* **184**, 395 (1990).
- [35] W. Wegscheider, J. Olajos, U. Menczgar, W. Dondl, and G. Abstreiter, Fabrication and properties of epitaxially stabilized Ge / α -Sn heterostructures on Ge(001), *Journal of Crystal Growth* **123**, 75 (1992).
- [36] P. Desjardins, T. Spila, O. Gurdal, N. Taylor, and J. E. Greene, Hybrid surface roughening modes during low-temperature heteroepitaxy: Growth of fully-strained metastable Ge(1-x)Sn(x) alloys on Ge(001)2X1, *Physical Review B* **60**, 15993 (1999).
- [37] O. Gurdal, M. A. Hasan, M. R. Sardela, J. E. Greene, H. H. Radamson, J. E. Sundgren, and G. V. Hansson, Growth of metastable Ge_{1-x}Sn_x/Ge strained layer superlattices on Ge(001)2 \times 1 by temperature-modulated molecular beam epitaxy, *Applied Physics Letters* **67**, 956 (1995).
- [38] O. Gurdal, P. Desjardins, J. R. Carlsson, N. Taylor, H. H. Radamson, J. E. Sundgren, and J. E. Greene, Low-temperature growth and critical epitaxial thicknesses of fully strained metastable Ge_{1-x}Sn_x(x \leq 0.26) alloys on Ge(001)2 \times 1, *Journal of Applied Physics* **83**, 162 (1998).
- [39] K. A. Bratland, Y. L. Foo, T. Spila, H.-S. Seo, R. T. Haasch, P. Desjardins, and J. E. Greene, Sn-mediated Ge/Ge(001) growth by low-temperature molecular-beam epitaxy: Surface smoothening and enhanced epi-

- taxial thickness, *Journal of Applied Physics* **97**, 044904 (2005).
- [40] G. He and H. A. Atwater, Synthesis of epitaxial $\text{Sn}_x\text{Ge}_{1-x}$ alloy films by ion-assisted molecular beam epitaxy, *Applied Physics Letters* **664**, 664 (1995).
 - [41] G. He and H. A. Atwater, Interband Transitions in $\text{Sn}_x\text{Ge}_{1-x}$ Alloys, *Physical Review Letters* **79**, 1937 (1997).
 - [42] R. Ragan and H. A. Atwater, Measurement of the direct energy gap of coherently strained $\text{Sn}_x\text{Ge}_{1-x}/\text{Ge}(001)$ heterostructures, *Applied Physics Letters* **77**, 3418 (2000).
 - [43] Y. Chibane, B. Bouhafs, and M. Ferhat, Unusual structural and electronic properties of $\text{Sn}_x\text{Ge}_{1-x}$ alloys, *Physica Status Solidi (B) Basic Research* **240**, 116 (2003).
 - [44] V. R. D'Costa, C. S. Cook, A. G. Birdwell, C. L. Littler, M. Canonico, S. Zollner, J. Kouvetakis, and J. Menéndez, Optical critical points of thin-film $\text{Ge}_{1-y}\text{Sn}_y$ alloys: A comparative $\text{Ge}_{1-y}\text{Sn}_y/\text{Ge}_{1-x}\text{Six}$ study, *Physical Review B* **73**, 125207 (2006).
 - [45] W. J. Yin, X. G. Gong, and S. H. Wei, Origin of the unusually large band-gap bowing and the breakdown of the band-edge distribution rule in the $\text{Sn}_x\text{Ge}_{1-x}$ alloys, *Physical Review B - Condensed Matter and Materials Physics* **78**, 1 (2008).
 - [46] H. P. Perez Ladron de Guevara, A. G. Rodriguez, H. Navarro-Contreras, and M. A. Vidal, $\text{Ge}_{1-x}\text{Sn}_x$ alloys pseudomorphically grown on $\text{Ge}(001)$, *Applied Physics Letters* **83**, 4942 (2003).
 - [47] H. P. Ladron de Guevara, A. G. Rodriguez, H. Navarro-Contreras, and M. A. Vidal, Determination of the optical energy gap of $\text{Ge}_{1-x}\text{Sn}_x$ alloys with $0 \leq x \leq 0.14$, *Applied Physics Letters* **84**, 4532 (2004).
 - [48] J. Taraci, S. Zollner, M. R. McCartney, J. Menendez, M. A. Santana-Aranda, D. J. Smith, A. Haaland, A. V. Tutukin, G. Gundersen, G. Wolf, and J. Kouvetakis, Synthesis of silicon-based infrared semiconductors in the Ge-Sn system using molecular chemistry methods, *Journal of the American Chemical Society* **123**, 10980 (2001).
 - [49] M. Bauer, J. Taraci, J. Tolle, A. V. Chizmeshya, S. Zollner, D. J. Smith, J. Menendez, C. Hu, and J. Kouvetakis, Ge-Sn semiconductors for band-gap and lattice engineering, *Applied Physics Letters* **81**, 2992 (2002).
 - [50] M. R. Bauer, C. S. Cook, P. Aella, J. Tolle, J. Kouvetakis, P. A. Crozier, A. V. Chizmeshya, D. J. Smith, and S. Zollner, SnGe superstructure materials for Si-based infrared optoelectronics, *Applied Physics Letters* **83**, 3489 (2003).
 - [51] M. Bauer, C. Ritter, P. A. Crozier, J. Ren, J. Menendez, G. Wolf, and J. Kouvetakis, Synthesis of ternary SiGeSn semiconductors on $\text{Si}(100)$ via $\text{Sn}_x\text{Ge}_{1-x}$ buffer layers, *Applied Physics Letters* **83**, 2163 (2003).
 - [52] S. Wirths, D. Buca, and S. Mantl, Si-Ge-Sn alloys: From growth to applications, *Progress in Crystal Growth and Characterization of Materials* **62**, 1 (2016).
 - [53] M. Yamazaki, S. Takeuchi, O. Nakatsuka, A. Sakai, M. Ogawa, and S. Zaima, Scanning tunneling microscopy observation of initial growth of Sn and Ge $1-x$ Sn x layers on $\text{Ge}(001)$ substrates, *Applied Surface Science* **254**, 6048 (2008).
 - [54] S. Takeuchi, Y. Shimura, O. Nakatsuka, S. Zaima, M. Ogawa, and A. Sakai, Growth of highly strained $\text{Ge}_{1-x}\text{Sn}_x$ /virtual Ge by a Sn precipitation controlled compositionally step-graded method, *Applied Physics Letters* **92**, 10.1063/1.2945629 (2008).
 - [55] S. Gupta, B. Magyari-Köpe, Y. Nishi, and K. C. Saraswat, Achieving direct band gap in germanium through integration of Sn alloying and external strain, *Journal of Applied Physics* **113**, 10.1063/1.4792649 (2013).
 - [56] A. V. G. Chizmeshya, C. Ritter, J. Tolle, C. Cook, J. Menéndez, and J. Kouvetakis, Fundamental Studies of $\text{P}(\text{GeH}_3)_3$, $\text{As}(\text{GeH}_3)_3$, and $\text{Sb}(\text{GeH}_3)_3$: Practical n-Dopants for New Group IV Semiconductors, *Chemistry of Materials* **18**, 6266 (2006).
 - [57] S. Su, B. Cheng, C. Xue, W. Wang, Q. Cao, H. Xue, W. Hu, G. Zhang, Y. Zuo, and Q. Wang, GeSn p-i-n photodetector for all telecommunication bands detection, *Optics Express* **19**, 6400 (2011).
 - [58] G. Han, S. Su, C. Zhan, Q. Zhou, Y. Yang, L. Wang, P. Guo, W. Wei, C. P. Wong, Z. X. Shen, B. Cheng, and Y. C. Yeo, High-mobility germanium-tin (GeSn) P-channel MOSFETs featuring metallic source/drain and sub-370°C process modules, *Technical Digest - International Electron Devices Meeting, IEDM*, 402 (2011).
 - [59] S. Gupta, R. Chen, B. Magyari-Köpe, H. Lin, B. Yang, A. Nainani, Y. Nishi, J. S. Harris, and K. C. Saraswat, GeSn technology: Extending the Ge electronics roadmap, *Technical Digest - International Electron Devices Meeting, IEDM*, 398 (2011).
 - [60] M. Oehme, J. Werner, M. Gollhofer, M. Schmid, M. Kaschel, E. Kasper, and J. Schulze, Room-Temperature Electroluminescence From GeSn Light-Emitting Pin Diodes on Si, *IEEE Photonics Technology Letters* **23**, 1751 (2011).
 - [61] R. Roucka, J. Mathews, R. T. Beeler, J. Tolle, J. Kouvetakis, and J. Menéndez, Direct gap electroluminescence from $\text{Si}/\text{Ge}_{1-y}\text{Sn}_y$ p-i-n heterostructure diodes, *Applied Physics Letters* **98**, 0 (2011).
 - [62] B. Vincent, F. Gencarelli, H. Bender, C. Merckling, B. Douhard, D. H. Petersen, O. Hansen, H. H. Henrichsen, J. Meererschaut, W. Vandervorst, M. Heyns, R. Loo, and M. Caymax, Undoped and in-situ B doped GeSn epitaxial growth on Ge by atmospheric pressure-chemical vapor deposition, *Applied Physics Letters* **99**, 10.1063/1.3645620 (2011).
 - [63] S. Wirths, D. Buca, A. T. Tiedemann, B. Hollander, P. Bernardy, T. Stoica, D. Grutzmacher, and S. Mantl, Epitaxial Growth of $\text{Ge}_{1-x}\text{Sn}_x$ by Reduced Pressure CVD Using SnCl_4 and Ge_2H_6 , *ECS Transactions* **50**, 885 (2013).
 - [64] R. Soref, Mid-infrared photonics in silicon and germanium, *Nature Photonics* **4**, 495 (2010).
 - [65] Y. Zhou, Y. Miao, S. Ojo, H. Tran, G. Abernathy, J. M. Grant, S. Amoah, G. Salamo, W. Du, J. Liu, J. Margetis, J. Tolle, Y.-h. Zhang, G. Sun, R. A. Soref, B. Li, and S.-Q. Yu, Electrically injected GeSn lasers on Si operating up to 100 K, *Optica* **7**, 924 (2020).
 - [66] D. Buca, A. Bjelajac, D. Spirito, O. Concepción, M. Gromovyi, E. Sakat, X. Lafosse, L. Ferlazzo, N. von den Driesch, Z. Ikonik, D. Grützmacher, G. Capellini, and M. El Kurdi, Room Temperature Lasing in GeSn Microdisks Enabled by Strain Engineering, *Advanced Optical Materials* **10**, 2201024 (2022).
 - [67] B. Marzban, L. Seidel, V. Kiyek, T. Liu, M. Zöllner, Z. Ikonik, G. Capellini, D. Buca, J. Schulze, M. Oehme,

- and J. Witzens, Modeling and design of an electrically pumped SiGeSn microring laser, in *Silicon Photonics XVII*, March, edited by G. T. Reed and A. P. Knights (SPIE, 2022) p. 18.
- [68] A. Elbaz, R. Arefin, E. Sakat, B. Wang, E. Herth, G. Patriarche, A. Foti, R. Ossikovski, S. Sauvage, X. Checoury, K. Pantzas, I. Sagnes, J. Chrétien, L. Casiez, M. Bertrand, V. Calvo, N. Pauc, A. Chelnokov, P. Boucaud, F. Boeuf, V. Reboud, J.-M. Hartmann, and M. El Kurdi, Reduced Lasing Thresholds in GeSn Microdisk Cavities with Defect Management of the Optically Active Region, *ACS Photonics* **7**, 2713 (2020).
- [69] Q. M. Thai, N. Pauc, J. Aubin, M. Bertrand, J. Chrétien, V. Delaye, A. Chelnokov, J.-M. Hartmann, V. Reboud, and V. Calvo, GeSn heterostructure microdisk laser operating at 230 K, *Optics Express* **26**, 32500 (2018).
- [70] B. Marzban, D. Stange, D. Rainko, Z. Ikonik, D. Buca, and J. Witzens, Modeling of a SiGeSn quantum well laser, *Photonics Research* **9**, 1234 (2021).
- [71] Y. Dong, W. Wang, D. Lei, X. Gong, Q. Zhou, S. Y. Lee, W. K. Loke, S.-F. Yoon, E. S. Tok, G. Liang, and Y.-C. Yeo, Suppression of dark current in germanium-tin on silicon p-i-n photodiode by a silicon surface passivation technique, *Optics Express* **23**, 18611 (2015).
- [72] S. Gupta, E. Simoen, R. Loo, O. Madia, D. Lin, C. Merckling, Y. Shimura, T. Conard, J. Lauwaert, H. Vrielinck, and M. Heyns, Density and Capture Cross-Section of Interface Traps in GeSnO₂ and GeO₂ Grown on Heteroepitaxial GeSn, *ACS Applied Materials and Interfaces* **8**, 13181 (2016).
- [73] M. Morea, C. E. Brendel, K. Zang, J. Suh, C. S. Fenrich, Y. C. Huang, H. Chung, Y. Huo, T. I. Kamins, K. C. Saraswat, and J. S. Harris, Passivation of multiple-quantum-well Ge_{0.97}Sn_{0.03}/Ge p-i-n photodetectors, *Applied Physics Letters* **110**, 0 (2017).
- [74] D. Stange, N. von den Driesch, T. Zabel, F. Armand-Pilon, D. Rainko, B. Marzban, P. Zaumseil, J.-M. Hartmann, Z. Ikonik, G. Capellini, S. Mantl, H. Sigg, J. Witzens, D. Grützmacher, and D. Buca, GeSn/SiGeSn Heterostructure and Multi Quantum Well Lasers, *ACS Photonics* **5**, 4628 (2018).
- [75] Q. Chen, Y. Jung, H. Zhou, S. Wu, X. Gong, Y.-c. Huang, K. H. Lee, L. Zhang, D. Nam, J. Liu, J.-w. Luo, W. Fan, and C. S. Tan, GeSn/Ge Multiquantum-Well Vertical-Cavity Surface-Emitting p-i-n Structures and Diode Emitters on a 200 mm Ge-on-Insulator Platform, *ACS Photonics* 10.1021/acsp Photonics.2c01934 (2023).
- [76] S. Xu, W. Wang, Y.-C. Huang, Y. Dong, S. Masudy-Panah, H. Wang, X. Gong, and Y.-C. Yeo, High-speed photo detection at two-micron-wavelength: technology enablement by GeSn/Ge multiple-quantum-well photodiode on 300 mm Si substrate, *Optics Express* **27**, 5798 (2019).
- [77] Y. Dong, W. Wang, S. Y. Lee, D. Lei, X. Gong, W. K. Loke, S.-F. Yoon, G. Liang, and Y.-C. Yeo, Germanium-tin multiple quantum well on silicon avalanche photodiode for photodetection at two micron wavelength, *Semiconductor Science and Technology* **31**, 095001 (2016).
- [78] M. Wanitzek, M. Oehme, C. Spieth, D. Schwarz, L. Seidel, and J. Schulze, GeSn-on-Si Avalanche Photodiodes for Short-Wave Infrared Detection, in *ESSCIRC 2022-IEEE 48th European Solid State Circuits Conference (ESSCIRC)* (IEEE, 2022) pp. 169–172.
- [79] J. Zheng, L. Li, T. Zhou, Y. Zuo, C. Li, B. Cheng, and Q. Wang, Growth of Crystalline Ge_{1-x}Sn_x Films on Si (100) by Magnetron Sputtering, *ECS Solid State Letters* **3**, P111 (2014).
- [80] G. Chen, Y. Yu, Y. Shi, N. Li, W. Luo, L. Cao, A. J. Danner, A. Q. Liu, and X. Zhang, High-Speed Photodetectors on Silicon Photonics Platform for Optical Interconnect, *Laser and Photonics Reviews* 10.1002/lpor.202200117 (2022).
- [81] M. R. M. Atalla, S. Assali, S. Koelling, A. Attiaoui, and O. Moutanabbir, Dark current in monolithic extended-SWIR GeSn PIN photodetectors, *Applied Physics Letters* **122**, 031103 (2023), arXiv:2203.03409.
- [82] G. E. Chang, S. Q. Yu, J. Liu, H. H. Cheng, R. A. Soref, and G. Sun, Achievable Performance of Uncooled Homojunction GeSn Mid-Infrared Photodetectors, *IEEE Journal of Selected Topics in Quantum Electronics* **28**, 10.1109/JSTQE.2021.3065204 (2022).
- [83] S. Ghosh, R. Bansal, G. Sun, R. A. Soref, H.-H. Cheng, and G.-E. Chang, Design and Optimization of GeSn Waveguide Photodetectors for 2- μ m Band Silicon Photonics, *Sensors* **22**, 3978 (2022).
- [84] C.-H. Liu, R. Bansal, C.-W. Wu, Y.-T. Jheng, and G.-E. Chang, GeSn Waveguide Photodetectors with Vertical p-i-n Heterostructure for Integrated Photonics in the 2 μ m Wavelength Band, *Advanced Photonics Research* **3**, 2100330 (2022).
- [85] C. Li, X. Gao, K. Guan, W. Li, Z. Ma, G. Xu, Z. Li, S. Yang, N. Wang, and C. Xue, Influence of photonic crystals on the performance parameters of GeSn vertical-structure photodiodes, *Optics & Laser Technology* **163**, 109375 (2023).
- [86] V. Reboud, D. Buca, H. Sigg, J. M. Hartmann, Z. Ikonik, N. Pauc, V. Calvo, P. Rodriguez, and A. Chelnokov, Lasing in Group-IV Materials, in *Topics in Applied Physics*, Vol. 139, edited by D. Lockwood and L. Pavesi (Springer Cham, 2021) pp. 105–195, arXiv:2012.10220.
- [87] L. Casiez, M. Bertrand, J. Chretien, A. Quintero, Q. M. Thai, M. Frauenrath, O. Lartigue, P. Barritault, N. Bernier, P. Rodriguez, A. Chelnokov, J. M. Hartmann, N. Pauc, V. Calvo, and V. Reboud, GeSn heterostructures LEDs for gas detection, 2020 IEEE Photonics Conference, IPC 2020 - Proceedings, 16 (2020).
- [88] D. Stange, N. von den Driesch, D. Rainko, S. Roesgaard, I. Povstugar, J.-M. Hartmann, T. Stoica, Z. Ikonik, S. Mantl, D. Grützmacher, and D. Buca, Short-wave infrared LEDs from GeSn/SiGeSn multiple quantum wells, *Optica* **4**, 185 (2017).
- [89] L. Peng, X. Li, J. Zheng, X. Liu, M. Li, Z. Liu, C. Xue, Y. Zuo, and B. Cheng, Room-temperature direct-bandgap electroluminescence from type-I GeSn/SiGeSn multiple quantum wells for 2 μ m LEDs, *Journal of Luminescence* **228**, 117539 (2020).
- [90] R. Bansal, Y.-T. Jheng, K.-C. Lee, H. H. Cheng, and G.-E. Chang, GeSn Vertical Heterostructure p-i-n Waveguide Light Emitting Diode for 2 μ m Band Silicon Photonics, *IEEE Electron Device Letters* **44**, 364 (2023).
- [91] M. Liu, Y. Junk, Y. Han, D. Yang, J. H. Bae, M. Frauenrath, J.-M. Hartmann, Z. Ikonik, F. Bärwolf, A. Mai, D. Grützmacher, J. Knoch, D. Buca, and Q.-T. Zhao, Vertical GeSn nanowire MOSFETs for CMOS beyond silicon, *Communications Engineering* **2**, 7 (2023).

- [92] J. Doherty, S. Biswas, E. Galluccio, C. A. Broderick, A. Garcia-Gil, R. Duffy, E. P. O'Reilly, and J. D. Holmes, Progress on Germanium-Tin Nanoscale Alloys, *Chemistry of Materials* **32**, 4383 (2020).
- [93] K. Momma and F. Izumi, VESTA 3 for three-dimensional visualization of crystal, volumetric and morphology data, *Journal of Applied Crystallography* **44**, 1272 (2011).
- [94] B. Predel, Ge-Sn (Germanium-Tin), in *Ga-Gd - Hf-Zr*, edited by O. Madelung (Springer-Verlag, Berlin/Heidelberg, 1996) pp. 1–4.
- [95] M. P. Polak, P. Scharoch, and R. Kudrawiec, The electronic band structure of Ge 1- x Sn x in the full composition range: indirect, direct, and inverted gaps regimes, band offsets, and the Burstein–Moss effect, *Journal of Physics D: Applied Physics* **50**, 195103 (2017).
- [96] C. Xu, D. Ringwala, D. Wang, L. Liu, C. D. Poweleit, S. L. Chang, H. L. Zhuang, J. Menéndez, and J. Kouvetakis, Synthesis and Fundamental Studies of Si-Compatible (Si)GeSn and GeSn Mid-IR Systems with Ultrahigh Sn Contents, *Chemistry of Materials* **31**, 9831 (2019).
- [97] C. Xu, C. L. Senaratne, R. J. Culbertson, J. Kouvetakis, and J. Menéndez, Deviations from Vegard's law in semiconductor thin films measured with X-ray diffraction and Rutherford backscattering: The Ge 1- y Sn y and Ge 1- x Si x cases, *Journal of Applied Physics* **122**, 125702 (2017).
- [98] S. Magalhaes, M. Dias, B. Nunes, F. Oliveira, M. F. Cerqueira, and E. Alves, Confronting Vegard's rule in Ge 1- x Sn x epilayers: from fundamentals to the effect of defects, *Journal of Physics D: Applied Physics* **55**, 295301 (2022).
- [99] J. Shen, J. Zi, X. Xie, and P. Jiang, Ab initio calculation of the structure of the random alloys, *Physical Review B - Condensed Matter and Materials Physics* **56**, 12084 (1997).
- [100] F. Gencarelli, D. Grandjean, Y. Shimura, B. Vincent, D. Banerjee, A. Vantomme, W. Vandervorst, R. Loo, M. Heyns, and K. Temst, Extended X-ray absorption fine structure investigation of Sn local environment in strained and relaxed epitaxial Ge 1- x Sn x films, *Journal of Applied Physics* **117**, 095702 (2015).
- [101] R. Beeler, R. Roucka, A. V. G. Chizmeshya, J. Kouvetakis, and J. Menéndez, Nonlinear structure-composition relationships in the Ge_{1-y}Sn_y/Si(100) (y|0.15) system, *Physical Review B* **84**, 035204 (2011).
- [102] S. Assali, J. Nicolas, S. Mukherjee, A. Dijkstra, and O. Moutanabbir, Atomically uniform Sn-rich GeSn semiconductors with 3.0-3.5 μ m room-temperature optical emission, *Applied Physics Letters* **112**, 1 (2018).
- [103] B. Cao, S. Chen, X. Jin, J. Liu, and T. Li, Short-Range Order in GeSn Alloy, *ACS Applied Materials & Interfaces* **12**, 57245 (2020), arXiv:2010.02991.
- [104] J. Z. Lentz, J. C. Woicik, M. Bergschneider, R. Davis, A. Mehta, K. Cho, and P. C. McIntyre, Local ordering in Ge/Ge-Sn semiconductor alloy core/shell nanowires revealed by extended x-ray absorption fine structure (EXAFS), *Applied Physics Letters* **122**, 10.1063/5.0136746 (2023).
- [105] J. D. Fuhr, C. I. Ventura, and R. A. Barrio, Formation of non-substitutional β -Sn defects in Ge 1- x Sn x alloys, *Journal of Applied Physics* **114**, 193508 (2013).
- [106] W. Windl and S.-C. Chien, Free-Energy Parameterization and Thermodynamics in Si–Ge–Sn Alloys, *physica status solidi (b)* **259**, 10.1002/pssb.202100590 (2022).
- [107] S. Liu, A. C. Covian, X. Wang, C. T. Cline, A. Akey, W. Dong, S. Yu, and J. Liu, 3D Nanoscale Mapping of Short-Range Order in GeSn Alloys, *Small Methods* **6**, 2200029 (2022), arXiv:2203.05667.
- [108] Z. Song, W. Fan, C. S. Tan, Q. Wang, D. Nam, D. H. Zhang, and G. Sun, Corrigendum: Band structure of Ge 1- x Sn x alloy: a full-zone 30-band $k \cdot p$ model, *New Journal of Physics* **22**, 019502 (2020).
- [109] J. D. Gallagher, C. L. Senaratne, C. Xu, P. Sims, T. Aoki, D. J. Smith, J. Menéndez, and J. Kouvetakis, Non-radiative recombination in Ge_{1-y}Sn_y light emitting diodes: The role of strain relaxation in tuned heterostructure designs, *Journal of Applied Physics* **117**, 0 (2015).
- [110] Y. Chibane and M. Ferhat, Electronic structure of Sn_x Ge_{1-x} alloys for small Sn compositions: Unusual structural and electronic properties, *Journal of Applied Physics* **107**, 10.1063/1.3326162 (2010).
- [111] P. Moontragoon, R. A. Soref, and Z. Ikonik, The direct and indirect bandgaps of unstrained Si x Ge 1- x- y Sn y and their photonic device applications, *Journal of Applied Physics* **112**, 073106 (2012).
- [112] A. Kumar, M. P. Komalan, H. Lenka, A. K. Kambham, M. Gilbert, F. Gencarelli, B. Vincent, and W. Vandervorst, Atomic insight into Ge_{1-x}Sn_x using atom probe tomography, *Ultramicroscopy* **132**, 171 (2013).
- [113] Z. Song, W. Fan, C. S. Tan, Q. Wang, D. Nam, D. H. Zhang, and G. Sun, Band Structure of Strained Ge_{1-x} ~ Sn_x Alloy: A Full-Zone 30-Band $k \cdot p$ Model, *IEEE Journal of Quantum Electronics* **56**, 1 (2020).
- [114] G.-E. Chang, S.-w. Chang, and S. L. Chuang, Strain-Balanced Ge_zSn_{1-z}-Si_xGe_ySn_{1-x-y} Multiple-Quantum-Well Lasers, *IEEE Journal of Quantum Electronics* **46**, 1813 (2010).
- [115] J. Michel, J. Liu, and L. C. Kimerling, High-performance Ge-on-Si photodetectors, *Nature Photonics* **4**, 527 (2010).
- [116] C. Eckhardt, K. Hummer, and G. Kresse, Indirect-to-direct gap transition in strained and unstrained Sn_xGe_{1-x} alloys, *Physical Review B - Condensed Matter and Materials Physics* **89**, 1 (2014).
- [117] V. R. D'Costa, W. Wang, and Y.-C. Yeo, Near-bandgap optical properties of pseudomorphic GeSn alloys grown by molecular beam epitaxy, *Journal of Applied Physics* **120**, 063104 (2016).
- [118] N. S. Fernando, R. A. Carrasco, R. Hickey, J. Hart, R. Hazbun, S. Schoeche, J. N. Hilfiker, J. Kolodzey, and S. Zollner, Band gap and strain engineering of pseudomorphic Ge 1- x - y Si x Sn y alloys on Ge and GaAs for photonic applications, *Journal of Vacuum Science & Technology B, Nanotechnology and Microelectronics: Materials, Processing, Measurement, and Phenomena* **36**, 021202 (2018).
- [119] K. Zelazna, M. P. Polak, P. Scharoch, J. Serafiniczuk, M. Gladysiewicz, J. Misiewicz, J. Dekoster, and R. Kudrawiec, Electronic band structure of compressively strained Ge 1- x Sn x with x | 0.11 studied by contactless electorelectance, *Applied Physics Letters* **106**, 142102 (2015).
- [120] L. Jiang, J. D. Gallagher, C. L. Senaratne, T. Aoki, J. Mathews, J. Kouvetakis, and J. Menéndez, Composi-

- tional dependence of the direct and indirect band gaps in Ge $1-y$ Sn y alloys from room temperature photoluminescence: implications for the indirect to direct gap crossover in intrinsic and n -type materials, *Semiconductor Science and Technology* **29**, 115028 (2014).
- [121] H. Lin, R. Chen, W. Lu, Y. Huo, T. I. Kamins, and J. S. Harris, Investigation of the direct band gaps in Ge $_{1-x}$ Sn $_x$ alloys with strain control by photoreflectance spectroscopy, *Applied Physics Letters* **100**, 10.1063/1.3692735 (2012).
- [122] H. Perez Ladron de Guevara, A. G. Rodriguez, H. Navarro-Contreras, and M. A. Vidal, Nonlinear behavior of the energy gap in Ge $_{1-x}$ Sn $_x$ alloys at 4K, *Applied Physics Letters* **91**, 161909 (2007).
- [123] S. Q. Liu and S. T. Yen, Extraction of eight-band $k \cdot p$ parameters from empirical pseudopotentials for GeSn, *Journal of Applied Physics* **125**, 10.1063/1.5099073 (2019).
- [124] T. D. Eales, I. P. Marko, S. Schulz, E. O'Halloran, S. Ghetmiri, W. Du, Y. Zhou, S. Q. Yu, J. Margetis, J. Tolle, E. P. O'Reilly, and S. J. Sweeney, Ge $_{1-x}$ Sn $_x$ alloys: Consequences of band mixing effects for the evolution of the band gap Γ -character with Sn concentration, *Scientific Reports* **9**, 1 (2019).
- [125] E. J. O'Halloran, C. A. Broderick, D. S. P. Tanner, S. Schulz, and E. P. O'Reilly, Comparison of first principles and semi-empirical models of the structural and electronic properties of Ge $_{1-x}$ Sn $_x$ alloys, *Optical and Quantum Electronics* **51**, 314 (2019), arXiv:1908.02833.
- [126] G. Landwehr and S. Uchida, The Germanium Grain Boundary: A Disordered Two-Dimensional Electronic System, in *Localization and Metal-Insulator Transitions* (Springer US, Boston, MA, 1985) pp. 379–391.
- [127] I. Vladimirov, M. Kühn, T. Gefner, F. May, and R. T. Weitz, Energy barriers at grain boundaries dominate charge carrier transport in an electron-conductive organic semiconductor, *Scientific Reports* **8**, 1 (2018).
- [128] S. Tsurekawa, K. Kido, S. Hamada, T. Watanabe, and T. Sekiguchi, Electrical activity of grain boundaries in polycrystalline silicon - influences of grain boundary structure, chemistry and temperature, *Zeitschrift für Metallkunde* **96**, 197 (2005).
- [129] T. Imajo, T. Ishiyama, K. Nozawa, T. Suemasu, and K. Toko, Acceptor defects in polycrystalline Ge layers evaluated using linear regression analysis, *Scientific Reports* **12**, 14941 (2022).
- [130] M. Grundmann, *The Physics of Semiconductors*, Graduate Texts in Physics (Springer Berlin Heidelberg, Berlin, Heidelberg, 2010) p. 744.
- [131] R. People and J. C. Bean, Calculation of critical layer thickness versus lattice mismatch for Ge x Si $1-x$ /Si strained-layer heterostructures, *Applied Physics Letters* **47**, 322 (1985).
- [132] W. Wang, Q. Zhou, Y. Dong, E. S. Tok, and Y.-C. Yeo, Critical thickness for strain relaxation of Ge $1-x$ Sn x ($x \leq 0.17$) grown by molecular beam epitaxy on Ge(001), *Applied Physics Letters* **106**, 232106 (2015).
- [133] J. Nicolas, S. Assali, S. Mukherjee, A. Lotnyk, and O. Moutanabbir, Dislocation Pipe Diffusion and Solute Segregation during the Growth of Metastable GeSn, *Crystal Growth & Design* **20**, 3493 (2020), arXiv:2003.01308.
- [134] S. Mukherjee, S. Assali, and O. Moutanabbir, Atomic Pathways of Solute Segregation in the Vicinity of Nanoscale Defects, *Nano Letters* **21**, 9882 (2021), arXiv:2107.00800.
- [135] L. M. Giovane, H.-C. Luan, A. M. Agarwal, and L. C. Kimerling, Correlation between leakage current density and threading dislocation density in SiGe p-i-n diodes grown on relaxed graded buffer layers, *Applied Physics Letters* **78**, 541 (2001).
- [136] S. Kondratenko, S. Derenko, Y. I. Mazur, H. Stanchu, A. V. Kuchuk, V. S. Lysenko, P. Lytvyn, S.-Q. F. Yu, and G. J. Salamo, Impact of defects on photoexcited carrier relaxation dynamics in GeSn thin films, *Journal of Physics: Condensed Matter* 10.1088/1361-648x/abc4ce (2020).
- [137] H. Tetzner, I. A. Fischer, O. Skibitzki, M. M. Mirza, C. L. Manganelli, G. Luongo, D. Spirito, D. J. Paul, M. De Seta, and G. Capellini, Current leakage mechanisms related to threading dislocations in Ge-rich SiGe heterostructures grown on Si(001), *Applied Physics Letters* **119**, 153504 (2021).
- [138] S. Sze and K. K. Ng, *America*, edited by V. K. Jain and A. Verma, Environmental Science and Engineering, Vol. 10 (John Wiley & Sons, Inc., Hoboken, NJ, USA, 2006) pp. 739–751.
- [139] J. S. Park, J. Bai, M. Curtin, B. Adekore, M. Carroll, and A. Lochtefeld, Defect reduction of selective Ge epitaxy in trenches on Si(001) substrates using aspect ratio trapping, *Applied Physics Letters* **90**, 1 (2007).
- [140] H. C. Luan, D. R. Lim, K. K. Lee, K. M. Chen, J. G. Sandland, K. Wada, and L. C. Kimerling, High-quality Ge epilayers on Si with low threading-dislocation densities, *Applied Physics Letters* **75**, 2909 (1999).
- [141] J. Aubin, J. M. Hartmann, A. Gassenq, J. L. Rouviere, E. Robin, V. Delaye, D. Cooper, N. Mollard, V. Reboud, and V. Calvo, Growth and structural properties of step-graded, high Sn content GeSn layers on Ge, *Semiconductor Science and Technology* **32**, 10.1088/1361-6641/aa8084 (2017).
- [142] R. Loo, G. Wang, L. Souriau, J. Lin, S. Takeuchi, G. Brammertz, and M. Caymax, Epitaxial Ge on Standard STI Patterned Si Wafers: High Quality Virtual Substrates for Ge pMOS and III/V nMOS, *ECS Transactions* **25**, 335 (2009).
- [143] G. Wang, R. Loo, E. Simoen, L. Souriau, M. Caymax, M. M. Heyns, and B. Blanpain, A model of threading dislocation density in strain-relaxed Ge and GaAs epitaxial films on Si (100), *Applied Physics Letters* **94**, 102115 (2009).
- [144] N. von den Driesch, S. Wirths, R. Troitsch, G. Musler, U. Breuer, O. Moutanabbir, D. Grützmacher, and D. Buca, Thermally activated diffusion and lattice relaxation in (Si)GeSn materials, *Physical Review Materials* **4**, 033604 (2020).
- [145] H. Li, Y. X. Cui, K. Y. Wu, W. K. Tseng, H. H. Cheng, and H. Chen, Strain relaxation and Sn segregation in GeSn epilayers under thermal treatment, *Applied Physics Letters* **102**, 251907 (2013).
- [146] H. Groiss, M. Glaser, M. Schatzl, M. Brehm, D. Gerthsen, D. Roth, P. Bauer, and F. Schäffler, Free-running Sn precipitates: an efficient phase separation mechanism for metastable Ge $_{1-x}$ Sn $_x$ epilayers, *Scientific Reports* **7**, 16114 (2017).
- [147] A. Kuchuk, P. Lytvyn, Y. Mazur, H. Stanchu, S. Kondratenko, F. de Oliveira, S. Malyuta, M. Teodoro, M. Benamara, S.-Q. Yu, and G. Salamo, Sn-guided

- self-grown Ge stripes banded by GeSn Nanowires: Formation mechanism and electric-field-induced switching from p- to n-type conduction, *Applied Surface Science* **604**, 154443 (2022).
- [148] S. Wu, L. Zhang, B. Son, Q. Chen, H. Zhou, and C. S. Tan, Insights into the Origins of Guided Microtrenches and Microholes/rings from Sn Segregation in Germanium-Tin Epilayers, *The Journal of Physical Chemistry C* **124**, 20035 (2020).
- [149] C. Schulte-Braucks, E. Hofmann, S. Glass, N. von den Driesch, G. Mussler, U. Breuer, J.-m. Hartmann, P. Zaumseil, T. Schröder, Q.-t. Zhao, S. Mantl, and D. Buca, Schottky barrier tuning via dopant segregation in NiGeSn-GeSn contacts, *Journal of Applied Physics* **121**, 205705 (2017).
- [150] M. Friesel, U. Sodervall, and W. Gust, Diffusion of tin in germanium studied by secondary ion mass spectrometry, *Journal of Applied Physics* **78**, 5351 (1995).
- [151] I. Riihimäki, A. Virtanen, S. Rinta-Anttila, P. Pusa, J. Raisanen, and The ISOLDE Collaboration, Vacancy-impurity complexes and diffusion of Ga and Sn in intrinsic and p-doped germanium, *Applied Physics Letters* **91**, 091922 (2007).
- [152] Y. Panayiotatos, V. Saltas, A. Chroneos, and F. Valianatos, Tin diffusion in germanium: a thermodynamic approach, *Journal of Materials Science: Materials in Electronics* **28**, 9936 (2017).
- [153] A. Antonelli and J. Bernholc, Pressure effects on self-diffusion in silicon, *Physical Review B* **40**, 10643 (1989).
- [154] M. J. Aziz, Thermodynamics of diffusion under pressure and stress: Relation to point defect mechanisms, *Applied Physics Letters* **70**, 2810 (1997).
- [155] J.-H. Choi, K.-D. Na, S.-C. Lee, and C. S. Hwang, First-principles study on the formation of a vacancy in Ge under biaxial compressive strain, *Thin Solid Films* **518**, 6373 (2010).
- [156] The atomic diffusion coefficient follows the Arrhenius-type law $D = D_0 \exp(-E_a/kT)$, where E_a is the activation energy for diffusion.
- [157] P. Zaumseil, Y. Hou, M. A. Schubert, N. von den Driesch, D. Stange, D. Rainko, M. Virgilio, D. Buca, and G. Capellini, The thermal stability of epitaxial GeSn layers, *APL Materials* **6**, 076108 (2018).
- [158] C. Xu, T. Hu, A. Zhang, D. A. Ringwala, J. Menéndez, and J. Kouvetakis, Synthesis of short-wave infrared Ge_{1-y}Sn_y semiconductors directly on Si(100) via ultralow temperature molecular routes for monolithic integration applications, *Journal of Vacuum Science & Technology A* **40**, 063405 (2022).
- [159] H. V. Stanchu, A. V. Kuchuk, Y. I. Mazur, K. Pandey, F. M. de Oliveira, M. Benamara, M. D. Teodoro, S.-Q. Yu, and G. J. Salamo, Quantitative Correlation Study of Dislocation Generation, Strain Relief, and Sn Outdiffusion in Thermally Annealed GeSn Epilayers, *Crystal Growth & Design* **21**, 1666 (2021).
- [160] V. Bonino, N. Pauc, V. Calvo, M. Frauenrath, J.-M. Hartmann, A. Chelnokov, V. Reboud, M. Rosenthal, and J. Segura-Ruiz, Microstructuring to Improve the Thermal Stability of GeSn Layers, *ACS Applied Materials & Interfaces* **14**, 22270 (2022).
- [161] M. R. Braun, J. Z. Lentz, I. Bishnoi, A. C. Meng, L. Casalena, H. Cheng, and P. C. McIntyre, Oxide Decomposition and Sn Surface Segregation on Core/Shell Ge/GeSn Nanowires, *ACS Applied Electronic Materials* **4**, 5406 (2022).
- [162] H. Jia, P. Jurczak, J. Yang, M. Tang, K. Li, H. Deng, M. Dang, S. Chen, and H. Liu, Impact of ex-situ annealing on strain and composition of MBE grown GeSn, *Journal of Physics D: Applied Physics* **53**, 485104 (2020).
- [163] T. Tsukamoto, N. Hirose, A. Kasamatsu, T. Mimura, T. Matsui, and Y. Suda, Investigation of Sn surface segregation during GeSn epitaxial growth by Auger electron spectroscopy and energy dispersive x-ray spectroscopy, *Applied Physics Letters* **106**, 1 (2015).
- [164] N. Taoka, G. Capellini, N. Von Den Driesch, D. Buca, P. Zaumseil, M. A. Schubert, W. M. Klesse, M. Montanari, and T. Schroeder, Sn migration control at high temperature due to high deposition speed for forming high-quality GeSn layer, *Applied Physics Express* **9**, 10.7567/APEX.9.031201 (2016).
- [165] S. Zaima, O. Nakatsuka, N. Taoka, M. Kurosawa, W. Takeuchi, and M. Sakashita, Growth and applications of GeSn-related group-IV semiconductor materials, *Sci. Technol. Adv. Mater* **16**, 43502 (2015).
- [166] J. Zheng, Z. Liu, C. Xue, C. Li, Y. Zuo, B. Cheng, and Q. Wang, Recent progress in GeSn growth and GeSn-based photonic devices, *Journal of Semiconductors* **39**, 061006 (2018).
- [167] Y. Miao, G. Wang, Z. Kong, B. Xu, X. Zhao, X. Luo, H. Lin, Y. Dong, B. Lu, L. Dong, J. Zhou, J. Liu, and H. H. Radamson, Review of Si-Based GeSn CVD Growth and Optoelectronic Applications, *Nanomaterials* **11**, 2556 (2021).
- [168] T. Tsukamoto, N. Hirose, A. Kasamatsu, T. Mimura, T. Matsui, and Y. Suda, Formation of GeSn layers on Si (001) substrates at high growth temperature and high deposition rate by sputter epitaxy method, *Journal of Materials Science* **50**, 4366 (2015).
- [169] Y. Miao, Y. Wang, H. Hu, X. Liu, H. Su, J. Zhang, J. Yang, Z. Tang, X. Wu, J. Song, R. Xuan, and H. Zhang, Characterization of crystalline GeSn layer on tensile-strained Ge buffer deposited by magnetron sputtering, *Materials Science in Semiconductor Processing* **85**, 134 (2018).
- [170] I. Dascalescu, N. C. Zoita, A. Slav, E. Matei, S. Iftimie, F. Comanescu, A.-M. Lepadatu, C. Palade, S. Lazanu, D. Buca, V. S. Teodorescu, M. L. Ciurea, M. Braic, and T. Stoica, Epitaxial GeSn Obtained by High Power Impulse Magnetron Sputtering and the Heterojunction with Embedded GeSn Nanocrystals for Shortwave Infrared Detection, *ACS Applied Materials & Interfaces* **12**, 33879 (2020).
- [171] H. Huang, D. Zhao, C. Qi, J. Huang, Z. Zeng, B. Zhang, and S. Lu, Effect of Growth Temperature on Crystallization of Ge_{1-x}Sn_x Films by Magnetron Sputtering, *Crystals* **12**, 1810 (2022).
- [172] R. R. Lietaen, J. W. Seo, S. Decoster, A. Vantomme, S. Peters, K. C. Bustillo, E. E. Haller, M. Menghini, and J.-P. Locquet, Tensile strained GeSn on Si by solid phase epitaxy, *Applied Physics Letters* **102**, 052106 (2013).
- [173] T. Sadoh, A. Ooato, J.-H. Park, and M. Miyao, High Sn-concentration (~8%) GeSn by low-temperature (~150°C) solid-phase epitaxy of a-GeSn/c-Ge, *Thin Solid Films* **602**, 20 (2016).
- [174] K. Moto, T. Sugino, R. Matsumura, H. Ikenoue, M. Miyao, and T. Sadoh, Low-temperature (<200°C) solid-phase crystallization of high substitutional Sn con-

- centration (10%) GeSn on insulator enhanced by weak laser irradiation, *AIP Advances* **7**, 10.1063/1.4993220 (2017).
- [175] S. Dev, K. R. Khiangte, and S. Lodha, Wafer-scale mono-crystalline GeSn alloy on Ge by sputtering and solid phase epitaxy, *Journal of Physics D: Applied Physics* **53**, 21LT01 (2020).
- [176] K. Gao, S. Prucnal, R. Huebner, C. Baetz, I. Skorupa, Y. Wang, W. Skorupa, M. Helm, and S. Zhou, Ge_{1-x}Sn_x alloys synthesized by ion implantation and pulsed laser melting, *Applied Physics Letters* **105**, 042107 (2014).
- [177] K. Inenaga, R. Motomura, M. Ishimaru, R. Nakamura, and H. Yasuda, Liquid-mediated crystallization of amorphous GeSn under electron beam irradiation, *Journal of Applied Physics* **127**, 10.1063/5.0006416 (2020).
- [178] S. Prucnal, Y. Berencen, M. Wang, L. Rebohle, R. Kudrawiec, M. Polak, V. Zviagin, R. Schmidt-Grund, M. Grundmann, J. Grenzer, M. Turek, A. Drożdżel, K. Pysznia, J. Zuk, M. Helm, W. Skorupa, and S. Zhou, Band gap renormalization in n-type GeSn alloys made by ion implantation and flash lamp annealing, *Journal of Applied Physics* **125**, 203105 (2019).
- [179] G. He and H. A. Atwater, Synthesis of epitaxial Sn_xGe_{1-x} alloy films by ion-assisted molecular beam epitaxy, *Applied Physics Letters* **68**, 664 (1996).
- [180] J. Zheng, Z. Liu, Y. Zhang, Y. Zuo, C. Li, and C. Xue, Growth of high-Sn content (28%) GeSn alloy films by sputtering epitaxy, *Journal of Crystal Growth* **492**, 29 (2018).
- [181] D. Imbrenda, R. Hickey, R. A. Carrasco, N. S. Fernando, J. VanDerslice, S. Zollner, and J. Kolodzey, Infrared dielectric response, index of refraction, and absorption of germanium-tin alloys with tin contents up to 27% deposited by molecular beam epitaxy, *Applied Physics Letters* **113**, 10.1063/1.5040853 (2018).
- [182] M. Oehme, K. Kosteck, M. Schmid, F. Oliveira, E. Kasper, and J. Schulze, Epitaxial growth of strained and unstrained GeSn alloys up to 25% Sn, *Thin Solid Films* **557**, 169 (2014).
- [183] R. Hickey, N. Fernando, S. Zollner, J. Hart, R. Hazbun, and J. Kolodzey, Properties of pseudomorphic and relaxed germanium 1-x tin x alloys (x ≤ 0.185) grown by MBE, *Journal of Vacuum Science & Technology B, Nanotechnology and Microelectronics: Materials, Processing, Measurement, and Phenomena* **35**, 021205 (2017).
- [184] N. Taoka, G. Capellini, V. Schlykow, M. Montanari, P. Zaumseil, O. Nakatsuka, S. Zaima, and T. Schroeder, Electrical and optical properties improvement of GeSn layers formed at high temperature under well-controlled Sn migration, *Materials Science in Semiconductor Processing* **57**, 48 (2017).
- [185] E. Kasper, M. Kittler, M. Oehme, and T. Argyiurov, Germanium tin: silicon photonics toward the mid-infrared [Invited], *Photonics Research* **1**, 69 (2013).
- [186] M. A. Mircovich, C. Xu, D. A. Ringwala, C. D. Poweleit, J. Menéndez, and J. Kouvetakis, Extended Compositional Range for the Synthesis of SWIR and LWIR Ge_{1-y}Sn_y Alloys and Device Structures via CVD of SnH₄ and Ge₃H₈, *ACS Applied Electronic Materials* **3**, 3451 (2021).
- [187] G. Ehrlich, Atomic events at lattice steps and clusters: a direct view of crystal growth processes, *Surface Science* **331-333**, 865 (1995).
- [188] M. Nerding, L. Oberbeck, T. A. Wagner, R. B. Bergmann, and H. P. Strunk, Single to polycrystalline transition in silicon growth by ion-assisted deposition at low temperatures, *Journal of Applied Physics* **93**, 2570 (2003).
- [189] A. Cullis, Strain-Induced Modulations in the Surface Morphology of Heteroepitaxial Layers, *MRS Bulletin* **21**, 21 (1996).
- [190] C. Xu, P. M. Wallace, D. A. Ringwala, S. L. Chang, C. D. Poweleit, J. Kouvetakis, and J. Menéndez, Mid-infrared (3-8 μm) Ge_{1-y}Sn_y alloys (0.15 ≤ y ≤ 0.30): Synthesis, structural, and optical properties, *Applied Physics Letters* **114**, 0 (2019).
- [191] W. Dou, M. Benamara, A. Mosleh, J. Margetis, P. Grant, Y. Zhou, S. Al-Kabi, W. Du, J. Tolle, B. Li, M. Mortazavi, and S.-Q. Yu, Investigation of GeSn Strain Relaxation and Spontaneous Composition Gradient for Low-Defect and High-Sn Alloy Growth, *Scientific Reports* **8**, 5640 (2018).
- [192] S. Assali, J. Nicolas, and O. Moutanabbir, Enhanced Sn incorporation in GeSn epitaxial semiconductors via strain relaxation, *Journal of Applied Physics* **125**, 025304 (2019).
- [193] J. Rathore, A. Nanwani, S. Mukherjee, S. Das, O. Moutanabbir, and S. Mahapatra, Composition uniformity and large degree of strain relaxation in MBE-grown thick GeSn epitaxial layers, containing 16% Sn, *Journal of Physics D: Applied Physics* **54**, 10.1088/1361-6463/abe1e8 (2021).
- [194] J. Aubin, J. M. Hartmann, A. Gassenq, L. Milord, N. Pauc, V. Reboud, and V. Calvo, Impact of thickness on the structural properties of high tin content GeSn layers, *Journal of Crystal Growth* **473**, 20 (2017).
- [195] C. L. Senaratne, P. M. Wallace, J. D. Gallagher, P. E. Sims, J. Kouvetakis, and J. Menéndez, Direct gap Ge_{1-y}Sn_y alloys: Fabrication and design of mid-IR photodiodes, *Journal of Applied Physics* **120**, 10.1063/1.4956439 (2016).
- [196] W. Dou, Y. Zhou, J. Margetis, S. A. Ghetmiri, S. Al-Kabi, W. Du, J. Liu, G. Sun, R. A. Soref, J. Tolle, B. Li, M. Mortazavi, and S.-Q. Yu, Optically pumped lasing at 3 μm from compositionally graded GeSn with tin up to 23%, *Optics Letters* **43**, 4558 (2018).
- [197] A. Attiaoui and O. Moutanabbir, Indirect-to-direct band gap transition in relaxed and strained Ge_{1-x}Si_xSn_y ternary alloys, *Journal of Applied Physics* **116**, 10.1063/1.4889926 (2014).
- [198] M. R. M. Atalla, S. Assali, A. Attiaoui, C. Lemieux-Leduc, A. Kumar, S. Abdi, and O. Moutanabbir, All-Group IV Transferable Membrane Mid-Infrared Photodetectors, *Advanced Functional Materials* **31**, 2006329 (2021).
- [199] T. Ueno, T. Irisawa, Y. Shiraki, A. Uedono, and S. Tanigawa, Low temperature buffer growth for modulation doped SiGe/Ge/SiGe heterostructures with high hole mobility, *Thin Solid Films* **369**, 320 (2000).
- [200] A. P. Knights, R. M. Gwilliam, B. J. Sealy, T. J. Grasyby, C. P. Parry, D. J. F. Fulgoni, P. J. Phillips, T. E. Whall, E. H. C. Parker, and P. G. Coleman, Growth temperature dependence for the formation of vacancy clusters in Si/Si_{0.64}Ge_{0.36}/Si structures, *Journal of Applied Physics* **89**, 76 (2001).
- [201] L. Qian, J. Tong, W. Fan, J. S. Pan, and D. H. Zhang, Growth of Direct Bandgap Ge_{1-x}Sn_x Alloys by Mod-

- ified Magnetron Sputtering, *IEEE Journal of Quantum Electronics* **56**, 1 (2020).
- [202] G. Lin, K. Qian, H. Ding, J. Qian, J. Xu, J. Wang, S. Ke, W. Huang, S. Chen, and C. Li, Effective strain relaxation of GeSn single crystal with Sn content of 16.5% on Ge grown by high-temperature sputtering, *Applied Surface Science* **623**, 157086 (2023).
- [203] J. Zheng, S. Wang, Z. Liu, H. Cong, C. Xue, C. Li, Y. Zuo, B. Cheng, and Q. Wang, GeSn p-i-n photodetectors with GeSn layer grown by magnetron sputtering epitaxy, *Applied Physics Letters* **108**, 2 (2016).
- [204] T. Tsukamoto, K. Ikeno, N. Hirose, A. Kasamatsu, T. Matsui, and Y. Suda, Sn distribution in Ge/GeSn heterostructures formed by sputter epitaxy method, *Journal of Crystal Growth* **604**, 127045 (2023).
- [205] H. Khelidj, A. Portavoce, M. Bertoglio, M. Descoins, L. Patout, K. Hoummada, A. Hallén, A. Charaï, M. Benoudia, and D. Mangelinck, Ge(Sn) growth on Si(001) by magnetron sputtering, *Materials Today Communications* **26**, 101915 (2021).
- [206] T. Tsukamoto, N. Hirose, A. Kasamatsu, T. Matsui, and Y. Suda, Effects of Low-Temperature GeSn Buffer Layers on Sn Surface Segregation During GeSn Epitaxial Growth, *Electronic Materials Letters* 10.1007/s13391-019-00179-y (2019).
- [207] Yang, Hu, Miao, Dong, Wang, Wang, and Xuan, High-quality GeSn Layer with Sn Composition up to 7Sputtering for Optoelectronic Application, *Materials* **12**, 2662 (2019).
- [208] J. Zheng, W. Huang, Z. Liu, C. Xue, C. Li, Y. Zuo, B. Cheng, and Q. Wang, Influence of H₂ on strain evolution of high-Sn-content Ge_{1-x}Sn_x alloys, *Journal of Materials Science* **52**, 431 (2017).
- [209] E. Napolitani and G. Impellizzeri, Chapter Three - Ion Implantation Defects and Shallow Junctions in Si and Ge, in *Defects in Semiconductors*, Semiconductors and Semimetals, Vol. 91, edited by L. Romano, V. Privitera, and C. Jagadish (Elsevier, 2015) pp. 93–122.
- [210] T. Drüsedau, M. Löhmann, F. Klabunde, and T.-M. John, Investigations on energy fluxes in magnetron sputter-deposition: implications for texturing and nanoporosity of metals, *Surface and Coatings Technology* **133-134**, 126 (2000).
- [211] J. T. Gudmundsson, Physics and technology of magnetron sputtering discharges, *Plasma Sources Science and Technology* **29**, 10.1088/1361-6595/abb7bd (2020).
- [212] T. Takagi, Ion-surface interactions during thin film deposition, *Journal of Vacuum Science & Technology A: Vacuum, Surfaces, and Films* **2**, 382 (1984).
- [213] F. Auret, S. Coelho, W. Meyer, C. Nyamhere, M. Hayes, and J. Nel, Electrical Characterization of Defects Introduced During Sputter Deposition of Schottky Contacts on n-type Ge, *Journal of Electronic Materials* **36**, 1604 (2007).
- [214] F. D. Auret, S. M. Coelho, G. Myburg, P. J. van Rensburg, and W. E. Meyer, Defect introduction in Ge during inductively coupled plasma etching and Schottky barrier diode fabrication processes, *Thin Solid Films* **518**, 2485 (2010).
- [215] A. Sakai and T. Tatsumi, Ge growth on Si using atomic hydrogen as a surfactant, *Applied Physics Letters* **64**, 52 (1994).
- [216] T. Asano, N. Taoka, K. Hozaki, W. Takeuchi, M. Sakashita, O. Nakatsuka, and S. Zaima, Impact of hydrogen surfactant on crystallinity of Ge 1-x Sn x epitaxial layers, *Japanese Journal of Applied Physics* **54**, 04DH15 (2015).
- [217] H. Johll, M. Samuel, R. Y. Koo, H. C. Kang, Y. C. Yeo, and E. S. Tok, Influence of hydrogen surface passivation on Sn segregation, aggregation, and distribution in GeSn/Ge(001) materials, *Journal of Applied Physics* **117**, 10.1063/1.4921594 (2015).
- [218] H. Ye and J. Yu, Germanium epitaxy on silicon, *Science and Technology of Advanced Materials* **15**, 024601 (2014).
- [219] B. Cunningham, J. O. Chu, and S. Akbar, Heteroepitaxial growth of Ge on (100) Si by ultrahigh vacuum, chemical vapor deposition, *Applied Physics Letters* **59**, 3574 (1991).
- [220] L. Colace, G. Masini, F. Galluzzi, G. Assanto, G. Capellini, L. Di Gaspere, E. Palange, and F. Evangelisti, Metal-semiconductor-metal near-infrared light detector based on epitaxial Ge/Si, *Applied Physics Letters* **72**, 3175 (1998).
- [221] J. Matthews and A. Blakeslee, Defects in epitaxial multilayers, *Journal of Crystal Growth* **27**, 118 (1974).
- [222] D. D. Cannon, J. Liu, Y. Ishikawa, K. Wada, D. T. Danielson, S. Jongthammanurak, J. Michel, and L. C. Kimerling, Tensile strained epitaxial Ge films on Si(100) substrates with potential application in L-band telecommunications, *Applied Physics Letters* **84**, 906 (2004).
- [223] H. Hanafusa, N. Hirose, A. Kasamatsu, T. Mimura, T. Matsui, and Y. Suda, Ge flat layer growth on heavily phosphorus-doped Si(001) by sputter epitaxy, *Japanese Journal of Applied Physics* **51**, 2 (2012).
- [224] T. Tsukamoto, N. Hirose, A. Kasamatsu, T. Mimura, T. Matsui, and Y. Suda, Effects of boron dopants of Si (001) substrates on formation of Ge layers by sputter epitaxy method, *Applied Physics Letters* **103**, 10.1063/1.4826501 (2013).
- [225] T. Tsukamoto, N. Hirose, A. Kasamatsu, T. Mimura, T. Matsui, and Y. Suda, Control of surface flatness of Ge layers directly grown on Si (001) substrates by DC sputter epitaxy method, *Thin Solid Films* **592**, 34 (2015).
- [226] G. S. Zeng, C. L. Liu, and S. H. Chen, Effect of substrate biasing on the epitaxial growth and structural properties of rf magnetron sputtered germanium buffer layer on silicon, *Coatings* **11**, 0 (2021).
- [227] Z. Liu, X. Hao, J. Huang, A. Ho-Baillie, and M. A. Green, Reduction of Threading Dislocation Density in Sputtered Ge/Si(100) Epitaxial Films by Continuous-Wave Diode Laser-Induced Recrystallization, *ACS Applied Energy Materials* **1**, 1893 (2018).
- [228] W. Yeh, A. Matsumoto, K. Sugihara, and H. Hayase, Sputter Epitaxial Growth of Flat Germanium Film with Low Threading-Dislocation Density on Silicon (001), *ECS Journal of Solid State Science and Technology* **3**, Q195 (2014).
- [229] S. M. Pietralunga, M. Feré, M. Lanata, D. Piccinin, G. Radnóczy, F. Misják, A. Lamperti, M. Martinelli, and P. M. Ossi, Heteroepitaxial sputtered Ge on Si (100): Nanostructure and interface morphology, *Europhysics Letters* **88**, 10.1209/0295-5075/88/28005 (2009).
- [230] S. Otsuka, T. Mori, Y. Morita, N. Uchida, Y. Liu, S.-i. O'uchi, H. Fuketa, S. Migita, M. Masahara, and T. Matsukawa, Structural and electrical characterization of epitaxial Ge thin films on Si(001) formed by sputtering, *Japanese Journal of Applied Physics* **56**, 04CB01

- (2017).
- [231] M. Steglich, C. Patzig, L. Berthold, F. Schrempel, K. Fücksel, T. Höche, E.-B. Kley, and A. Tünnermann, Heteroepitaxial Ge-on-Si by DC magnetron sputtering, *AIP Advances* **3**, 072108 (2013).
 - [232] G. Bajor, K. C. Cadien, M. A. Ray, J. E. Greene, and P. S. Vijayakumar, Growth of high quality epitaxial Ge films on (100)Si by sputter deposition, *Applied Physics Letters* **40**, 696 (1982).
 - [233] Y. Arroyo Rojas Dasilva, R. Kozak, R. Erni, and M. D. Russell, Structural defects in cubic semiconductors characterized by aberration-corrected scanning transmission electron microscopy, *Ultramicroscopy* **176**, 11 (2017).
 - [234] Y. B. Bolkhovityanov and L. V. Sokolov, Ge-on-Si films obtained by epitaxial growing: edge dislocations and their participation in plastic relaxation, *Semiconductor Science and Technology* **27**, 043001 (2012).
 - [235] J. S. Speck, M. A. Brewer, G. Beltz, A. E. Romanov, and W. Pompe, Scaling laws for the reduction of threading dislocation densities in homogeneous buffer layers, *Journal of Applied Physics* **80**, 3808 (1996).
 - [236] A. Marzegalli, M. Brunetto, M. Salvalaglio, F. Montalenti, G. Nicotra, M. Scuderi, C. Spinella, M. De Seta, and G. Capellini, Onset of plastic relaxation in the growth of Ge on Si(001) at low temperatures: Atomic-scale microscopy and dislocation modeling, *Physical Review B* **88**, 165418 (2013).
 - [237] The *slip plane* is the plane containing both the dislocation line and **b**, within which a dislocation can *glide* [412]. Gliding involves the switching of interatomic bonds, with no diffusion [234].
 - [238] A. Sakai, T. Tatsumi, and K. Aoyama, Growth of strain-relaxed Ge films on Si(001) surfaces, *Applied Physics Letters* **71**, 3510 (1997).
 - [239] F. Rovaris, M. H. Zoellner, P. Zaumseil, A. Marzegalli, L. Di Gaspere, M. De Seta, T. Schroeder, P. Storck, G. Schwalb, G. Capellini, and F. Montalenti, Dynamics of crosshatch patterns in heteroepitaxy, *Physical Review B* **100**, 085307 (2019).
 - [240] E. P. Kvam, D. M. Maher, and C. J. Humphreys, Variation of dislocation morphology with strain in Ge x Si 1-x epilayers on (100)Si, *Journal of Materials Research* **5**, 1900 (1990).
 - [241] J. Zou, X. Z. Liao, D. J. H. Cockayne, and Z. M. Jiang, Alternative mechanism for misfit dislocation generation during high-temperature Ge(Si)/Si (001) island growth, *Applied Physics Letters* **81**, 1996 (2002).
 - [242] Y. Huangfu, W. Zhan, X. Hong, X. Fang, G. Ding, and H. Ye, Heteroepitaxy of Ge on Si(001) with pits and windows transferred from free-standing porous alumina mask, *Nanotechnology* **24**, 10.1088/0957-4484/24/18/185302 (2013).
 - [243] D. Leonhardt, S. Ghosh, and S. M. Han, Origin and removal of stacking faults in Ge islands nucleated on Si within nanoscale openings in SiO₂, *Journal of Applied Physics* **110**, 073516 (2011).
 - [244] M. Y. Gutkin, K. N. Mikaelyan, and I. A. Ovidko, Generation and evolution of partial misfit dislocations and stacking faults in thin-film heterostructures, *Physics of the Solid State* **43**, 42 (2001).
 - [245] E. Maras, O. Trushin, A. Stukowski, T. Ala-Nissila, and H. Jónsson, Global transition path search for dislocation formation in Ge on Si(001), *Computer Physics Communications* **205**, 13 (2016), arXiv:1601.06597.
 - [246] J. M. Hartmann, A. Abbadie, A. M. Papon, P. Holliger, G. Rolland, T. Billon, J. M. Fedeli, M. Rouviere, L. Vivien, and S. Laval, Reduced pressure-chemical vapor deposition of Ge thick layers on Si(001) for 1.3-1.55- μ m photodetection, *Journal of Applied Physics* **95**, 5905 (2004).
 - [247] A. E. Romanov, W. Pompe, G. Beltz, and J. S. Speck, Modeling of threading dislocation density reduction in heteroepitaxial layers: II. Effective dislocation kinetics, *Physica Status Solidi (B) Basic Research* **199**, 33 (1997).
 - [248] O. Skibitzki, M. H. Zoellner, F. Rovaris, M. A. Schubert, Y. Yamamoto, L. Persichetti, L. Di Gaspere, M. De Seta, R. Gatti, F. Montalenti, and G. Capellini, Reduction of threading dislocation density beyond the saturation limit by optimized reverse grading, *Physical Review Materials* **4**, 103403 (2020).
 - [249] L. B. Freund and S. Suresh, *Thin Film Materials* (Cambridge University Press, 2004).
 - [250] V. T. Gillard, W. D. Nix, and L. B. Freund, Role of dislocation blocking in limiting strain relaxation in heteroepitaxial films, *Journal of Applied Physics* **76**, 7280 (1994).
 - [251] B. Pichaud, M. Putero, and N. Burle, Elemental dislocation mechanisms involved in the relaxation of heteroepitaxial semiconducting systems, *Physica Status Solidi (A) Applied Research* **171**, 251 (1999).
 - [252] E. A. Stach, R. Hull, R. M. Tromp, F. M. Ross, M. C. Reuter, and J. C. Bean, In-situ transmission electron microscopy studies of the interaction between dislocations in strained SiGe/Si (001) heterostructures, *Philosophical Magazine A* **80**, 2159 (2000).
 - [253] V. Terzieva, L. Souriau, M. Caymax, D. P. Brunco, A. Moussa, S. Van Elshocht, R. Loo, F. Clemente, A. Satta, and M. Meuris, Benefits and side effects of high temperature anneal used to reduce threading dislocation defects in epitaxial Ge layers on Si substrates, *Thin Solid Films* **517**, 172 (2008).
 - [254] Y. Yamamoto, P. Zaumseil, M. A. Schubert, and B. Tillack, Influence of annealing conditions on threading dislocation density in Ge deposited on Si by reduced pressure chemical vapor deposition, *Semiconductor Science and Technology* **33**, 124007 (2018).
 - [255] At 300K, TEC of Ge and Si are respectively $5.910 \cdot 10^{-6} \text{ } ^\circ\text{C}^{-1}$ and $2.6 \cdot 10^{-6} \text{ } ^\circ\text{C}^{-1}$.
 - [256] R. Hull and J. C. Bean, New insights into the microscopic motion of dislocations in covalently bonded semiconductors by in-situ transmission electron microscope observations of misfit dislocations in thin strained epitaxial layers, *Physica Status Solidi (a)* **138**, 533 (1993).
 - [257] L. Wei, Y. Miao, Y. Ding, C. Li, H. Lu, and Y.-F. Chen, Ultra high hole mobility in Ge films grown directly on Si (100) through interface modulation, *Journal of Crystal Growth* **548**, 125838 (2020).
 - [258] Y. H. Tan and C. S. Tan, Growth and characterization of germanium epitaxial film on silicon (001) using reduced pressure chemical vapor deposition, *Thin Solid Films* **520**, 2711 (2012).
 - [259] V. A. Shah, A. Dobbie, M. Myronov, and D. R. Leadley, High quality relaxed Ge layers grown directly on a Si(0 0 1) substrate, *Solid-State Electronics* **62**, 189 (2011).
 - [260] Y. Yamamoto, P. Zaumseil, T. Arguirov, M. Kittler, and B. Tillack, Low threading dislocation density Ge deposited on Si (100) using RPCVD, *Solid-State Elec-*

- tronics **60**, 2 (2011).
- [261] D. Choi, Y. Ge, J. S. Harris, J. Cagnon, and S. Stemmer, Low surface roughness and threading dislocation density Ge growth on Si (0 0 1), *Journal of Crystal Growth* **310**, 4273 (2008).
- [262] A. Nayfeh, C. O. Chui, K. C. Saraswat, and T. Yonehara, Effects of hydrogen annealing on heteroepitaxial-Ge layers on Si: Surface roughness and electrical quality, *Applied Physics Letters* **85**, 2815 (2004).
- [263] T. Nishimura, S. Kabuyanagi, W. Zhang, C. H. Lee, T. Yajima, K. Nagashio, and A. Toriumi, Atomically flat planarization of Ge(100), (110), and (111) surfaces in H₂ annealing, *Applied Physics Express* **7**, 5 (2014).
- [264] H.-Y. Yu, S.-I. Cheng, J.-H. Park, A. K. Okay, M. C. Onbaşlı, B. Ercan, Y. Nishi, and K. C. Saraswat, High quality single-crystal germanium-on-insulator on bulk Si substrates based on multistep lateral over-growth with hydrogen annealing, *Applied Physics Letters* **97**, 063503 (2010).
- [265] A. Toriumi and T. Nishimura, Germanium CMOS potential from material and process perspectives: Be more positive about germanium, *Japanese Journal of Applied Physics* **57**, 010101 (2018).
- [266] S. Kobayashi, Y. Nishi, and K. Saraswat, Effect of isochronal hydrogen annealing on surface roughness and threading dislocation density of epitaxial Ge films grown on Si, *Thin Solid Films* **518**, S136 (2010).
- [267] J. Hartmann, A. Abbadie, J. Barnes, J. Fédéli, T. Billon, and L. Vivien, Impact of the H₂ anneal on the structural and optical properties of thin and thick Ge layers on Si; Low temperature surface passivation of Ge by Si, *Journal of Crystal Growth* **312**, 532 (2010).
- [268] L. Barbisan, A. Marzegalli, and F. Montalenti, Atomic-scale insights on the formation of ordered arrays of edge dislocations in Ge/Si(001) films via molecular dynamics simulations, *Scientific Reports* **12**, 1 (2022).
- [269] A. Kumar, J. Demeulemeester, J. Bogdanowicz, J. Bran, D. Melkonyan, C. Fleischmann, F. Gencarelli, Y. Shimura, W. Wang, R. Loo, and W. Vandervorst, On the interplay between relaxation, defect formation, and atomic Sn distribution in Ge(1-x)Sn(x) unraveled with atom probe tomography, *Journal of Applied Physics* **118**, 10.1063/1.4926473 (2015).
- [270] H. Stanchu, A. V. Kuchuk, Y. I. Mazur, J. Margetis, J. Tolle, J. Richter, S.-Q. Yu, and G. J. Salamo, X-ray diffraction study of strain relaxation, spontaneous compositional gradient, and dislocation density in GeSn/Ge/Si(100) heterostructures, *Semiconductor Science and Technology* **35**, 075009 (2020).
- [271] N. Bhargava, M. Coppinger, J. Prakash Gupta, L. Wielunski, and J. Kolodzey, Lattice constant and substitutional composition of GeSn alloys grown by molecular beam epitaxy, *Applied Physics Letters* **103**, 041908 (2013).
- [272] F. Gencarelli, B. Vincent, J. Demeulemeester, A. Vantomme, A. Moussa, A. Franquet, A. Kumar, H. Bender, J. Meersschaut, W. Vandervorst, R. Loo, M. Caymax, K. Temst, and M. Heyns, Crystalline Properties and Strain Relaxation Mechanism of CVD Grown GeSn, *ECS Journal of Solid State Science and Technology* **2**, P134 (2013).
- [273] H. Cai, K. Qian, Y. An, G. Lin, S. Wu, H. Ding, W. Huang, S. Chen, J. Wang, and C. Li, Thickness-dependent behavior of strain relaxation and Sn segregation of GeSn epilayer during rapid thermal annealing, *Journal of Alloys and Compounds* **904**, 164068 (2022).
- [274] H. H. Cheng, W. P. Huang, V. I. Mashanov, and G. Sun, Local intermixing on Ge/Si heterostructures at low temperature growth, *Journal of Applied Physics* **108**, 044314 (2010).
- [275] D. Huang, R. Ji, L. Yao, J. Jiao, X. Chen, C. Li, W. Huang, S. Chen, and S. Ke, Strain-induced abnormal Ge/Si inter-diffusion during hetero-epitaxy process, *Vacuum* **196**, 110735 (2022).
- [276] S. Gupta, E. Simoen, R. Loo, Y. Shimura, C. Porret, F. Gencarelli, K. Paredis, H. Bender, J. Lauwaert, H. Vrielinck, and M. Heyns, Electrical properties of extended defects in strain relaxed GeSn, *Applied Physics Letters* **113**, 022102 (2018).
- [277] J. D. Gallagher, C. L. Senaratne, P. Sims, T. Aoki, J. Menéndez, and J. Kouvetakis, Electroluminescence from GeSn heterostructure pin diodes at the indirect to direct transition, *Applied Physics Letters* **106**, 10.1063/1.4913688 (2015).
- [278] F. Wan, C. Xu, X. Wang, G. Xu, B. Cheng, and C. Xue, Study of strain evolution mechanism in Ge_{1-x}Sn_x materials grown by low temperature molecular beam epitaxy, *Journal of Crystal Growth* **577**, 126399 (2022).
- [279] G. Ju, M. Tabuchi, Y. Takeda, and H. Amano, Role of threading dislocations in strain relaxation during GaInN growth monitored by real-time X-ray reflectivity, *Applied Physics Letters* **110**, 262105 (2017).
- [280] F. Castioni, L. Henry, L. Casiez, N. Bernier, V. Reboud, J. Chretien, N. Pauc, V. Calvo, J. Richy, A. Jannaud, V. Delaye, E. Robin, J.-M. Hartmann, and P. Bayle-Guillemaud, Impact of strain on Si and Sn incorporation in (Si)GeSn alloys by STEM analyses, *Journal of Applied Physics* **132**, 195306 (2022).
- [281] The concentration of vacancies is given by $N = N_0 * \exp(E_f/kT)$, where N_0 is the density of sites the defect can occupy and E_f is the formation energy [282]. At 300 K, with $N_0 = 4.41 \cdot 10^{22}$ at/cm⁻³, this expression yields $N \ll 1$ at/cm⁻³.
- [282] J. R. Weber, A. Janotti, and C. G. Van de Walle, Defects in Germanium, in *Photonics and Electronics with Germanium*, edited by K. Wada and L. C. Kimerling (Wiley-VCH Verlag GmbH & Co. KGaA, Weinheim, Germany, 2015) pp. 1–23.
- [283] E. N. Sgourou, A. Daskalopulu, L. H. Tsoukalas, G. Stamoulis, R. V. Vovk, and A. Chroneos, Seventy-Five Years since the Point-Contact Transistor: Germanium Revisited, *Applied Sciences* **12**, 11993 (2022).
- [284] K. Kuitunen, F. Tuomisto, J. Slotte, and I. Capan, Divacancy clustering in neutron-irradiated and annealed n-type germanium, *Physical Review B - Condensed Matter and Materials Physics* **78**, 1 (2008).
- [285] V. Markevich, A. Peaker, S. Lastovskii, L. Murin, V. Litvinov, V. Emtsev, and L. Dobaczewski, Interstitial-related defect reactions in electron-irradiated oxygen-rich Ge crystals: A DLTS study, *Physica B: Condensed Matter* **404**, 4533 (2009).
- [286] H. Gossmann, P. Asoka-Kumar, T. C. Leung, B. Nielsen, K. G. Lynn, F. C. Unterwald, and L. C. Feldman, Point defects in Si thin films grown by molecular beam epitaxy, *Applied Physics Letters* **61**, 540 (1992).
- [287] H. Jorke, H.-J. Herzog, and H. Kibbel, Kinetics of ordered growth of Si on Si(100) at low temperatures, *Physical Review B* **40**, 2005 (1989).

- [288] Y. Bai, M. T. Bulsara, and E. A. Fitzgerald, Photoluminescence and secondary ion mass spectrometry investigation of unintentional doping in epitaxial germanium thin films grown on III-V compound by metal-organic chemical vapor deposition, *Journal of Applied Physics* **111**, 013502 (2012).
- [289] K. M. Shoukri, Y. M. Haddara, A. P. Knights, and P. G. Coleman, Impact of growth conditions on vacancy-type defects in silicon-germanium structures grown by molecular-beam epitaxy, *Applied Physics Letters* **86**, 131923 (2005).
- [290] J. Slotte, I. Makkonen, and F. Tuomisto, Review—Defect Identification with Positron Annihilation Spectroscopy in Narrow Band Gap Semiconductors, *ECS Journal of Solid State Science and Technology* **5**, P3166 (2016).
- [291] H. av Skardi, A. Bro Hansen, A. Mesli, and A. Nylandsted Larsen, The di-vacancy in particle-irradiated, strain-relaxed SiGe, *Nuclear Instruments and Methods in Physics Research Section B: Beam Interactions with Materials and Atoms* **186**, 195 (2002).
- [292] J. Slotte, S. Kilpeläinen, N. Segercrantz, K. Mizohata, J. Räisänen, and F. Tuomisto, In Situ Positron Annihilation Spectroscopy Analysis on Low-Temperature Irradiated Semiconductors, Challenges and Possibilities, *physica status solidi (a)* **218**, 2000232 (2021).
- [293] J. Slotte and F. Tuomisto, Advances in positron annihilation spectroscopy of Si, Ge and their alloys, *Materials Science in Semiconductor Processing* **15**, 669 (2012).
- [294] M. Christian Petersen, A. Nylandsted Larsen, and A. Mesli, Divacancy defects in germanium studied using deep-level transient spectroscopy, *Physical Review B* **82**, 075203 (2010).
- [295] M. Elsayed, N. Arutyunov, R. Krause-Rehberg, G. Oganessian, and V. Kozlovski, Formation and annealing of vacancy-P complexes in proton-irradiated germanium, *Acta Materialia* **100**, 1 (2015).
- [296] J. R. Weber, A. Janotti, P. Rinke, and C. G. Van de Walle, Dangling-bond defects and hydrogen passivation in germanium, *Applied Physics Letters* **91**, 142101 (2007).
- [297] C. Van de Walle, J. Weber, and A. Janotti, Role of hydrogen at germanium/dielectric interfaces, *Thin Solid Films* **517**, 144 (2008).
- [298] A. Chroneos, Isovalent impurity-vacancy complexes in germanium, *physica status solidi (b)* **244**, 3206 (2007).
- [299] A. Chroneos, Effect of germanium substrate loss and nitrogen on dopant diffusion in germanium, *Journal of Applied Physics* **105**, 056101 (2009).
- [300] N. Kuganathan, R. W. Grimes, and A. Chroneos, Nitrogen-vacancy defects in germanium, *AIP Advances* **12**, 045110 (2022).
- [301] V. P. Markevich, V. V. Litvinov, L. Dobaczewski, J. L. Lindström, L. I. Murin, S. V. Vetrov, I. D. Hawkins, and A. R. Peaker, Vacancy-oxygen complex in Ge crystals, *Physica B: Condensed Matter* **340-342**, 844 (2003).
- [302] J. Kujala, T. Südkamp, J. Slotte, I. Makkonen, F. Tuomisto, and H. Bracht, Vacancy-donor complexes in highly n-type Ge doped with As, P and Sb, *Journal of Physics: Condensed Matter* **28**, 335801 (2016).
- [303] A. Vohra, A. Khanam, J. Slotte, I. Makkonen, G. Pourtois, C. Porret, R. Loo, and W. Vandervorst, Heavily phosphorus doped germanium: Strong interaction of phosphorus with vacancies and impact of tin alloying on doping activation, *Journal of Applied Physics* **125**, 225703 (2019).
- [304] A. Vohra, A. Khanam, J. Slotte, I. Makkonen, G. Pourtois, R. Loo, and W. Vandervorst, Evolution of phosphorus-vacancy clusters in epitaxial germanium, *Journal of Applied Physics* **125**, 025701 (2019).
- [305] A. Chroneos, H. Bracht, R. W. Grimes, and B. P. Uberuaga, Vacancy-mediated dopant diffusion activation enthalpies for germanium, *Applied Physics Letters* **92**, 1 (2008).
- [306] F. Aurret, P. J. van Rensburg, M. Hayes, J. Nel, S. Coelho, W. Meyer, S. Decoster, V. Matias, A. Vantomme, and D. Smeets, Electrical characterization of defects in heavy-ion implanted n-type Ge, *Nuclear Instruments and Methods in Physics Research Section B: Beam Interactions with Materials and Atoms* **257**, 169 (2007).
- [307] H. Höhler, N. Atodiressei, K. Schroeder, R. Zeller, and P. H. Dederichs, Vacancy complexes with oversized impurities in Si and Ge, *Physical Review B* **71**, 035212 (2005).
- [308] S. Decoster, S. Cottenier, U. Wahl, J. G. Correia, and A. Vantomme, Lattice location study of ion implanted Sn and Sn-related defects in Ge, *Physical Review B - Condensed Matter and Materials Physics* **81**, 1 (2010).
- [309] E. Kamiyama, K. Sueoka, O. Nakatsuka, N. Taoka, S. Zaima, K. Izunome, and K. Kashima, Analysis for positions of Sn atoms in epitaxial Ge_{1-x}Sn_x film in low temperature depositions, *Thin Solid Films* **557**, 173 (2014).
- [310] D. Rainko, D. Stange, N. von den Driesch, C. Schulte-Braucks, G. Mussler, Z. Ikonc, J. M. Hartmann, M. Luysberg, S. Mantl, D. Grützmacher, and D. Buca, (Si)GeSn nanostructures for light emitters (2016) p. 98910W.
- [311] S. Su, W. Wang, B. Cheng, G. Zhang, W. Hu, C. Xue, Y. Zuo, and Q. Wang, Epitaxial growth and thermal stability of Ge_{1-x}Sn_x alloys on Ge-buffered Si(001) substrates, *Journal of Crystal Growth* **317**, 43 (2011).
- [312] In Ref. [311], they claim χ_{min} is equal for Sn and Ge, but precise values are not reported.
- [313] C. I. Ventura, J. D. Fuhr, and R. A. Barrio, Nonsubstitutional single-atom defects in the Ge_{1-x}Sn_x alloy, *Physical Review B* **79**, 155202 (2009).
- [314] Y. Shimura, N. Tsutsui, O. Nakatsuka, A. Sakai, and S. Zaima, Low temperature growth of Ge_{1-x}Sn_x buffer layers for tensile-strained Ge layers, *Thin Solid Films* **518**, S2 (2010).
- [315] A. Chroneos, C. Jiang, R. W. Grimes, U. Schwingenschlögl, and H. Bracht, Defect interactions in Sn_{1-x}Ge_x random alloys, *Applied Physics Letters* **94**, 252104 (2009).
- [316] F. Tuomisto and I. Makkonen, Defect identification in semiconductors with positron annihilation: Experiment and theory, *Reviews of Modern Physics* **85**, 1583 (2013).
- [317] S. Assali, M. Elsayed, J. Nicolas, M. O. Liedke, A. Wagner, M. Butterling, R. Krause-Rehberg, and O. Moutanabbir, Vacancy complexes in nonequilibrium germanium-tin semiconductors, *Applied Physics Letters* **114**, 251907 (2019).
- [318] J. Slotte, F. Tuomisto, J. Kujala, A. M. Holm, N. Segercrantz, S. Kilpeläinen, K. Kuitunen, E. Simoen, F. Gencarelli, R. Loo, and Y. Shimura, (Invited) Positron Annihilation Spectroscopy on Open-Volume

- Defects in Group IV Semiconductors, ECS Transactions **64**, 241 (2014).
- [319] E. Kamiyama, S. Nakagawa, K. Sueoka, T. Ohmura, T. Asano, O. Nakatsuka, N. Taoka, S. Zaima, K. Izunome, and K. Kashima, Effect of Sn atoms on incorporation of vacancies in epitaxial Ge 1-x Sn x film grown at low temperature, *Applied Physics Express* **7**, 1 (2014).
- [320] A. Chronos, C. A. Londos, and H. Bracht, A-centers and isovalent impurities in germanium: Density functional theory calculations, *Materials Science and Engineering B: Solid-State Materials for Advanced Technology* **176**, 453 (2011).
- [321] O. Nakatsuka, Y. Shimura, W. Takeuchi, N. Taoka, and S. Zaima, Development of epitaxial growth technology for Ge1-xSn x alloy and study of its properties for Ge nanoelectronics, *Solid-State Electronics* **83**, 82 (2013).
- [322] E. Kamiyama, K. Sueoka, K. Terasawa, T. Yamah, O. Nakatsuka, S. Zaima, K. Izunome, K. Kashima, and H. Uchida, Atom probe tomography study on Ge1 - x - ySnxCy hetero-epitaxial film on Ge substrates, *Thin Solid Films* **592**, 54 (2015).
- [323] A. Khanam, A. Vohra, J. Slotte, I. Makkonen, R. Loo, G. Pourtois, and W. Vandervorst, A demonstration of donor passivation through direct formation of V-As i complexes in As-doped Ge 1-x Sn x, *Journal of Applied Physics* **127**, 195703 (2020).
- [324] V. P. Markevich, A. R. Peaker, B. Hamilton, V. V. Litvinov, Y. M. Pokotilo, S. B. Lastovskii, J. Coutinho, A. Carvalho, M. J. Rayson, and P. R. Briddon, Tin-vacancy complex in germanium, *Journal of Applied Physics* **109**, 10.1063/1.3574405 (2011).
- [325] V. P. Markevich, A. R. Peaker, B. Hamilton, V. V. Litvinov, Y. M. Pokotilo, A. N. Petukh, S. B. Lastovskii, J. Coutinho, M. J. Rayson, and P. R. Briddon, Radiation-induced defect reactions in tin-doped Ge crystals, *Solid State Phenomena* **178-179**, 392 (2011).
- [326] A. Vohra, I. Makkonen, G. Pourtois, J. Slotte, C. Porret, E. Rosseel, A. Khanam, M. Tirrito, B. Douhard, R. Loo, and W. Vandervorst, Source/Drain Materials for Ge nMOS Devices: Phosphorus Activation in Epitaxial Si, Ge, Ge 1-x Sn x and Si y Ge 1-x-y Sn x, *ECS Journal of Solid State Science and Technology* **9**, 044010 (2020).
- [327] S. Xu, *GERMANIUM-TIN PHOTO DETECTORS FOR APPLICATIONS IN THE TWO MICRON WAVELENGTH RANGE*, Ph.D. thesis, National University of Singapore (2019).
- [328] Y.-H. Hsieh, W.-Y. Hsieh, H.-H. Tseng, Y.-K. Liu, H. H. Cheng, and G.-E. Chang, Enhanced infrared optical absorption in GeSn alloys for full-telecommunication photodetection, in *International Photonics and Optoelectronics Meetings*, Vol. 95 (OSA, Washington, D.C., 2012) p. ITh3B.3.
- [329] From Ref. [130], the dependence of the absorption coefficient can be approximated to $\alpha \propto (E - E_g)^{-1/2}$. Given the bowing behavior of $E_{g,GeSn}$, the data is fitted using the square root of a second-degree polynomial $f(x_{Sn})$.
- [330] Q. Zhang, Y. Liu, J. Yan, C. Zhang, Y. Hao, and G. Han, Theoretical investigation of tensile strained GeSn waveguide with Si₃N₄ liner stressor for mid-infrared detector and modulator applications, *Optics Express* **23**, 7924 (2015).
- [331] H. Tran, W. Du, S. A. Ghetmiri, A. Mosleh, G. Sun, R. A. Soref, J. Margetis, J. Tolle, B. Li, H. A. Naseem, and S.-Q. Yu, Systematic study of Ge 1-x Sn x absorption coefficient and refractive index for the device applications of Si-based optoelectronics, *Journal of Applied Physics* **119**, 103106 (2016).
- [332] H. Li, C. Chang, H. H. Cheng, G. Sun, and R. A. Soref, Disorder-induced enhancement of indirect absorption in a GeSn photodetector grown by molecular beam epitaxy, *Applied Physics Letters* **108**, 191111 (2016).
- [333] J. Menéndez, J. Tolle, V. R. D'Costa, Y. Fang, J. Mathews, R. Roucka, and J. Kouvetakis, Sn-alloying as a means of increasing the optical absorption of Ge at the C - and L -telecommunication bands, *Semiconductor Science and Technology* **24**, 115006 (2009).
- [334] H. Kumar and R. Basu, Noise Analysis of Group IV Material-Based Heterojunction Phototransistor for Fiber-Optic Telecommunication Networks, *IEEE Sensors Journal* **18**, 9180 (2018).
- [335] A. K. Pandey, R. Basu, and G. E. Chang, Gain performance of GeSn based n-p-n heterojunction phototransistor, *Proceedings of the International Conference on Numerical Simulation of Optoelectronic Devices, NUSOD 2018-Novem*, 35 (2018).
- [336] A. K. Pandey, R. Basu, and G. E. Chang, Optimized Ge1-xSnx/Ge multiple-quantum-well heterojunction phototransistors for high-performance SWIR photodetection, *IEEE Sensors Journal* **18**, 5842 (2018).
- [337] R. Roucka, J. Mathews, C. Weng, R. Beeler, J. Tolle, J. Menendez, and J. Kouvetakis, High-Performance Near-IR Photodiodes: A Novel Chemistry-Based Approach to Ge and Ge-Sn Devices Integrated on Silicon, *IEEE Journal of Quantum Electronics* **47**, 213 (2011).
- [338] G.-E. Chang, R. Basu, B. Mukhopadhyay, and P. K. Basu, Design and Modeling of GeSn-Based Heterojunction Phototransistors for Communication Applications, *IEEE Journal of Selected Topics in Quantum Electronics* **22**, 425 (2016).
- [339] W. Wang, Y. Dong, S. Y. Lee, W. K. Loke, X. Gong, S. F. Yoon, G. Liang, and Y. C. Yeo, Germanium-Tin heterojunction phototransistor: Towards high-efficiency low-power photodetection in short-wave infrared range, *Digest of Technical Papers - Symposium on VLSI Technology 2016-Septe*, 2015 (2016).
- [340] P. Tao, W. Tang, Y. Wang, J. Shi, H. H. Cheng, and X. Wu, Optoelectronic properties for the compressively strained Ge1-xSnx films grown on Ge(004), *Materials Research Express* **7**, 10.1088/2053-1591/ab7a63 (2020).
- [341] S. Adachi, Optical dispersion relations for GaP, GaAs, GaSb, InP, InAs, InSb, Al x Ga 1-x As, and In 1-x Ga x As y P 1-y, *Journal of Applied Physics* **66**, 6030 (1989).
- [342] E. Simoen, F. De Stefano, G. Eneman, B. De Jaeger, C. Claeys, and F. Crupi, On the temperature and field dependence of trap-assisted tunneling current in Ge p+n junctions, *IEEE Electron Device Letters* **30**, 562 (2009).
- [343] C. Claeys, E. Simoen, G. Eneman, K. Ni, A. Hikavyy, R. Loo, S. Gupta, C. Merckling, A. Alian, and M. Caymax, Review—Device Assessment of Electrically Active Defects in High-Mobility Materials, *ECS Journal of Solid State Science and Technology* **5**, P3149 (2016).
- [344] O. Madelung, Elements of the IVth group and IV-IV compounds, in *Semiconductors: Data Handbook* (Springer Berlin Heidelberg, Berlin, Heidelberg, 2004)

- pp. 7–70.
- [345] E. Simoen, G. Brouwers, R. Yang, G. Eneman, M. B. Gonzalez, F. Leys, B. De Jaeger, J. Mitard, D. Brunco, L. Souriau, N. Cody, S. Thomas, L. Lajaunie, M. David, and M. Meuris, Is there an impact of threading dislocations on the characteristics of devices fabricated in strained-Ge substrates?, *physica status solidi c* **6**, 1912 (2009).
 - [346] E. Simoen, C. Claeys, A. Oliveira, P. Agopian, J. Martino, B. Hsu, G. Eneman, E. Rosseel, R. Loo, H. Arimura, N. Horiguchi, W.-C. Wen, and H. Nakashima, Device-Based Threading Dislocation Assessment in Germanium Hetero-Epitaxy, in *2019 34th Symposium on Microelectronics Technology and Devices (SBMicro)*, Vol. 50 (IEEE, 2019) pp. 1–6.
 - [347] M. B. Gonzalez, G. Eneman, G. Wang, B. De Jaeger, E. Simoen, and C. Claeys, Analysis of the Temperature Dependence of Trap-Assisted Tunneling in Ge pFET Junctions, *Journal of The Electrochemical Society* **158**, H955 (2011).
 - [348] G. Eneman, E. Simoen, R. Yang, B. De Jaeger, G. Wang, J. Mitard, G. Hellings, D. Brunco, R. Loo, K. De Meyer, M. R. Caymax, C. Claeys, M. Meuris, and M. Heyns, Defects, Junction Leakage and Electrical Performance of Ge pFET Devices, *ECS Transactions* **19**, 195 (2009).
 - [349] N. A. DiLello, D. K. Johnstone, and J. L. Hoyt, Characterization of dark current in Ge-on-Si photodiodes, *Journal of Applied Physics* **112**, 054506 (2012).
 - [350] P. N. Grillo, S. A. Ringel, and E. A. Fitzgerald, Effect of composition on deep levels in heteroepitaxial GeSi_{1-x} layers and evidence for dominant intrinsic recombination-generation in relaxed Ge layers on Si, *Journal of Electronic Materials* **25**, 1028 (1996).
 - [351] E. Simoen, P. Clauws, and J. Vennik, DLTS of grown-in dislocations in p- and n- type high-purity germanium, *Solid State Communications* **54**, 1025 (1985).
 - [352] M. Sande, L. Goethem, L. Laet, and H. Guislain, Dislocations in high-purity germanium and its relation to γ -ray detector performance, *Applied Physics A Solids and Surfaces* **40**, 257 (1986).
 - [353] S. A. Shevchenko, Electrical conductivity of germanium with dislocation grids, *Journal of Experimental and Theoretical Physics* **88**, 66 (1999).
 - [354] A. Carvalho, V. Torres, V. Markevich, J. Coutinho, V. Litvinov, A. Peaker, R. Jones, and P. Briddon, Identification of stable and metastable forms of centers in germanium, *Physica B: Condensed Matter* **401-402**, 192 (2007).
 - [355] J. Fage-Pedersen, A. N. Larsen, and A. Mesli, Irradiation-induced defects in Ge studied by transient spectroscopies, *Physical Review B* **62**, 10116 (2000).
 - [356] P. Clauws, Oxygen related defects in germanium, *Materials Science and Engineering: B* **36**, 213 (1996).
 - [357] C. Nyamhere, A. Das, F. Aurret, A. Chawanda, C. Pineda-Vargas, and A. Venter, Deep level transient spectroscopy (DLTS) study of defects introduced in antimony doped Ge by 2MeV proton irradiation, *Physica B: Condensed Matter* **406**, 3056 (2011).
 - [358] F. Berg Rasmussen, R. Jones, and S. Öberg, Nitrogen in germanium: Identification of the pair defect, *Physical Review B* **50**, 4378 (1994).
 - [359] I. A. Gulyas, C. A. Stephenson, Q. Meng, S. R. Bank, and M. A. Wistey, The carbon state in dilute germanium carbides, *Journal of Applied Physics* **129**, 10.1063/1.5112057 (2021).
 - [360] E. Simoen, B. Vincent, C. Merckling, F. Gencarelli, L.-K. Chu, and R. Loo, Deep-Level Transient Spectroscopy of MOS Capacitors on GeSn Epitaxial Layers, *ECS Transactions* **50**, 279 (2013).
 - [361] F. H. Baumann and W. Schröter, Deformation-Induced Defects in p-Type Germanium, *Physica Status Solidi (a)* **79**, K123 (1983).
 - [362] M. Stavola, Hydrogen in Silicon and Germanium, in *Proceedings of the 5th International Symposium on Advanced Science and Technology of Silicon Materials (JSPS Si Symposium)* (Hawaii, USA, 2008) pp. 337–343.
 - [363] E. E. Haller, W. L. Hansen, and F. S. Goulding, Physics of ultra-pure germanium, *Advances in Physics* **30**, 93 (1981).
 - [364] L. Dobaczewski, K. B. Nielsen, N. Zangenberg, B. B. Nielsen, A. R. Peaker, and V. P. Markevich, Donor level of bond-center hydrogen in germanium, *Physical Review B* **69**, 245207 (2004).
 - [365] W. Takeuchi, T. Asano, Y. Inuzuka, M. Sakashita, O. Nakatsuka, and S. Zaima, Characterization of Shallow- and Deep-Level Defects in Undoped Ge 1-x Sn x Epitaxial Layers by Electrical Measurements, *ECS Journal of Solid State Science and Technology* **5**, P3082 (2016).
 - [366] M.-Y. Ryu, Y. K. Yeo, M. Ahoujja, T. Harris, R. Beeler, and J. Kouvetakis, Degenerate parallel conducting layer and conductivity type conversion observed from p-Ge 1-y Sn y (y = 0.06%) grown on n-Si substrate, *Applied Physics Letters* **101**, 131110 (2012).
 - [367] S. Gupta, E. Simoen, H. Vrielinck, C. Merckling, B. Vincent, F. Gencarelli, R. Loo, and M. Heyns, Identification of Deep Levels Associated with Extended and Point Defects in GeSn Epitaxial Layers Using DLTs, *ECS Transactions* **53**, 251 (2013).
 - [368] B. Baert, S. Gupta, F. Gencarelli, R. Loo, E. Simoen, and N. D. Nguyen, Electrical characterization of p-GeSn/n-Ge diodes with interface traps under dc and ac regimes, *Solid-State Electronics* **110**, 65 (2015).
 - [369] M. Hogsed, K. Choe, N. Miguel, B. Wang, and J. Kouvetakis, Radiation-induced electron and hole traps in Ge_{1-x}Sn_x (x = 0-0.094), *Journal of Applied Physics* **127**, 0 (2020).
 - [370] I. Capan, B. Pivac, I. Hawkins, V. Markevich, A. Peaker, L. Dobaczewski, and R. Jaćimović, Neutron-irradiation-induced defects in germanium: A Laplace deep level transient spectroscopy study, *Vacuum* **84**, 32 (2009).
 - [371] S. M. M. Coelho, F. D. Aurret, P. J. Janse van Rensburg, and J. M. Nel, Electrical characterization of defects introduced in n-Ge during electron beam deposition or exposure, *Journal of Applied Physics* **114**, 173708 (2013).
 - [372] J. Vanhellefont, J. Lauwaert, A. Witecka, P. Śpiewak, I. Romandic, and P. Clauws, Experimental and theoretical study of the thermal solubility of the vacancy in germanium, *Physica B: Condensed Matter* **404**, 4529 (2009).
 - [373] P. Ščajev, V. Soriūtė, G. Kreiza, T. Malinauskas, S. Stanionytė, P. Onufrijevs, A. Medvids, and H.-H.

- Cheng, Temperature dependent carrier lifetime, diffusion coefficient, and diffusion length in Ge 0.95 Sn 0.05 epilayer, *Journal of Applied Physics* **128**, 115103 (2020).
- [374] L. I. Khirunen, M. G. Sosnin, A. V. Duvanskii, N. V. Abrosimov, and H. Riemann, Divacancy-tin related defects in irradiated germanium, *Journal of Applied Physics* **123**, 161595 (2018).
- [375] V. P. Markevich, I. D. Hawkins, A. R. Peaker, V. V. Litvinov, L. I. Murin, L. Dobaczewski, and J. L. Lindström, Electronic properties of vacancy-oxygen complex in Ge crystals, *Applied Physics Letters* **81**, 1821 (2002).
- [376] S. Brotzmann, H. Bracht, J. L. Hansen, A. N. Larsen, E. Simoen, E. E. Haller, J. S. Christensen, and P. Werner, Diffusion and defect reactions between donors, C, and vacancies in Ge. I. Experimental results, *Physical Review B* **77**, 235207 (2008).
- [377] M. Carroll, J. Sheng, and J. C. Verley, Low-Temperature Hetero-Epitaxial Growth of Ge on Si by High Density Plasma Chemical Vapor Deposition, *MRS Proceedings* **934**, 0934 (2006).
- [378] A. Stesmans, T. Nguyen Hoang, and V. V. Afanas'ev, Hydrogen interaction kinetics of Ge dangling bonds at the Si 0.25Ge0.75/SiO₂ interface, *Journal of Applied Physics* **116**, 10.1063/1.4880739 (2014).
- [379] S. J. Pearton and J. M. Kahn, Dislocations in germanium: Effects of plasma hydrogenation, *Physica Status Solidi (a)* **78**, K65 (1983).
- [380] Kusumandari, N. Taoka, W. Takeuchi, M. Fukudome, M. Sakashita, O. Nakatsuka, and S. Zaima, Broad defect depth distribution in germanium substrates induced by CF₄ plasma, *Applied Physics Letters* **103**, 033511 (2013).
- [381] S.-Y. Wen, L. He, Y.-H. Zhu, and J.-W. Luo, Excimer laser annealing suppresses the bubbles in the recrystallization of argon-implantation induced amorphous germanium, *Journal of Applied Physics* **133**, 045703 (2023).
- [382] I. Chambouleyron and A. R. Zanatta, Nitrogen in germanium, *Journal of Applied Physics* **84**, 1 (1998).
- [383] C. Schulte-Braucks, K. Narimani, S. Glass, N. Von Den Driesch, J. M. Hartmann, Z. Ikonik, V. V. Afanas'ev, Q. T. Zhao, S. Mantl, and D. Buca, Correlation of Bandgap Reduction with Inversion Response in (Si)GeSn/High-k/Metal Stacks, *ACS Applied Materials and Interfaces* **9**, 9102 (2017).
- [384] L. I. Khirunen, Y. V. Pomozov, M. G. Sosnin, N. V. Abrosimov, and H. Riemann, The interaction between divacancies and shallow dopants in irradiated Ge:Sn, in *AIP Conference Proceedings*, Vol. 1583 (2014) pp. 75–79.
- [385] M. Kaukonen, R. Jones, S. Öberg, and P. R. Briddon, Tin-vacancy complexes in silicon, *Physical Review B - Condensed Matter and Materials Physics* **64**, 2452131 (2001).
- [386] Q. Chen, S. Wu, L. Zhang, W. Fan, and C. S. Tan, Simulation of High-Efficiency Resonant-Cavity-Enhanced GeSn Single-Photon Avalanche Photodiodes for Sensing and Optical Quantum Applications, *IEEE Sensors Journal* **21**, 14789 (2021).
- [387] M. Oehme, K. Kosteck, K. Ye, S. Bechler, K. Ulbricht, M. Schmid, M. Kaschel, M. Gollhofer, R. Körner, W. Zhang, E. Kasper, and J. Schulze, GeSn-on-Si normal incidence photodetectors with bandwidths more than 40 GHz, *Optics Express* **22**, 839 (2014).
- [388] T. Mizoguchi, T. Imajo, J. Chen, T. Sekiguchi, T. Sue-masu, and K. Toko, Composition dependent properties of p- and n-type polycrystalline group-IV alloy thin films, *Journal of Alloys and Compounds* **887**, 161306 (2021).
- [389] B. Julsgaard, N. von den Driesch, P. Tidemand-Lichtenberg, C. Pedersen, Z. Ikonik, and D. Buca, Carrier lifetime of GeSn measured by spectrally resolved picosecond photoluminescence spectroscopy, *Photonics Research* **8**, 788 (2020).
- [390] C. Schulte-Braucks, *Investigation of GeSn as novel group IV semiconductor for electronic applications*, Vol. 168 (2017).
- [391] O. Nakatsuka, N. Tsutsui, Y. Shimura, S. Takeuchi, A. Sakai, and S. Zaima, Mobility Behavior of Ge 1- x Sn x Layers Grown on Silicon-on-Insulator Substrates, *Japanese Journal of Applied Physics* **49**, 04DA10 (2010).
- [392] Vacancies cannot form upon cooling down in equilibrium conditions, as thermodynamics predict they are less stable compared to room temperature.
- [393] S. Ghosh, B. Mukhopadhyay, G. Sen, and P. K. Basu, Performance analysis of GeSn/SiGeSn quantum well infrared photodetector in terahertz wavelength region, *Physica E: Low-Dimensional Systems and Nanostructures* **115**, 113692 (2020).
- [394] D. Schroder, The concept of generation and recombination lifetimes in semiconductors, *IEEE Transactions on Electron Devices* **29**, 1336 (1982).
- [395] Only valid if σ_n, σ_p do not differ by more than 2 orders of magnitude.
- [396] E. Gaubas and J. Vanhellemont, Dependence of carrier lifetime in germanium on resistivity and carrier injection level, *Applied Physics Letters* **89**, 142106 (2006).
- [397] N. Derhacopian, P. Fine, J. T. Walton, Y. K. Wong, C. S. Rossington, and P. N. Luke, Determination of Surface Recombination Velocity and Bulk Lifetime in Detector Grade Silicon and Germanium Crystals, *IEEE Transactions on Nuclear Science* **41**, 1026 (1994).
- [398] S. Saito, F. Y. Gardes, A. Z. Al-Attili, K. Tani, K. Oda, Y. Suwa, T. Ido, Y. Ishikawa, S. Kako, S. Iwamoto, and Y. Arakawa, Group IV Light Sources to Enable the Convergence of Photonics and Electronics, *Frontiers in Materials* **1**, 1 (2014).
- [399] J. J. Sheng, D. Leonhardt, S. M. Han, S. W. Johnston, J. G. Cederberg, and M. S. Carroll, Empirical correlation for minority carrier lifetime to defect density profile in germanium on silicon grown by nanoscale interfacial engineering, *Journal of Vacuum Science & Technology B, Nanotechnology and Microelectronics: Materials, Processing, Measurement, and Phenomena* **31**, 051201 (2013).
- [400] R. Geiger, J. Frigerio, M. J. Süess, D. Chrastina, G. Isella, R. Spolenak, J. Faist, and H. Sigg, Excess carrier lifetimes in Ge layers on Si, *Applied Physics Letters* **104**, 062106 (2014).
- [401] G. Grzybowski, R. Roucka, J. Mathews, L. Jiang, R. T. Beeler, J. Kouvetakis, and J. Menéndez, Direct versus indirect optical recombination in Ge films grown on Si substrates, *Physical Review B* **84**, 205307 (2011), arXiv:1106.3300.
- [402] M. K. Hudait, S. W. Johnston, M. B. Clavel, S. Bhattacharya, S. Karthikeyan, and R. Joshi, High carrier lifetimes in epitaxial germanium-tin/Al(In)As heterostructures

- tures with variable tin compositions, *Journal of Materials Chemistry C* **10**, 10530 (2022).
- [403] S. Kako, K. Oda, T. Ido, and Y. Arakawa, Excess carrier lifetime in epitaxially grown layers of germanium on silicon, in *2015 IEEE 12th International Conference on Group IV Photonics (GFP)*, Vol. 2015-Octob (IEEE, 2015) pp. 171–172.
- [404] E. Rogowicz, J. Kopaczek, J. Kutrowska-Girzycka, M. Myronov, R. Kudrawiec, and M. Syperek, Carrier Dynamics in Thin Germanium–Tin Epilayers, *ACS Applied Electronic Materials* **3**, 344 (2021).
- [405] E. Vitiello, S. Rossi, C. A. Broderick, G. Gravina, A. Balocchi, X. Marie, E. P. O’Reilly, M. Myronov, and F. Pezzoli, Continuous-Wave Magneto-Optical Determination of the Carrier Lifetime in Coherent Ge_{1-x}Sn_x/Ge Heterostructures, *Physical Review Applied* **14**, 1 (2020).
- [406] S. De Cesari, A. Balocchi, E. Vitiello, P. Jahandar, E. Grilli, T. Amand, X. Marie, M. Myronov, and F. Pezzoli, Spin-coherent dynamics and carrier lifetime in strained Ge_{1-x}Sn_x semiconductors on silicon, *Physical Review B* **99**, 1 (2019).
- [407] R. Geiger, *ETH*, Ph.D. thesis, ETH (2016).
- [408] S. A. Srinivasan, M. Pantouvaki, P. Verheyen, G. Lepaee, P. Absil, J. Van Campenhout, and D. Van Thoulout, Carrier lifetime assessment in integrated Ge waveguide devices, in *2015 IEEE 12th International Conference on Group IV Photonics (GFP)*, Vol. 2015-Octob (IEEE, 2015) pp. 167–168.
- [409] B. R. Conley, J. Margetis, W. Du, H. Tran, A. Mosleh, S. A. Ghetmiri, J. Tolle, G. Sun, R. Soref, B. Li, H. A. Naseem, and S.-Q. Yu, Si based GeSn photoconductors with a 1.63 A/W peak responsivity and a 2.4 μm long-wavelength cutoff, *Applied Physics Letters* **105**, 221117 (2014).
- [410] *Pseudomorphic* refers to a film that grows epitaxially without relaxing the strain induced by a lattice-mismatched substrate. *Lattice-matched* refers to epitaxial growth in absence of lattice mismatch.
- [411] S. Dominici, H. Wen, F. Bertazzi, M. Goano, and E. Bellotti, Numerical study on the optical and carrier recombination processes in GeSn alloy for E-SWIR and MWIR optoelectronic applications, *Optics Express* **24**, 26363 (2016).
- [412] D. Hull and D. Bacon, *Introduction to Dislocations* (Elsevier, 2011).